University of New Hampshire
University of New Hampshire Scholars' Repository

Master's Theses and Capstones Student Scholarship

Spring 2011

The effect of cutting force model coefficient variability on process planning in milling

Firat Eren
University of New Hampshire, Durham

Follow this and additional works at: https://scholars.unh.edu/thesis

Recommended Citation
Eren, Firat, "The effect of cutting force model coefficient variability on process planning in milling" (2011). *Master's Theses and Capstones*. 629.
https://scholars.unh.edu/thesis/629

This Thesis is brought to you for free and open access by the Student Scholarship at University of New Hampshire Scholars' Repository. It has been accepted for inclusion in Master's Theses and Capstones by an authorized administrator of University of New Hampshire Scholars' Repository. For more information, please contact nicole.hentz@unh.edu.

THE EFFECT OF CUTTING FORCE MODEL COEFFICIENT VARIABILITY ON PROCESS PLANNING IN MILLING

by

Firat Eren

B.S., Sabanci University, 2008

THESIS

Submitted to the University of New Hampshire

in Partial Fulfillment of the Requirements for the Degree of

Master of Science

in

Mechanical Engineering

May, 2011

UMI Number: 1498955

All rights reserved

INFORMATION TO ALL USERS
The quality of this reproduction is dependent upon the quality of the copy submitted.

In the unlikely event that the author did not send a complete manuscript
and there are missing pages, these will be noted. Also, if material had to be removed,
a note will indicate the deletion.

UMI®
Dissertation Publishing

UMI 1498955
Copyright 2011 by ProQuest LLC.
All rights reserved. This edition of the work is protected against
unauthorized copying under Title 17, United States Code.

ProQuest®

ProQuest LLC
789 East Eisenhower Parkway
P.O. Box 1346
Ann Arbor, MI 48106-1346

This thesis has been examined and approved.

Thesis Director, Dr. Barry K. Fussell

Professor of Mechanical Engineering

Thesis Co-Director, Dr. Robert B. Jerard

Professor of Mechanical Engineering

Dr. Phil Ramsey

Adjunct and Visiting Faculty of Mathematics & Statistics

04/29/2011

Date

DEDICATIONS

To my grandfather, *Arzuman Eren*

ACKNOWLEDGEMENTS

I would like to thank Prof. Fussell and Prof. Jerard for their continual patience, support and guidance throughout this study. I feel very lucky to be a part of their research group at the Design and Manufacturing Lab. I believe that I learned a lot from them.

I would also like to thank to Prof. Ramsey for his time evaluating this thesis.

I feel the utmost gratitude for Prof. Celikkol. If it wasn't for him, I would not have the chance to study at the UNH. I also thank him for his support and friendship inside and outside of the university. I am also grateful for his wife Mira, for her hospitality.

Valuable help and support of my lab friends whom I worked with during three years are greatly appreciated. Thanks to Raed Hassan for teaching me how to use the FADAL CNC milling machine and to Chris Suprock for expanding my horizons with his brilliant innovative ideas. I also would like to thank Justin, Andrew, Saman, Minhyong and Yong for their friendship and making the lab a more enjoyable place.

I want to mention Basak Sahin whose support and existence is invaluable to me.

The financial support from NSF Grants DMI-0620996 and IIP-0810434 and the Department of Mechanical Engineering is greatly appreciated.

Finally, I would like to thank to my family. I felt their love and support at every instant during the three years.

TABLE OF CONTENTS

LIST OF TABLES

LIST OF FIGURES

LIST OF SYMBOLS

ϕ = angular position of cutting tool, (deg)

ϕ_{st} = angle at which tooth enters material, (deg)

ϕ_{ex} = angle at which tooth exits material, (deg)

ω = angular velocity of cutting tool, (rad/s)

a = axial depth of cut, (mm)

f = feedrate (mm/min)

f_t = feed per tooth, (mm)

h = chip thickness, (mm)

K_{RC} = model coefficient for radial shearing force component, (N/mm^2)

K_{RE} = model coefficient for radial friction force component, (N/mm)

K_{TC} = model coefficient for tangential shearing force component, (N/mm^2)

K_{TE} = model coefficient for tangential friction force component, (N/mm)

F_r = force on the tool in the radial direction, (N)

F_t = force on the tool tangential to the perimeter, (N)

F_{res} = resultant force on the tool, (N)

F_x = force along the x-axis of the mill, (N)

$\overline{F_x}$ = average force in the x-direction, (N)

F_y = force along the y-axis of the mill, (N)

$\overline{F_y}$ = average force in the y-direction, (N)

N_t = number of teeth on the cutting tool

F = vector of average forces in x and y direction

G = geometry matrix related to the cut geometry

K = force model coefficient vector

A = elements of the G matrix

δ = tool deflection, (mm)

L = tool length, (mm)

E = elastic modulus, (N/mm^2)

I = second moment of inertia (mm^4)

D_{eff} = effective tool diameter, (mm)

σ_b = bending stress, (N/mm^2)

D = tool diameter, (mm)

s_{est} = standard error of the estimate

ABSTRACT

THE EFFECT OF CUTTING FORCE MODEL COEFFICIENT VARIABILITY ON PROCESS PLANNING IN MILLING

by

Firat Eren

University of New Hampshire, May 2011

This thesis describes the effect of force model uncertainty on process planning. Specifically, the statistical variations in model predicted machining forces while cutting aluminum, carbon steel, stainless steel and titanium are determined. An accurate estimate of the variability is essential for use in process planning to determine appropriate factors of safety when setting cutting conditions that are both safe and efficient.

Force model coefficient calibration is described and the variability in the coefficients is determined through a least squares regression of a large number of experimental cuts. It is shown that the variability increases with changes in the calibration cutting conditions, e.g. radial depth of cut and spindle speed. Monte Carlo simulations of the cutting force are then used to determine the mean and standard deviation of the resultant peak force. A factor of safety is established for process

planning using the mean plus three standard deviations. Statistically, 99.86% of the actual peak cutting forces should fall below the predicted value. The maximum expected peak force can be determined for each tool move in a NC program and used to select safe cutting conditions.

CHAPTER 1

INTRODUCTION

1.1 Introduction

Force model uncertainty is investigated in this research to quantify its effect on process planning. In process planning, selecting the best possible feedrates is subject to constraints like tool health, part quality and machine tool limitations [1]. Based on these constraints, feedrates are optimized to maintain predicted cutting forces for each tool move. In this study, a linear milling force model [2] is utilized to predict cutting forces. Assigning a Factor of Safety (FS) value for the predicted cutting forces is practical for a process planner to set feedrates that will give a certain level of confidence that the cut will be safe. In a cutting process there are many conditions that have the potential to add to the force model uncertainty, e.g. variation in spindle speed, radial immersion, helix angle, cutter type, coolant type etc. In this research, the effect of the variations in the spindle speed and radial immersion are investigated to set FS values that will result in safe cutting conditions.

Models of the metal removal process have been developed and experimentally verified by many researchers [2, 3, 4]. Commercial software from vendors such as Third Wave, CGTech and VeritasCNC can be used to estimate cutting forces, a prerequisite for setting good cutting conditions. Previous research has illustrated how a properly calibrated force model can be used to select the best possible cutting conditions [1, 5, 6].

Extensive experimental investigation including thousands of cutting tests with a variety of tools and materials showed that model accuracy is only as good as the model coefficients [7]. With careful calibration it is possible to achieve good levels of accuracy. But model coefficient variability implies variability in the accuracy of cutting force estimates thereby impeding the usefulness of the models in selecting cutting conditions for process planning.

Model uncertainty as applied to machining has not been extensively studied but some good examples exist. The study performed by Kurdi et al [8] utilizes the Latin Hypercube method to quantify the uncertainty in stability and surface location errors including the correlation between the cutting coefficients and the tool model parameters. They conclude that taking the correlation into account reduces the output variation significantly. The work by Schmitz et al [9] on stability lobe generation in the presence of uncertainty shows how theoretical chatter limits are modified by uncertainty. Researchers at NIST [10] have also explored the effect of model uncertainty in turning operations with different chip breaker geometries utilizing a regression based model. The uncertainties in both data and the model were combined to obtain an expanded uncertainty which enables predictive modeling in a large range of conditions, i.e. machine tools and environments.

1.2 Thesis Overview

Chapter 1 is an introduction to force model uncertainty. Chapter 2 describes the cutting force model used in this research as well as the methods used for model coefficient calibration. Background information about the force model used in the research as well as process planning is given. The four model coefficients, K_{TC}, K_{TE}, K_{RC}, and K_{RE} and the calibration procedure for estimating these model coefficients are introduced. Chapter 3 describes the experiments performed for this research and the calibration results. Experimental design is shown, and calibration results for Aluminum 6061, Steel 1018, Stainless Steel 304 and Titanium Grade 2 are presented.

In Chapter 4, cutting model coefficient variability is discussed. Correlation matrices for the model coefficients are presented. The variation in the cutting coefficients generates variation in the force estimation for different cutting conditions. Monte Carlo simulations are run to obtain force probability distributions for different conditions. The simulation results are used to identify the effect of changing cutting conditions on the force predictions by observing the statistics, mean and standard deviation, of the force probability distribution results. Subsequently, they are used to set the Factor of Safety for the four different materials. The simulation results are experimentally validated in Chapter 5. Monte Carlo simulation results are used to form upper and lower confidence levels at 99.86% and 95 %. Measured peak forces for different cutting conditions, different spindle speed, radial immersion and chip thickness for the material of interest for this research are compared to the simulation results. A Case study with two methods is performed to validate the Factor of Safety values generated by Monte Carlo simulation. In Chapter 6, the effect of assigning ratios between the tangential and radial coefficients on the force probability density functions and the factor of safety are discussed. Mean and variance of the ratios of the calibrated radial to tangential coefficients for different cutting conditions are utilized in a multivariate normal distribution to estimate the radial coefficients in a Monte Carlo simulation. The change in factor of safety obtained with the ratio method is compared to the factor of safety obtained from the calibrated coefficients method. Chapter 7 summarizes the outcomes of the research, including a discussion of the potential practical applications as well as the limitations using the methods described in this research. This chapter also offers suggestions for further study.

CHAPTER 2

BACKGROUND

2.1 Introduction

In this chapter, the milling force model used in this research is introduced and the model calibration procedure is described. Background information about the process planning and feedrate selection process based on several constraints like tool bending stress and tool deflection is included.

2.2 Force Model

The mechanistic milling force model used in this research is described by Altintas [1]. Figure 2.1 defines the cutting geometry. The tangential force is split into a cutting or shearing component and a rubbing component [6],

$$F_t(\phi) = \left(K_{TC} \cdot h(\phi) + K_{TE}\right) a \qquad (2.1)$$

where K_{TC} and K_{TE} are the tangential coefficients, φ is the angle of tooth engagement, a is the length of tooth engaged in the cut and h is the instantaneous chip thickness which is defined as

$$h(\phi) = f_t \cdot \sin(\phi) \qquad (2.2)$$

where $\mathbf{f_t}$ is the feed per tooth, (mm/rev-tooth).

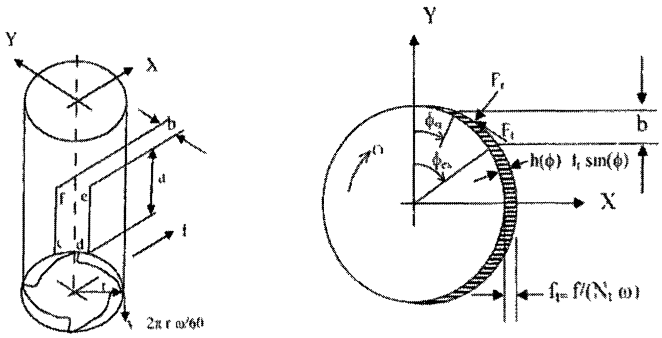

Figure 2.1: End Milling Cutting Geometry.

In a similar way the radial (F_r) force components are [1]:

$$F_r(\phi) = \left(K_{RC} \cdot h(\phi) + K_{RE}\right) a \tag{2.3}$$

where K_{RC} and K_{RE} are the radial cutting coefficients.

Tangential, radial and resultant forces can be related using an x-y reference frame to describe the motion of the tool relative to the workpiece [1, 4]:

$$F_x(\phi) = -F_t \cos(\phi) - F_r \sin(\phi) \tag{2.4}$$

$$F_y(\phi) = F_t \sin(\phi) - F_r \cos(\phi) \tag{2.5}$$

$$F_{res} = \sqrt{F_x^{\ 2} + F_y^{\ 2}} \tag{2.6}$$

Compared to other more complicated models [7], this linear model is simple to calibrate and extensive testing in our facility has demonstrated good accuracy and repeatability as long as the model is calibrated correctly.

2.3 Model Calibration

There are various methods to calibrate the model coefficients. Typically, a set of milling experiments are conducted at different feed rates with constant radial immersion and axial depth of cut. A single cutting tooth is used to eliminate the effect of run out. Average cutting forces in the x and y direction, obtained from the Kistler load cell, are plugged into equations (2.7) and (2.8) which are the integrated forms of the force equations given in (2.4), (2.5) and (2.6).

$$\overline{F}_x = \left\{ \begin{array}{l} \dfrac{Naf_t}{8\pi}\left[K_{TC}(\cos 2\phi_{ex} - \cos 2\phi_{st}) - K_{RC}(2\phi_{ex} - 2\phi_{st} - (\sin 2\phi_{ex} - \sin 2\phi_{st}))\right] \\ + \dfrac{Na}{2\pi}\left[-K_{TE}(\sin\phi_{ex} - \sin\phi_{st}) + K_{RE}(\cos\phi_{ex} - \cos\phi_{st})\right] \end{array} \right\} \tag{2.7}$$

$$\overline{F}_y = \left\{ \begin{array}{l} \dfrac{Naf_t}{8\pi}\left[K_{TC}\left(2\phi_{ex} - 2\phi_{st} - (\sin 2\phi_{ex} - \sin 2\phi_{st}\right) + K_{RC}(\cos 2\phi_{ex} - \cos 2\phi_{st})\right] \\ - \dfrac{Na}{2\pi}\left[K_{TE}(\cos\phi_{ex} - \cos\phi_{st}) + K_{RE}(\sin\phi_{ex} - \sin\phi_{st})\right] \end{array} \right\} \tag{2.8}$$

In the equations, N is the number of teeth, ϕ_{st} is the entry angle, ϕ_{ex} is the exit angle and f_t is the feed per tooth. Equations (2.7) and (2.8) can be combined into a matrix form as seen in (2.9) where K is the force model coefficient matrix and G depends on the cut geometry.

$$F = GK \tag{2.9}$$

$$\underbrace{\begin{bmatrix} \overline{F}_{x_\iota} \\ \overline{F}_{y_\iota} \end{bmatrix}}_{F} = \underbrace{\begin{bmatrix} A_{1x_\iota} & A_{2x_\iota} & A_{3x_\iota} & A_{4x_\iota} \\ A_{1y_\iota} & A_{2y_\iota} & A_{3y_\iota} & A_{4y_\iota} \end{bmatrix}}_{G} \underbrace{\begin{bmatrix} K_{TC} \\ K_{TE} \\ K_{RC} \\ K_{RE} \end{bmatrix}}_{K} \qquad (2.10)$$

F is the vector of average Kistler forces in the x and y directions for the cut. The G matrix is the x and y cut geometry matrix, related to the cut geometry in the x and y direction. The geometry matrix is multiplied by the model coefficient matrix, K, to get the average forces in x and y. The subscript ι in Equation 2.10 denotes the number of test conditions used to perform the calibration. Model calibration for this research is done using four different feedrate values. Thus, the size of the force vector F will be of 8x1, G matrix 8x4 and K vector 4x1.

The explicit form of the elements in the geometry matrix can be seen in the following equations. For the cut in the x direction the matrix elements are defined as,

$$A_{1x} = \frac{Naf_\iota}{8\pi} . (\cos 2\phi_{ex} - \cos 2\phi_{st}) \qquad (2.11)$$

$$A_{2x} = -\frac{Na}{2\pi} . (\sin \phi_{ex} - \sin \phi_{st}) \qquad (2.12)$$

$$A_{3x} = -\frac{Naf_\iota}{8\pi} .[2\phi_{ex} - 2\phi_{st} - (\sin 2\phi_{ex} - \sin 2\phi_{st})] \qquad (2.13)$$

$$A_{4x} = \frac{Na}{2\pi} .(\cos \phi_{ex} - \cos \phi_{st}) \qquad (2.14)$$

and for y direction, the matrix elements are the following;

$$A_{1y}=\frac{Naf_t}{8\pi}.[2\phi_{ex}-2\phi_{st}-(\sin 2\phi_{ex}-\sin 2\phi_{st})] \tag{2.15}$$

$$A_{2y}=-\frac{Na}{2\pi}.(\cos\phi_{ex}-\cos\phi_{st}) \tag{2.16}$$

$$A_{3y}=\frac{Naf_t}{8\pi}.(\cos 2\phi_{ex}-\cos 2\phi_{st}) \tag{2.17}$$

$$A_{4y}=-\frac{Na}{2\pi}.(\sin\phi_{ex}-\sin\phi_{st}) \tag{2.18}$$

Least squares estimation can be applied to (2.9) to calculate the cutting coefficients K_{TC}, K_{TE}, K_{RC} and K_{RE}, as follows,

$$\begin{bmatrix} K_{TC} \\ K_{TE} \\ K_{RC} \\ K_{RE} \end{bmatrix} = (G^T G)^{-1} G^T F \tag{2.19}$$

2.4 Process Planning

Previous research has demonstrated how a properly calibrated force model can be used to select the best possible cutting conditions. There is a set of constraints that has to be maintained to select the fastest feedrates possible. These constraints can be grouped as follows: part quality, tool health and machine tool limitations. Machine tool limitations describe the limits of the machine such as power, torque, velocity and acceleration. The part quality is affected by tool deflection and surface finish. From the basic strength of material beam analysis, the relationship between the cutting force and tool deflection is defined as:

$$\delta = \frac{F\,L^3}{3EI} \tag{2.20}$$

The cutting force F is assumed to be at the end of the tool length L, E is the elastic modulus and I is the moment of inertia which is estimated as

$$I = \frac{\pi\, {D_{eff}}^4}{64} \tag{2.21}$$

where D_{eff} is the effective tool diameter which is equal to 0.8 of the tool diameter, [1].

Another constraint for feedrate optimization is the surface quality estimation. For feedrate values ranging between 0.1 and 1.5 m/min [1], estimated roughness values with respect to the ideal conditions, where the tool runout and tool vibration is not taken into consideration, range between 0.0014 to 0.316 μm. However, in practice, surface roughness values for milling range from 0.2 to 25 μm. This leads to the conclusion that the estimated surface roughness values are negligible in comparison to the practical values. Feedrates are set based on an empirical relationship between the desired surface finish and the feedrate.

Tool health is determined by maximum chip thickness and bending stress. The maximum chip thickness is found by the use of equation (2.22) Excessive values of maximum chip thickness will cause tool breakage and accelerated tool wear.

$$h_{\max} = \frac{f}{N\omega} \tag{2.22}$$

Allowable values for a particular tool – workpiece material combination can be looked up in tables and may also be recommended by cutting tool manufacturers. In addition, if the bending stress experienced by the tool shank is excessive, the tool may also break. The bending stress, from basic strength of materials is defined as:

$$\sigma_b = \frac{F\,L\left(\frac{D}{2}\right)}{I} \tag{2.23}$$

Acceptable values for σ_b depend on the yield strength of the cutting tool.

Feedrate selection is limited by these constraints. Since the tool deflection and bending stress are functions of the cutting force, quantifying the uncertainty in the force model is essential for use in process planning to determine appropriate factors of safety when setting cutting conditions that are both safe and efficient. Factor of safety values obtained from this research can be used to determine a target force value. An iterative algorithm can then be used to find the feedrate corresponding to the constraining force.

2.5 Summary

In Chapter 2, the mechanistic milling force model used in this research is described and the model calibration procedure is explained. The model is calibrated by using the average cutting forces in x and y direction at four different feedrates with constant radial immersion and axial depth. By applying least squares regression to the force and geometry matrices, the model coefficients are obtained.

Constraints for process planning are introduced to select the best possible cutting conditions using a properly calibrated force model. Quantifying the uncertainty of the force model, we can set a Factor of Safety that results in safe and efficient cutting conditions.

CHAPTER 3

EXPERIMENTS AND CALIBRATION RESULTS

3.1 Introduction

Chapter 3 describes the experimental design for this research using four different materials, Aluminum 6061, Steel 1018, Stainless Steel 304 and Titanium Grade 2. Calibration results from tests of identical cutting conditions at specific radial immersion and spindle speed are presented for all of the materials. The calibration results for all different cutting conditions can be seen in Appendix C.

3.2 Experimental Design

Experiments were performed on four different material blocks with three different milling geometries. Blocks of 203mm long and 152mm wide, are machined using coolant and a 12.7mm diameter flat end mill tool with a single Sandvik Coromill 390 insert. Thicknesses of the blocks vary by material. Axial depth of cut for all of the experiments is 3.175mm.

Data from a large number of experiments were collected for the four different materials: Aluminum 6061, Steel 1018, Stainless Steel 304 and Titanium Grade 2. Three different radial depths of cut, four different spindle speeds and four different feed rates were used in the experiments. A lookup table [11] was used to determine the chip thickness and spindle speed range for each material. For each material, radial depth and spindle speed, model coefficients are obtained using measured average forces from the Kistler for the four different average chip thicknesses as shown in the Table 3.1.

Experiment	A	B	C	D
Radial immersion	¼, ½, ¾	¼, ½, ¾	¼, ½, ¾	¼, ½, ¾
Workpiece material	Al 6061	St 1018	StSt 304	Titanium Grd 2
Helix angle (degrees)	12	12	12	12
Workpiece thickness (mm)	50.8	25.4	12.7	12.7
Axial depth (mm)	3.175	3.175	3.175	3.175
h average (mm)	0.0254 0.0508 0.0762 0.1016	0.0254 0.03175 0.0381 0.0508	0.01905 0.0254 0.03175 0.0381	0.0127 0.01905 0.0254 0.0381
Spindle speed (rpm)	2600 3819* 5000 6200	2400 4000* 5600 6400	1600 2400* 3200 4400	1200 1800* 2400 2700
Sandvik Coromill 390 Insert * repeated 14 times	R390-11 T3 08E-NL H13A	R390-11 T3 08M-PM 1025	R390-11 T3 08E-ML 2030	R390-11 T3 08E-ML 2030

Table 3.1: Experimental Design for Model Calibration

Each calibration is performed for all combinations of radial immersions shown in row 1 and spindle speeds shown in row 7 of Table 3.1 using the specific Sandvik insert designated in the bottom row. For each experimental series A, B, C and D, one test for a specific spindle speed is repeated 14 times to quantify the baseline variability when all experimental conditions are identical. All other tests are repeated 3 times. For example, for Al 6061 at a spindle speed of 3819 rpm, the test is repeated 14 times while for 2600, 5000 and 6200 rpm the tests are repeated 3 times. So, for each material a total of 23 tests are performed with a total of 276 experiments (3 different rpm x 4 feed rates x 3 radial depths x 3 repetitions = 108 and 1 rpm x 4 feed rates x 3 radial depths x 14 repetitions = 168, 108+168=276).

3.3 Calibration Results

Force model coefficients for each test are sub-grouped into four categories for each material to look at the variation with respect to changing cutting conditions: 1) Identical cutting conditions (same spindle speed, same radial depth) 2) Only spindle speed changes with the same radial immersion. 3) Only radial immersion changes with same spindle speed. 4) Both spindle speed and radial immersion change. Table 3.2 shows the values of the regression matrices (as defined in Equation 2.10) used to calibrate the coefficients for one of the Aluminum tests at 3819 rpm, ¼ immersion. The calibration results from Table 3.2 are as follows: K_{TC} = 777.04 N/mm^2, K_{TE}=20.18 N/mm, K_{RC}=353.63 N/mm^2 and K_{RE}=24.62 N/mm.

	F (N)		(mm^2)	G (mm)	(mm^2)	(mm)
X1	7.3		0.0101	0.4376	-0.0083	-0.2527
Y1	25.62		0.0083	0.2527	0.0101	0.4376
X2	12.67		0.0202	0.4376	-0.0165	-0.2527
Y2	35.7		0.0165	0.2527	0.0202	0.4376
X3	17.61		0.0303	0.4376	-0.0248	-0.2527
Y3	46.91		0.0248	0.2527	0.0303	0.4376
X4	22.05		0.0404	0.4376	-0.0331	-0.2527
Y4	55.17		0.0331	0.2527	0.0404	0.4376

Table 3.2: Regression Matrices for Aluminum at 3819 rpm, ¼ Immersion.

Tables 3.3, 3.4, 3.5 and 3.6 show the coefficients for Al6061, Steel1018, Stainless Steel304 and Titanium Grade 2 calibrated from 14 identical tests. To form one row of the tables shown below, least squares regression must be applied to the regression matrices with corresponding average forces and geometry matrix, as shown in Table 3.2

	K_{TC} (N/mm^2)	**K_{TE} (N/mm)**	**K_{RC} (N/mm^2)**	**K_{RE} (N/mm)**
	777.04	20.18	353.63	24.62
	744.79	18.77	301.98	24.42
	698.58	18.72	275.31	22.40
	723.52	22.26	300.45	22.68
	756.10	21.68	352.17	20.62
	698.80	24.11	297.89	20.67
	762.76	20.78	345.67	17.79
	722.93	23.15	329.28	19.68
	794.69	20.07	320.94	18.40
	719.46	22.34	283.45	21.16
	730.23	19.89	311.40	22.89
	763.48	19.41	302.10	23.71
	751.56	18.74	317.22	23.94
	737.80	21.69	325.68	19.85
Mean	741.55	20.84	315.51	21.63
Stdev	28.17	1.73	24.17	2.22

Table 3.3: Calibration Results for Aluminum for 14 Identical Tests, 3819 rpm, ¼ Immersion.

	K_{TC} (N/mm²)	K_{TE} (N/mm)	K_{RC} (N/mm²)	K_{RE} (N/mm)
	1906.12	73.37	1061.20	89.85
	1932.10	43.83	992.01	80.23
	1904.16	50.14	1176.02	78.67
	1828.29	52.14	1012.38	82.65
	1809.12	53.62	1055.02	82.65
	1859.03	51.17	991.94	85.55
	1919.67	51.71	1114.39	82.65
	2057.34	47.08	1228.50	76.01
	1940.26	49.18	1070.91	81.33
	1894.17	51.45	1060.35	81.63
	1914.32	50.40	1050.92	80.90
	1776.77	54.69	1069.49	81.85
	1817.07	54.87	1032.56	83.77
	1884.35	50.69	1041.97	82.09
Mean	1890.32	54.07	1069.78	82.69
Stdev	70.14	8.67	65.67	3.78

Table 3.4: Calibration Results for Steel1018 for 14 Identical Tests, 4000 rpm, ¾ Immersion

	K_{TC} (N/mm²)	K_{TE} (N/mm)	K_{RC} (N/mm²)	K_{RE} (N/mm)
	2251.54	42.84	1335.00	64.38
	2898.54	29.54	1926.95	50.22
	2442.88	35.84	1492.65	67.55
	2174.94	47.90	1397.82	72.80
	1942.99	51.80	1021.52	81.35
	2168.16	45.44	1153.37	77.14
	2610.58	38.97	1413.97	70.41
	2714.19	35.03	1836.98	63.96
	2476.94	38.55	1596.72	63.61
	1997.08	53.73	1078.67	93.66
	2109.62	47.96	1260.97	77.53
	2289.47	43.12	1309.22	80.05
	2096.49	52.17	1250.14	86.33
	2622.33	40.11	1466.38	82.36
Mean	2342.55	43.07	1395.74	73.67
Stdev	289.41	7.19	260.45	11.24

Table 3.5: Calibration Results for Stainless Steel 304 for 14 Identical Tests, 2400 rpm, ¼ Immersion

	K_{TC} (N/mm^2)	K_{TE} (N/mm)	K_{RC} (N/mm^2)	K_{RE} (N/mm)
	1819.46	21.71	1038.00	37.47
	1888.45	22.19	1094.47	39.19
	1934.04	19.62	1098.15	34.48
	1859.52	20.21	1097.06	34.60
	1725.02	24.22	994.97	39.56
	1848.56	19.90	1088.03	34.12
	1662.33	24.05	921.95	40.02
	1930.66	21.12	1113.16	37.64
	1880.31	21.13	1124.60	35.83
	2001.84	18.70	1164.69	35.23
	1906.57	19.22	1108.87	36.26
	1862.40	19.34	1026.78	36.48
	1653.06	23.72	1011.60	37.60
	2005.11	17.74	1361.53	29.63
Mean	1855.52	20.92	1088.85	36.29
Stdev	109.78	2.05	100.63	2.70

Table 3.6: Calibration Results for Titanium for 14 Identical Tests, 1800 rpm, ½ Immersion.

It can be seen from the tables that the calibration coefficients for each material have variation when cutting with identical conditions (tests repeated with same spindle speed and same radial immersion). This is considered as random variation and therefore it forms the baseline of the coefficient variation with respect to the changing cutting conditions. It is expected that when spindle speed and/or radial immersion change, the variation of the cutting coefficients will increase. In Chapter 4, the contribution of each changing cutting condition to the force model uncertainty is presented in greater detail.

3.5 Summary

Experimental design for the force model calibrations are shown in this chapter. The experiments are performed on blocks of Aluminum 6061, Steel 1018, Stainless Steel 304 and Titanium Grade 2 with three different cutting geometries (¾, ½ and ¼ immersions) and four different spindle speeds, which vary by material, at four different feedrates. Tests with one spindle speed for all immersions, for each material are repeated 14 times.

Force model coefficients calibrated from the regression matrices are sub-grouped into four categories to look at the variations with respect to changing cutting conditions. The variation in the cutting coefficients is expected to be the smallest when the cutting conditions are identical and they are expected to increase with the changing cutting conditions. Calibration results for the identical cutting conditions for each material are presented.

CHAPTER 4

COEFFICIENT AND FORCE MODEL UNCERTAINTY

4.1 Introduction

In Chapter 4, correlation matrices tables for the four cutting coefficients (K_{TC}, K_{TE}, K_{RC}, and K_{RE}) for all of the materials are presented. Monte Carlo simulation results are presented to explain the effect of changing cutting conditions on the force estimations. For each material, a table of the Factor of Safety (FS) is provided. FS values are derived from the Monte Carlo simulations. In addition, for Steel 1018, tests with 5 new different types of inserts and tools with different material and geometries were conducted by varying radial depth, axial depth and tool radius to observe the change in FS when additional cutting parameters are varied.

4.2 Coefficient Uncertainty

One of the purposes of this study is to quantify the effect of the variability of the force model coefficients. There is always some variation in the cutting coefficients even if the cutting conditions are identical. Furthermore, the cutting coefficients are correlated with each other. Correlation matrices for these coefficients calibrated from identical cutting conditions for Titanium and Stainless steel can be seen in Tables 4.1-4.4.

$Corr(x_1,x_2)$	K_{TC}	K_{TE}	K_{RC}	K_{RE}
K_{TC}	1.00	-0.58	0.52	-0.44
K_{TE}	-0.58	1.00	-0.39	0.45
K_{RC}	0.52	-0.39	1.00	-0.63
K_{RE}	-0.44	0.45	-0.63	1.00

Table 4.1: Correlation Matrix Table of Model Coefficients for Aluminum, ¾ Immersion at 3819 rpm, 14 Cuts Using Identical Cutting Conditions.

$Corr(x_1,x_2)$	K_{TC}	K_{TE}	K_{RC}	K_{RE}
K_{TC}	1.00	-0.27	0.59	-0.47
K_{TE}	-0.27	1.00	-0.10	0.82
K_{RC}	0.59	-0.10	1.00	-0.58
K_{RE}	-0.47	0.82	-0.58	1.00

Table 4.2: Correlation Matrix Table of Model Coefficients for Steel 1018, ¾ Immersion at 4000 rpm, 14 Cuts Using Identical Cutting Conditions.

$Corr(x_1,x_2)$	K_{TC}	K_{TE}	K_{RC}	K_{RE}
K_{TC}	1.00	-0.94	0.92	-0.73
K_{TE}	-0.94	1.00	-0.90	0.85
K_{RC}	0.92	-0.90	1.00	-0.82
K_{RE}	-0.73	0.85	-0.82	1.00

Table 4.3: Correlation Matrix Table of Model Coefficients for Stainless Steel 304, ¼ Immersion at 2400 rpm, 14 Cuts Using Identical Cutting Conditions.

$Corr(x_1,x_2)$	K_{TC}	K_{TE}	K_{RC}	K_{RE}
K_{TC}	1.00	-0.87	0.82	-0.66
K_{TE}	-0.87	1.00	-0.76	0.83
K_{RC}	0.82	-0.76	1.00	-0.84
K_{RE}	-0.66	0.83	-0.84	1.00

Table 4.4: Correlation Matrix Table of Model Coefficients for Titanium Grade 2, ½ Immersion at 1800 rpm, 14 Cuts using Identical Cutting Conditions.

The numbers in the tables show the strength of the correlation between the coefficients. A positive number indicates a positive correlation between two coefficients while a negative number indicates a negative correlation between the variables. For example, K_{TC} –K_{TE} and K_{RC}-K_{RE} in Table 4.1 are inversely correlated, implying that these coefficients exhibit a "see-saw" effect, when one increases the other one decreases. However, K_{TC} - K_{RC} and K_{TE} - K_{RE} are positively correlated. There is also correlation between K_{TC} - K_{RE} and K_{TE} – K_{RC}. Correlation matrices are found from the covariance matrices which are evaluated in MATLAB [12], using the covariance function [13].

$$\mathrm{cov}(x_1,x_2) = E[(x_1-\mu_1)(x_2-\mu_2)] \tag{4.1}$$

where E is the mathematical expectation and μ_i=E(x_i) is the mean value. Equation 4.2 shows the correlation function which is evaluated from the covariance and standard deviations.

$$corr(x_1,x_2) = \frac{\mathrm{cov}(x_1,x_2)}{\sigma_{x_1}\sigma_{x_2}} \tag{4.2}$$

4.3 Force Probability Density Functions from Monte Carlo Simulations

The variation in the cutting coefficients generates a variation in force estimation. However, since there is correlation between the cutting coefficients, it is not possible to add the effect of the variation in them directly to the force estimation. In order to observe the estimated peak force distribution with respect to changing cutting conditions, i.e. radial depth and spindle speed, and/or identical conditions Monte Carlo simulation is run. A program was written in MATLAB using the *mvnrnd* function. By using this function, any number of cutting coefficients can be simulated based on a multivariate normal random distribution. Mean and covariance of the cutting coefficients for each case are utilized in multivariate random normal distributions to simulate any number of cutting coefficients.

In the Monte Carlo simulation, if the force distribution is to be simulated for a cut with identical cutting conditions, e.g. Aluminum 6061 is being cut at 3819 rpm with ¼ immersion, the mean and the covariance matrix of the sample, collected from 14 identical tests, determine the distribution of the cutting coefficients. The Monte Carlo simulation is based on the normal distribution. The force model is then used to calculate the maximum simulated force for the given cut geometry using the maximum chip thickness for the given cutting condition. The mean, standard deviations and covariance of the cutting coefficients of cutting conditions under interest are utilized in the force model. By running a Monte Carlo simulation, any number of cutting tests can be simulated at a particular cutting condition. In this study, 100,000 cutting tests are simulated. The Monte Carlo simulation results showing the force histogram for each of the four materials can be seen in Figures 4.1 to 4.4. The shape of all the histograms indicates a normal distribution that we define as the force PDF. Since there are 48 different cutting conditions for each material, it is impractical to do a force probability distribution analysis for each of them. A total of 4 probability distributions, an example from each material, are demonstrated using the identical test cases where the tests are repeated 14 times.

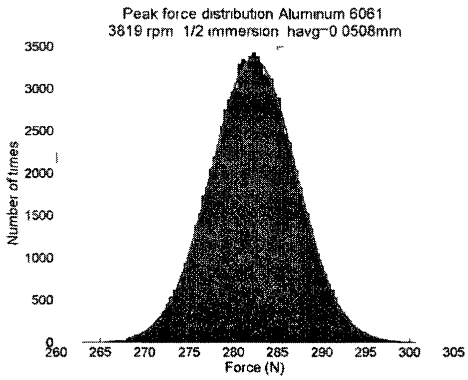

Figure 4.1: Force Histogram for Aluminum 6061

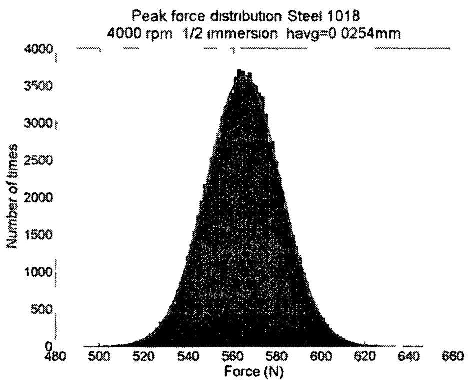

Figure 4.2: Force Histogram for Steel 1018.

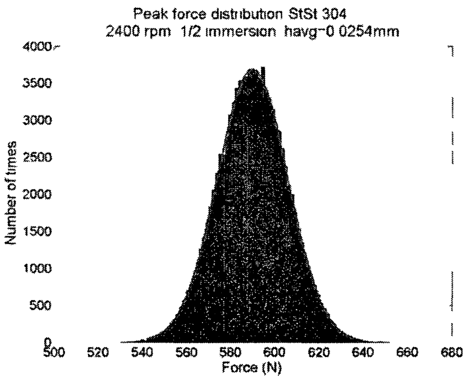

Figure 4.3: Force Histogram for Stainless Steel 304

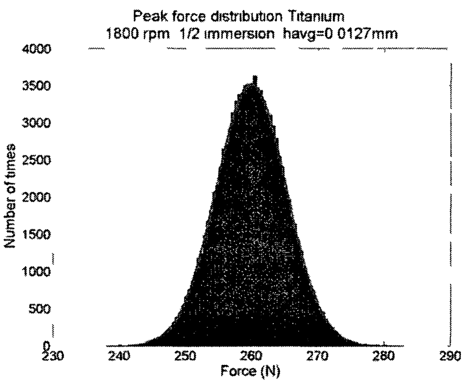

Figure 4.4: Force Histogram for Titanium Grade 2.

After running a Monte Carlo simulation for all four materials, it is possible to determine the peak force variation for different cases. A factor of safety for each case can then be determined by looking at the mean and standard deviation of the peak force probability density function tables. Table 4.5 shows the different cases considered. Row 1 of the table contains the statistics of the cuts with identical cutting conditions where each test is repeated 14 times. Row 2 shows the cases where spindle speeds are different but the radial depths are the same. Row 3 shows the cases where the radial depths are different but the spindle speed is the same. Finally, Row 4 has statistics of all of the cutting conditions, different radial depths and spindle speeds.

3819 rpm ½ immersion h_{avg} = 0.0508 mm	**Mean Peak Resultant Force (N)**	**Standard Deviation (N)**	**Sample size**
1-identical conditions	281.64	5.18	14
2-different spindle speed	279.22	11.52	23
3-different radial depth at 3819 rpm	289.61	8.30	42
4-different radial depth and spindle speed	286.85	16.02	69

Table 4.5. Aluminum 6061 Peak Resultant Force PDF Table

4000 rpm ½ immersion h_{avg}= 0.0254 mm	**Mean Peak Resultant Force (N)**	**Standard Deviation (N)**	**Sample size**
1-identical conditions	564.18	18.21	14
2-different spindle speed	577.76	32.87	23
3-different radial depth at 4000 rpm	563.76	19.44	42
4-different radial depth and spindle speed	577.95	33.57	69

Table 4.6. Steel 1018 Peak Resultant Force PDF Table.

2400 rpm ½ immersion h_{avg} = 0.0254 mm	**Mean Peak Resultant Force (N)**	**Standard Deviation (N)**	**Sample size**
1-identical conditions	589.45	17.11	14
2-different spindle speed	588.95	34.06	23
3-different radial depth at 2400 rpm	593.84	19.33	42
4-different radial depth and spindle speed	595.20	36.39	69

Table 4.7: Stainless Steel 304 Peak Resultant Force PDF Table

1800 rpm ½ immersion h_{avg} = 0.0127 mm	**Mean Peak Resultant Force (N)**	**Standard Deviation (N)**	**Sample size**
1-identical conditions	259.50	5.72	14
2-different spindle speed	263.43	8.93	23
3-different radial depth at 1800 rpm	256.68	11.41	42
4-different radial depth and spindle speed	261.49	12.21	69

Table 4.8: Titanium Grade 2 Peak Resultant Force PDF Table

In Tables 4.5, 4.6, 4.7 and 4.8 the second column shows the mean values of the maximum force based on simulation with 100,000 tests, the third column shows the standard deviation of these forces and fourth column indicates the sample size, i.e. the number of elements in the corresponding coefficients subset.

It can be seen from Tables 4.5, 4.6, 4.7 and 4.8 that the standard deviation is the smallest when the cutting conditions are identical and it is the biggest when cutting conditions (spindle speed and radial depth) are different. This is expected as the variation should be less when the cutting conditions are identical. For aluminum 6061, steel 1018 and stainless steel 304, a comparison of rows 2 and 3 leads to the conclusion that spindle speed causes more variability than radial depth. However, in titanium, radial depth is a more significant source of variation than spindle speed.

By using the mean and standard deviation values for any of the four materials in Tables 4.5 to 4.8 it is possible to determine a process planning factor of safety (FS) using equation 4.3.

$$FS = \frac{(mean + 3 \cdot std)}{mean} \tag{4.3}$$

In process planning, a factor of safety is necessary to ensure that the actual cutting forces will be less than the model estimated forces. This procedure is consistent with standard engineering practice when using any type of simulation model. In this study, we want to be 99.86% confident that the actual cutting forces while machining will be safe.

A Normal probability distribution plot defining the safe and unsafe regions can be seen in Figure 4.5

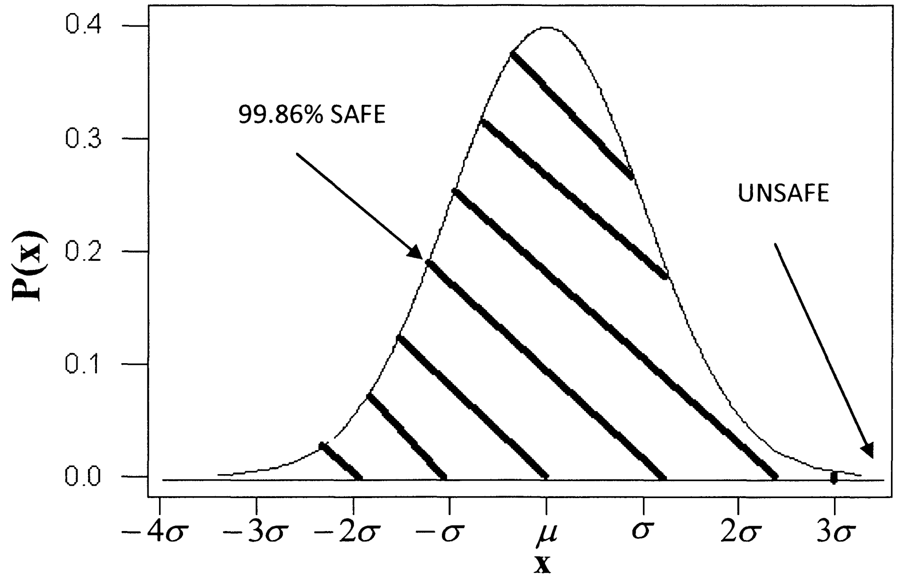

Figure 4.5: Probability Density Function

Table 4.9 is generated by using the mean and standard deviation values of Rows 1 and 4 of Tables 4.5 to 4.8. The first column shows the factor of safety required when the cutting conditions are absolutely identical to the calibration conditions. The second column shows the factor of safety when the radial depth and spindle speed are not identical to the calibration conditions.

Factor of Safety (Resultant Forces)		
	Identical Conditions	**Different RD and spindle speed**
Aluminum 6061	1.06	1.17
Steel 1018	1.10	1.17
Stainless Steel 304	1.09	1.16
Titanium Grade 2	1.07	1.16

Table 4.9: Factor of Safety Table for Resultant Forces.

By looking at Table 4.9, it can be said that for aluminum, if the cutting conditions such as radial depth and spindle speed are not known, then a factor of safety of 1.17 can be set. For example, if the breaking strength of the tool was 500N then the feedrates should be set to values such that the model estimated forces are calculated to be less than 427N (500/1.17). This force level would ensure a 99.86% probability that the actual forces encountered would be less than 500N. Table 4.9 also shows that when cutting conditions are the same, a lower factor of safety may be used.

4.4 Effect of Variation in Cutting Tool Type

When there is additional variation in the cutting parameters like tool geometry, tool material and axial depth, the FS is expected to change. To observe how much FS changes when additional machining parameters are added, new sets of experiments were conducted. These new sets of experiments were performed on Steel 1018 with the following 5 different inserts and tools of different geometry: Sandvik 08M-PL, Kennametal KC725M and Kennametal KC935M inserts as well as conventional coated and uncoated solid carbide tools of 30 degree helix angle. The geometry of Sandvik 08M-PL and Kennametal inserts is similar but the tool material is different. The tests were performed at 2400 and 4000 rpm; at ¼ and ¾ immersions; at tool radii of 12.7mm and 25.4mm and at axial depths of 3.175mm and 1.905mm. 16 tests were conducted for each cutter using the factorial experiment design table, Table 4.10, which can be seen below.

RD	RPM	Tool radius	Axial depth
1	1	1	1
2	1	1	1
1	2	1	1
1	1	2	1
1	1	1	2
1	1	2	2
1	2	2	1
2	2	1	1
2	1	1	2
2	1	2	1
1	2	1	2
1	2	2	2
2	2	2	1
2	2	1	2
2	1	2	2
2	2	2	2

Table 4.10: Orthogonal array for each tool

The levels for the variables of RPM, radial depth, tool radius and axial depth are described in the Table 4.11 below.

RPM	1	2400 rpm
	2	4000 rpm
RD	1	1/4 immersion
	2	3/4 immersion
Tool radius	1	12.7mm
	2	25.4mm
Axial depth	1	3.175mm
	2	1.905mm

Table 4.11: Levels for the variables in the experiments

The tests described above are conducted to calibrate the model coefficients, K_{TC}, K_{TE}, K_{RC} and K_{RE}. The values of the calibrated model coefficients can be seen in Appendix C. Monte Carlo simulation is then run in the same manner used to generate Table 4.9. Table 4.12 shows the mean and the standard deviation values of the distribution for the inserts as well as the conventional tools to obtain the Factor of Safety Table shown in Table 4.13.

4000 rpm ½ immersion h_{avg} = 0.0254 mm	**Mean Peak Resultant Force (N)**	**Standard Deviation (N)**	**Sample size**
(Inserts) Sandvik 08M-PM + Sandvik 08M-PL + KC725M + KC935M	572.38	67.83	117
Inserts+ Coated Carbide + Uncoated Carbide	545.70	92.09	149

Table 4.12: Insert and Conventional Tools Peak Resultant Force PDF Table.

The FS value in the second column in Table 4.13 is identical to Table 4.9, corresponding to the baseline tests. However, the other columns represent the FS resulting from the variation in different cutter types as well as different tool geometry, tool radius and axial depth. The third column of Table 4.13 shows the FS value of the inserts combined together, i.e. the coefficients from the Sandvik 08M-PM insert are combined with the coefficients from the tests conducted with Sandvik 08M-PL, KC725M and KC935M and a Monte Carlo simulation is run. The simulation results for this case can be seen in the first row of Table 4.12. Fourth column in Table 4.13 shows the FS value resulting from the combination of the inserts and the conventional solid carbide cutters (coated and uncoated) of 30 degree helix angle. Mean and standard deviation for this case can be seen in the second row of Table 4.12.

Factor of Safety (Resultant Forces)			
	Sandvik 08M-PM	**(Inserts) Sandvik 08M-PM + Sandvik 08M-PL + KC725M + KC935M**	**Inserts+ Coated Carbide + Uncoated Carbide**
Steel 1018 Different RD and spindle speed	1.17	1.36	1.5

Table 4.13: Factor of Safety Table for Resultant Forces.

It is observed from Table 4.12 that, when additional parameters are added, the FS increases. When the cutting coefficients from 4 types of inserts that exhibit slight change in tool geometry are combined with different axial depths and radiuses to estimate the peak resultant forces, the FS increases to 1.36. In addition, when the coefficients calibrated from the inserts and the conventional coated and uncoated solid carbide tools (exhibiting major change in tool geometry) are combined to estimate the peak resultant force distribution, the FS increases to 1.5.

4.5 Summary

In this chapter, correlation matrices for each material are presented. These tables show how strongly the model coefficients are correlated. K_{TC} –K_{TE} and K_{RC}-K_{RE} are inversely correlated, exhibiting the "see-saw" effect. However, K_{TC} - K_{RC} and K_{TE} - K_{RE} are positively correlated. There are also correlations between K_{TC} - K_{RE} and K_{TE} – K_{RC}. Since there is such a strong correlation between the coefficients, it is not possible to add the effect of variation in the coefficients to the force estimation. Thus Monte Carlo simulation is needed to observe the variations in the force estimations.

Monte Carlo simulation is run by creating 100,000 sets of force model coefficients with a statistical distribution that depends on the cutting conditions (identical conditions, only spindle speed changes etc) used when performing the model calibration. The mean, standard deviation and correlation matrix of the coefficients for the cutting test sub-groups described in Chapter 3 are utilized in a multivariate normal distribution. Then, the linear force model is run 100,000 times to yield a force probability distribution. This process is repeated for the four different cases (sub-groups) under consideration: 1) Identical conditions. 2) Different spindle speed with same radial depth. 3) Different radial depth with same spindle speed. 4) Different spindle speed and radial depth. The results from the simulations indicate that for Aluminum 6061, Steel 1018 and Stainless Steel 304 spindle speed is a more significant source of model coefficient variation than radial depth. However, in Titanium Grade 2, radial depth causes more variation than spindle speed. In addition to that, as expected, when cutting conditions are identical, the variation in the resultant forces is the smallest. On the contrary, when the sample includes the coefficients from all types of test conditions, the variation becomes larger.

Results for Steel 1018 indicate that to ensure safe and efficient cutting, the cutting conditions should be set such that the model estimated forces are 17% less than the maximum allowable forces. This procedure will ensure that the actual cutting forces will be less than a force which could either break the tool or deflect too much with a probability of 99.86%.

What happens when a cutting tool is used that has not undergone a calibration procedure to determine accurate cutting coefficients? To answer this question tests were conducted with different geometry, coating, axial and radial depths. It is observed that the required FS increases when these additional variations are introduced. Results from tests conducted with different types of inserts and conventional tools of different geometries at different tool radii, and axial depth show that when different types of inserts are used, the FS increases from 1.17 to 1.36. In addition, if the tests also include conventional coated and uncoated solid carbide tools, whose tool geometries are significantly different than the inserts, the FS increases from 1.36 to 1.5. These tests provide two valuable pieces of information: 1. Process planners must include a FS if they are using coefficients from a general table that doesn't include information about the cutting tool used in the calibration test. 2. Productivity can be significantly improved by getting calibration information from tests that are as close to the actual machining conditions as possible. This conclusion provides a good rationale for the value of on-line calibration performed while cutting a production part. In this way the calibration coefficients can be used with a FS between 1.1 and 1.2 as evidenced by Table 4.9

CHAPTER 5

EXPERIMENTAL VALIDATION

5.1 Introduction

This chapter compares experimentally measured forces to the probability distributions predicted by the Monte Carlo simulation method. Monte Carlo simulations are extended over a full range of chip thickness, in an attempt to generalize the factor of safety found for one chip thickness value. The changing cutting conditions case (changing radial depth and spindle speed) are used in the simulation for each material. Experimental resultant peak forces are compared with the results of the Monte Carlo simulated upper and lower force intervals.

A case study is performed using Steel 1018 with two different methods in order to experimentally validate the FS values generated by Monte Carlo simulations. In the first method, the cutting conditions are known and the force is simulated to get the mean peak target force. The target force is then multiplied by the Factor of Safety (FS) obtained from Monte Carlo simulations to determine the critical force level. Experimental forces, using the same cutting conditions, are obtained from the Kistler and compared with the simulated force. In the second method, the critical force is calculated based on the tool deflection constraints. This critical force is then divided by FS to get the target force. The feedrates are optimized to match the target force. Experimental cuts are performed at the optimized set feedrates and the measured forces are compared with the calculated force.

If the method is working correctly, the measured forces will be less than the target force with a 99.86% probability.

5.2 Methodology and Results

Experimental work is performed to verify the Monte Carlo simulation results in two ways. The first goal is to generalize the factor of safety values found for one chip thickness from the Monte Carlo simulation results in Chapter 4 over a full range of chip thicknesses. The second goal is to observe if the actual peak resultant forces during machining stay within the confidence levels set by the Monte Carlo simulations.

The calibration of the coefficients for all of the experimental tests is based on the average x and y force values. To compare simulation peak force results to experimental peak forces, the mean, standard deviation and the correlation of the coefficients are used to find force PDFs for the four different values of h_{avg} shown in Table 3.1 for each material. At each average chip thickness, h_{avg}, there are three sets of peak force values for three different radial immersions. The calibration tests are designed to have the same average chip thickness but peak forces are a function of peak chip thickness, h_{max}. Therefore, different radial depths result in different maximum chip thicknesses. Thus, for each set of forces shown in Figures 5.1-5.4 at the same chip thickness, the leftmost group is at ¾ immersion, the middle group is at ½ immersion and the rightmost group is at ¼ immersion (see Figure 5.1).

The number of test repetitions from Table 3.1 is limited to three at each spindle speed for each material instead of including all 14 repetitions at one spindle speed as it is desired to eliminate a possible bias towards that one spindle speed. In addition, all three types of radial immersions are included. Therefore, the total number of experimental conditions for each material is 4x4x3x3 (spindle speed x chip thickness x radial immersion x repetition) = 144. Monte Carlo simulations are run for all average chip thicknesses specified in Table 3.1 at a given radial immersion and spindle speed. Tables 5.1-5.4 show the mean, standard deviation and coefficient of variation, which is the ratio of standard deviation to the mean, obtained from the simulation. It should be noted that the coefficient of variation does not vary significantly with chip thickness. This observation is important and means that a single FS should work over the full range of chip thickness.

The mean and standard deviation values shown in Tables 5.1-5.4 can also be used to generate confidence limits which are graphically shown in Figures 5.1-5.4. Upper and lower confidence levels of 99.86% and 95% are formed by adding and subtracting 3σ and 2σ to the mean value. The experimentally measured resultant peak forces are shown on the graphs, indicating that the measured forces fall within the predicted confidence limits. The Kistler dynamometer used to measure forces has a natural frequency of around 950Hz and the data is filtered with a low pass Butterworth filter at 500Hz.

Al6061 **3819 rpm** **½ immersion**	**Mean (N)**	**Std. (N)**	**Cv**
1) h_{avg} = 0.0254mm different conditions	185.17	15.37	.083
2) h_{avg} = 0.0508 mm different conditions	283.56	22.80	.080
3) h_{avg} = 0.0762 mm different conditions	383.96	30.70	.080
4) h_{avg} = 0.1016 mm different conditions	482.79	39.05	.081

Table 5.1: Aluminum Peak Resultant Force PDF Table for Different Conditions, Case 4 of Table 4.5 for all h_{avg}, Sample Size = 36, Monte Carlo Simulation

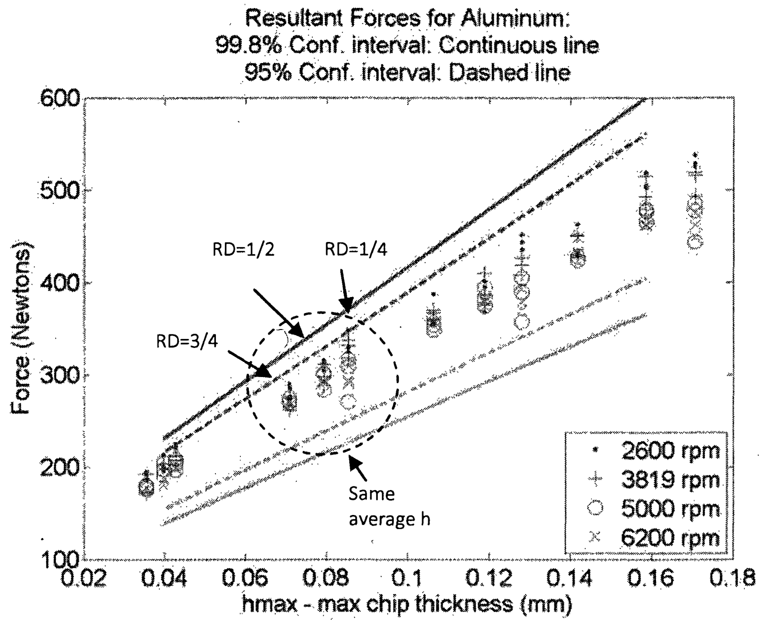

Figure 5.1: Experimental Resultant Forces Compared to the Monte Carlo Simulation Intervals for Aluminum.

Steel 1018 4000 rpm ½ immersion	**Mean (N)**	**Std. (N)**	**Cv**
1) h_{avg} = 0.0254mm different conditions	582.73	42.02	.072
2) h_{avg} = 0.03175 mm different conditions	647.03	43.59	.067
3) h_{avg} = 0.0381 mm different conditions	711.92	46.40	.065
4) h_{avg} = 0.0508 mm different conditions	841.92	54.89	.065

Table 5.2: Steel 1018 Peak Resultant Force PDF Table for Different Conditions, Case 4 of Table 4.6 for all $h_{avg,}$ Sample Size = 36, Monte Carlo Simulation

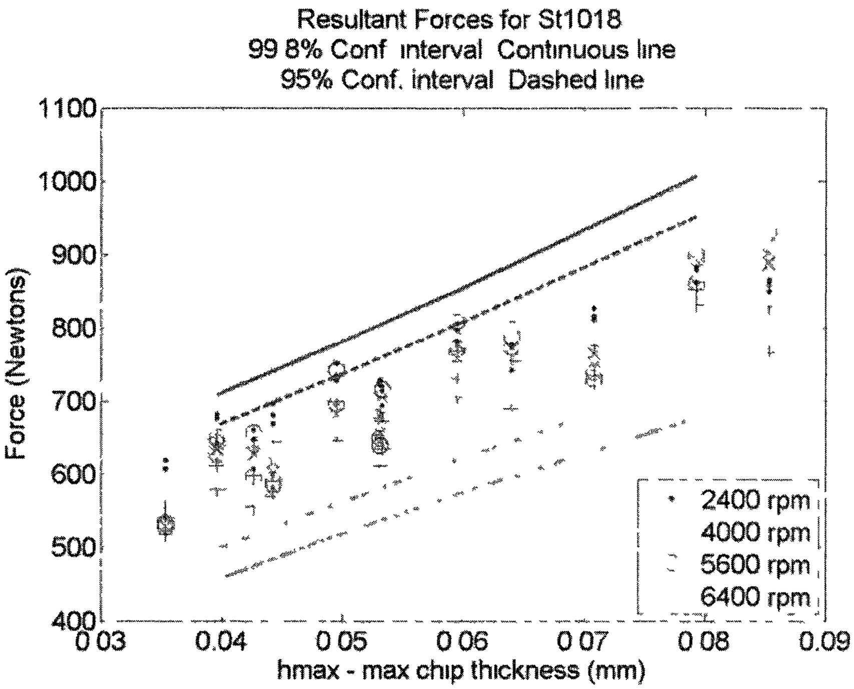

Figure 5.2: Experimental Resultant Forces Compared to the Monte Carlo Simulation Intervals for Steel 1018.

StSt 304 **2400 rpm** **½ immersion**	**Mean (N)**	**Std. (N)**	**Cv**
1) h_{avg} = 0 01905 mm different conditions	500 66	38.29	.076
2) h_{avg} = 0.0254 mm different conditions	647.03	43.52	073
3) h_{avg} = 0.03175 mm different conditions	711.92	50.16	073
4) h_{avg} = 0.0381 mm different conditions	770.45	58.34	076

Table 5.3: Stainless Steel 304 Peak Resultant Force PDF Table for Different Conditions, Case 4 of Table 4.7 for all h_{avg}, Sample Size = 36, Monte Carlo Simulation

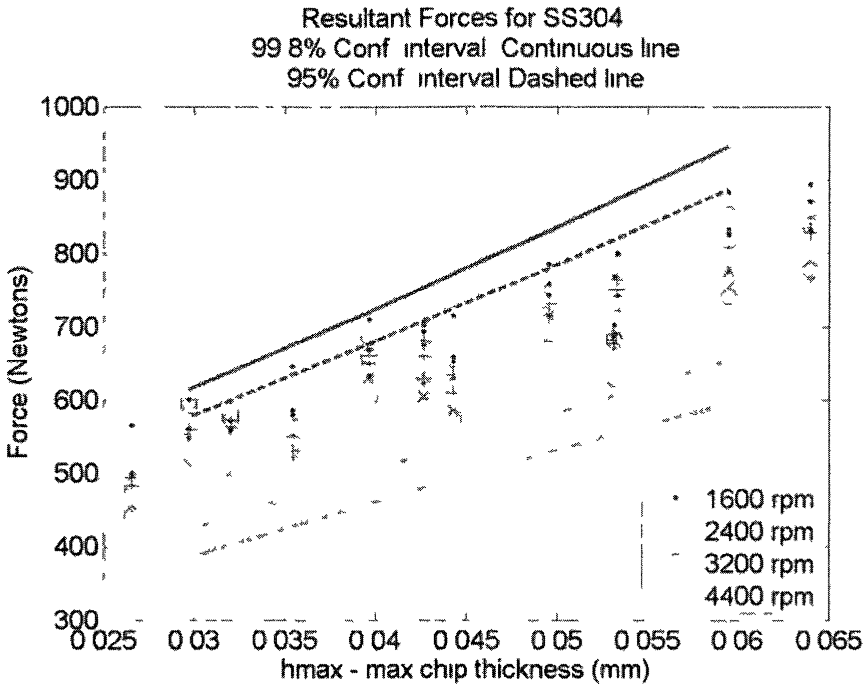

Figure 5.3: Experimental Resultant Forces Compared to the Monte Carlo Simulation Intervals for Stainless 304.

Titanium **1800 rpm** **½ immersion**	**Mean (N)**	**Std. (N)**	**Cv**
1) h_{avg} = 0 0127 mm different conditions	259 61	15 21	058
2) h_{avg} = 0 01905 mm different conditions	325 97	16 15	050
3) h_{avg} = 0 0254 mm different conditions	392 81	18 54	047
4) h_{avg} = 0 0381 mm different conditions	527 08	26 23	050

Table 5.4: Titanium Peak Resultant Force PDF Table for Different Conditions, Case 4 of Table 4.8 for all h_{avg}, Sample Size = 36, Monte Carlo Simulation

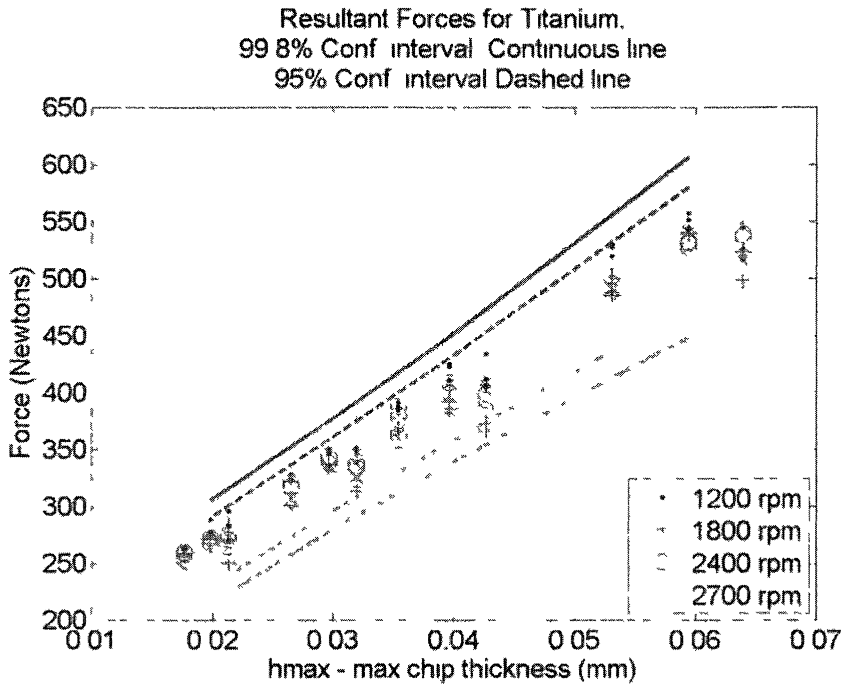

Figure 5.4: Experimental Resultant Forces Compared to the Monte Carlo Simulation Intervals for Titanium Grade 2.

Figures 5.1 to 5.4 show that the experimentally measured forces fall within the confidence intervals created by Monte Carlo simulation.

5.3 Case Study

A case study was performed to verify the FS values generated by Monte Carlo simulations for the cutting conditions that are different than the tests done to determine FS.

A Steel 1018 block underwent both up and down milling, using a three flute insert cutter with a 25.4 mm diameter, with four different radial immersions (slot, three quarters, half and quarter), four different spindle speeds (3000 rpm, 3500 rpm, 4000 rpm and 4500 rpm) and an axial depth of 2.54 mm. The cutting forces are simulated by two different methods: 1) Spindle speed, immersion and h_{avg} are known. A feedrate is calculated based on the spindle speed and h_{avg}. Then, the force is simulated based on this information including the effects of runout. The simulated force is multiplied by the FS to determine the force level not to be exceeded. Then, experimental resultant peak forces are plotted against the simulated and critical force levels. 2) The tolerance specified in [1] is used to calculate the critical force level. A target force is obtained by dividing the critical force level by the FS. The simulation program is then utilized in an iterative manner to determine the experimental feedrates. The experimental resultant peak forces are plotted against the predetermined critical and target force levels.

5.3.1 Method1: Known feedrate-calculated force

For a given cutting condition, a critical force not to be exceeded is determined as follows: e.g. for a half immersion cut at 3000 rpm, and a specified average chip thickness (h_{avg}) of 0.03175 mm, the feedrate is calculated and the resultant peak force is determined from the simulation, including runout with a magnitude of 0.01016 mm and locating angle of 145 degrees. The runout magnitude is measured with the tool in the FADAL 3 axis CNC milling machine using a dial indicator. The locating angle for the tool is estimated to match the profile shape of the measured force. The simulated resultant peak force is multiplied with a FS value for steel 1018 obtained from the Monte Carlo simulations (Table 4.9). Experiments are then run at the calculated feedrates. Experimental feedrates for method 1 can be seen in Table 5.5.

	G E O M E T R Y (up and down mill)			
RPM	**SLOT**	**¾ immersion**	**½ immersion**	**¼ immersion**
3000	448.84	398.98	448.84	598.47
3500	523.67	465.48	523.67	698.22
4000	598.47	531.97	598.47	797.96
4500	673.27	598.47	673.27	897.71

Table 5.5 – Feedrate table (mm/min) for Case Study, method 1: Fixed h_{avg}

The experiments are set such that the observed average chip thickness, h_{avg}, is the same for all of the cuts. But since the peak resultant forces depend on the maximum chip thickness, h_{max}, force levels vary with different radial immersions. Up milling and down milling case study results for a total of 32 tests can be seen in Figure 5.5 and Figure 5.6 respectively. The experimental peak resultant force magnitudes for down and up milling cases for case study one can be seen in Appendix C.

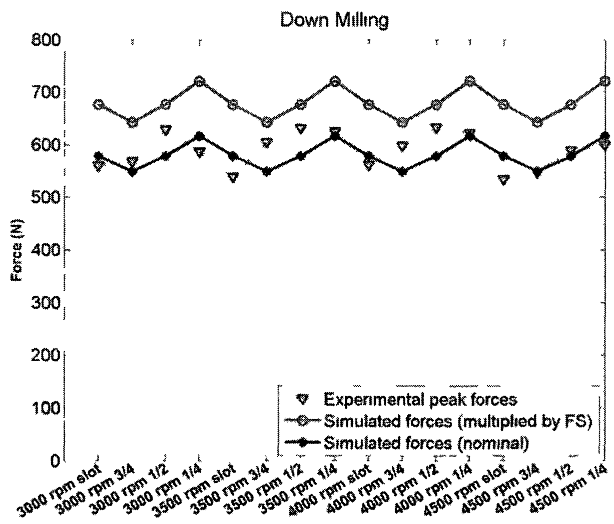

Figure 5.5: Case study Method 1 – Downmill results. Critical force level is the simulated peak resultant force multiplied by the factor of safety

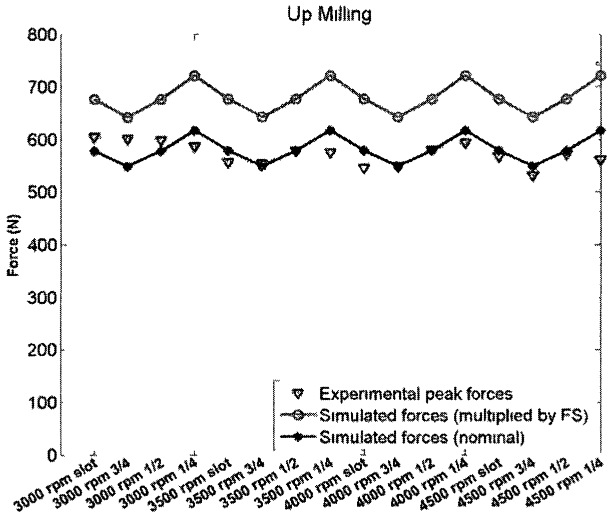

Figure 5.6: Case study Method 1 – Upmill results. Critical force level is the simulated peak resultant force multiplied by the factor of safety

The results from Figure 5.5 and Figure 5.6 show that experimental forces lie below the critical force level which is determined by using a FS obtained from the Monte Carlo simulations (Table 4.9). It is shown that the forces experienced by the tool during cutting will be less than the predicted forces with a probability of 99.86 %, under a variety of cutting conditions. It can also be noted that for downmilling, the variation in the experimental forces tend to be larger than in upmilling. Note that the model estimated forces are the same for both Up and Down milling since the model doesn't discriminate between the two cases.

5 3 2 Method 2 Known force-calculated feedrate

For this method, a critical force level not to be exceeded is determined by using the constraint equations for tool deflection and maximum bending stress (Eq 2.20 and Eq 2.22) [4]. The smallest force result out of the two constraint equations is used to get the target force which is then used in the force simulation to determine the feedrates by iteration. In this case study, the tool deflection formula yields a smaller force value and therefore tool deflection becomes the constraint for the process planning.

Calculation of the constraint force from tool deflection is now described. First, various tool parameters are given: Modulus of elasticity for cemented tungsten carbide is 675.10^3 MPa, Effective diameter of the tool is 20.32mm, tool length is 38.1mm and allowable tool deflection of 0.00152mm. Using this information in Eq. 2.20, the target force from the allowable deflection is calculated as 468 N. The allowable force from bending stress is calculated from Eq. 2.22 to be 3580 N based on a stress of 207 MPa and a tool diameter of 25.4mm. Since the force from deflection is smaller than the force from bending stress, it becomes the constraint for the process planning.

The calculated maximum allowable force from tool deflection is divided by a FS value of 1.17 for Steel 1018 (Table 4.9) to get the target force. Dividing 468 N by 1.17 gives 400 N as the target force by which to set the feedrates. The feedrates for the given cut geometries are determined by iterating the feedrate in the simulation program until the target peak force is obtained. The simulation includes tool runout of 0.01016 mm with a locating angle of 145 degrees. The experimental feedrates for method 2 can be seen in Table 5.6. Simulated and experimental forces for method 2 with up and down milling geometries can be seen in Figures 5.7 and 5.8 respectively.

	G E O M E T R Y (up and down mill)			
RPM	**SLOT**	**¾ immersion**	**½ immersion**	**¼ immersion**
3000	146.05	146.05	146.05	170.18
3500	170.18	170.18	170.18	198.12
4000	195.58	195.58	195.58	223.52
4500	218.44	218.44	218.44	254

Table 5.6: Feedrate table (mm/min) for Case Study, method 2: Fixed forces

The experiments for this method are designed such that the experimental resultant peak forces for all types of immersion yield the same peak force values. Since it requires a higher feedrate for ¼ immersion than the other 3 types of immersion to get the same target peak force, the feedrates are slightly higher for ¼ immersion than the other immersions for a specific cutting speed. The experimental peak resultant force magnitudes for down and up milling cases for this case study can be seen in Appendix C.

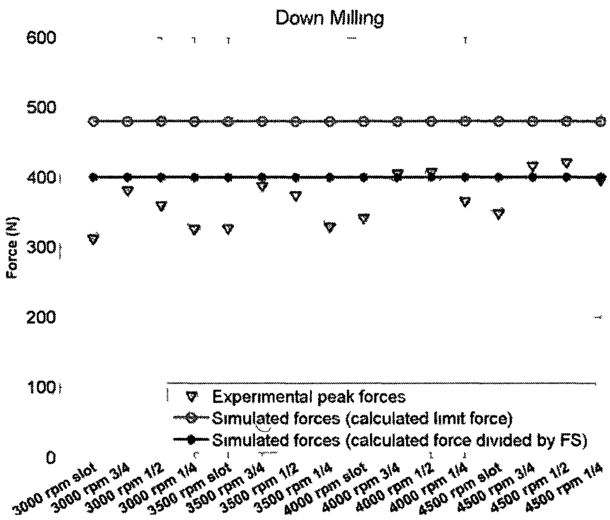

Figure 5.7: Case study Method 2 – Downmill results

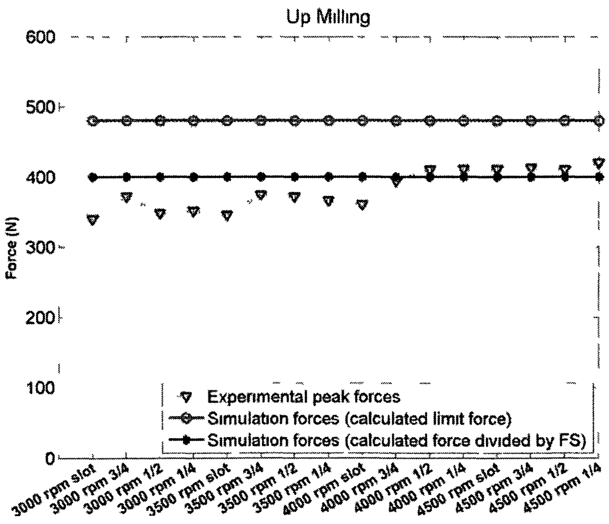

Figure 5.8: Case study Method 2 – Upmill results

Figures 5.7 and 5.8 indicate that the experimental peak forces remain in the safe zone for all of the test cases, below the critical force level corresponding to a 99.86% confidence level. It is again notable that the variation of the experimental forces in downmilling is larger than the variation in upmilling.

5.4 Summary

In chapter 5, experimental validation of the Monte Carlo simulations are performed. For each of the four materials, Monte Carlo simulations are run for a full range of chip thicknesses at ½ immersion. 95% and 99.86% confidence intervals are formed by adding 2 σ and 3 σ to the Monte Carlo simulation mean. The resultant peak forces from the tests include three repetitions with all types of immersions and spindle speeds, for a total number of 144 cases for each material. The tests fall within the confidence intervals created by Monte Carlo simulation.

A case study is also performed on a Steel 1018 block to verify the FS values generated by Monte Carlo simulations. In the first method, a peak force level is calculated from known cutting condition (known spindle speed, radial depth, chip thickness, feedrate and axial depth). That force level is then multiplied by the FS (1.17) to calculate the critical force level. We expect 99.86% of the measured forces to be below the critical force level. The results confirm that the measured peak forces do fall below the critical threshold.

In the second method, a constraint equation for tool deflection is used to get the maximum allowable force for a desired tolerance. The maximum allowable force is then divided by the FS for Steel 1018, 1.17 (as opposed to multiplying in method 1). Feedrates for the given cutting conditions are found iteratively in the simulation program. The experimental peak resultant forces all fall within the maximum allowable force line. This verifies that the FS obtained from Monte Carlo simulations can be used to enable safe and efficient cutting with 99.86% confidence, which is vital in process planning.

CHAPTER 6

RATIO ASSIGNMENT BETWEEN THE TANGENTIAL AND THE RADIAL COEFFICIENTS

6.1 Introduction

This chapter describes the effect of eliminating the need for the radial coefficient calibration by assigning a ratio of the radial coefficients to the tangential coefficients on the force probability density functions.

The Kistler dynamometer is a useful instrument for calibrating the tangential and the radial coefficients. However, due to its invasive nature and high cost, it is not practical to use the force dynamometer in industrial applications. In contrast, the power sensor made by Load Control Incorporated (LCI) [14] is an inexpensive and non-invasive instrument. Unfortunately, the power sensor is only capable of finding the tangential coefficients. It is worth investigating whether it is possible to calibrate the tangential coefficients with a power sensor and then use a ratio of radial to tangential coefficients to determine the radial coefficients. Maximum allowable force estimations for process planning could be performed based on these coefficients and a corresponding FS.

6.2 Coefficient Ratios

To assign a ratio between the tangential and radial coefficients, the calibration results from the calibration tests shown in shown in Appendix C, i.e. 69 coefficients for each material, have to be used. The mean and the variance of the two ratios (K_{RC}/K_{TC} and K_{RE}/K_{TE}) for 69 sets of coefficients can be seen in Table 6.1. To account for the ratio variation, the mean and the variance of these two ratios for each material are utilized in a multivariate normal random distribution to obtain 100,000 ratios in MATLAB. These randomly created ratios are multiplied with 100,000 tangential coefficients obtained from the multivariate normal distribution, to estimate the radial coefficients. Monte Carlo simulation is then run to see the effect of assigning ratios between the tangential and the radial coefficients on the force probability density functions, thus on the FS. The coefficients for all of the cutting conditions for each material can be seen in Appendix C.

	Mean K_{RC}/K_{TC}	**Mean K_{RE}/K_{TE}**	**Var K_{RC}/K_{TC}**	**Var K_{RE}/K_{TE}**
Al 6061	0.398	1.188	0.001	0.041
St1018	0.556	1.564	0.005	0.024
StSt 304	0.584	1.955	0.004	0.077
Titanium2	0.612	1.768	0.004	0.022

Table 6.1 – Mean and variance table of K_{RC}/K_{TC} and K_{RE}/K_{TE} for each material using calibration results from Appendix C

The values in Table 6.1 indicate that the variation in the cutting coefficients is less than the variation in the edge coefficients. In addition, the mean ratios of the cutting and edge constants are different for each material.

After running the Monte Carlo simulation using the calibrated tangential coefficients and the estimated radial coefficients, it is possible to obtain F.S values for each material. Table 6.2 shows the effect on the FS when using the ratio method instead of calibrating all four coefficients with the Kistler force data.

		CALIBRATED COEFFICIENTS METHOD	RATIO METHOD
ALUMINUM	**Mean (N)**	287.4	288.12
	Std (N)	17.05	17.41
	F.S	1.17	1.19
ST1018	**Mean (N)**	580.21	582.73
	Std (N)	33.66	47.91
	F.S	1.17	1.26
STST304	**Mean (N)**	593.41	596.1
	Std (N)	33.24	35.71
	F.S	1.16	1.21
TITANIUM 2	**Mean (N)**	260.3	260.4
	Std (N)	13.89	15.95
	F.S	1.16	1.19

Table 6.2 – Factor of safety tables for Calibrated Coefficients method and the Ratio method for different cutting conditions, 69 conditions

Results from Table 6.2 show that if the radial coefficients are assumed to be a fixed ratio of the tangential coefficients, the FS for Aluminum increases from 1.17 to 1.19. The required FS for ST1018, STST304 and Titanium 2 increase by 9%, 5% and 3% respectively.

These results indicate that estimating the radial coefficients from the calibrated tangential coefficients with a ratio uncertainty slightly skews the force distribution. However, these results may prove useful in process planning as it eliminates the need for an expensive and invasive force dynamometer at the expense of setting the cutting conditions (feedrate/spindle speed) slightly more conservative.

To have an idea about the accuracy of the force estimates obtained from both the calibrated coefficients method and the radial coefficients method, the standard error between the model estimates and the experimental forces is found for each material. In Table 6.3 the standard error values for both ratio and calibrated coefficients method for each material can be seen.

	STANDARD ERROR TABLE	
	CALIBRATED COEFFICIENTS (N)	**RATIO METHOD (N)**
ALUMINUM	21.37	21.53
ST1018	49.09	46.50
STST304	42.26	46.05
TITANIUM 2	24.88	21.35

Table 6.3 Standard Error Table comparing the calibrated coefficients method and the ratio method to experimental forces for all of the materials

The values in Table 6.3 are obtained by utilizing a perfect linear fit (slope=1 and intercept=0) to the experimental peak resultant forces and model estimated resultant forces. Then, using equation 6.1, the standard error of the estimates can be obtained,

$$s_{est} = \sqrt{\frac{\sum (y - y')^2}{n-2}} \tag{6.1}$$

where, y denotes the model predicted forces, y' is the estimates from the regression line and n is the number of samples.

In Table 6.3, it can be seen that in terms of standard error, there is no significant difference between the two methods. Figures 6.1-6.4 show the experimental peak resultant forces vs. model predicted peak resultant forces for each material for the ratio method.

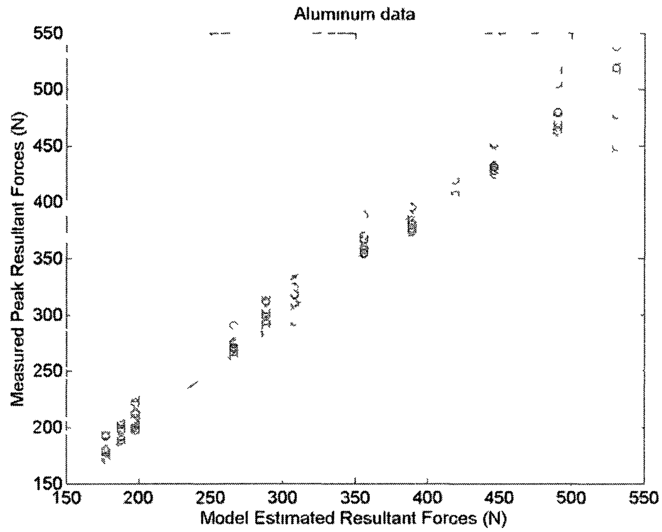

Figure 6.1 – Ratio Model Estimated vs. Measured Forces for Aluminum

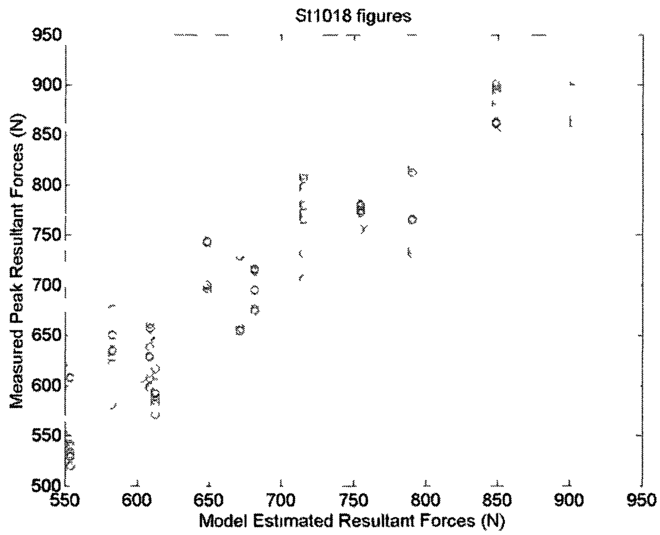

Figure 6.2 – Ratio Model Estimated vs. Measured Forces for Steel1018

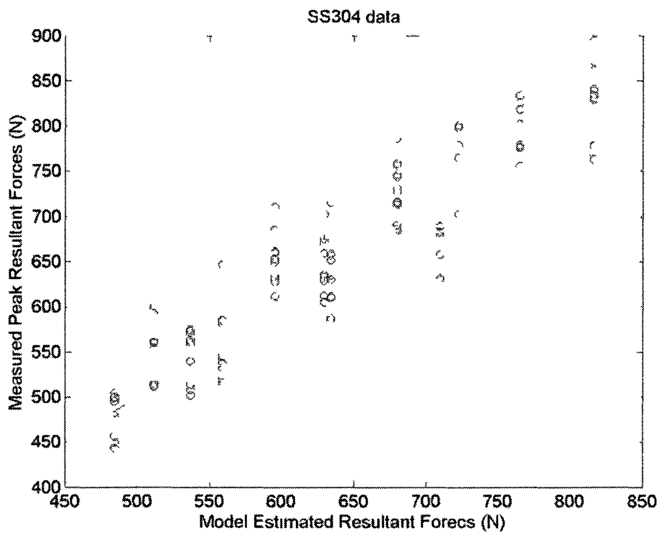

Figure 6.3 – Ratio Model Estimated vs. Measured Forces for SS304

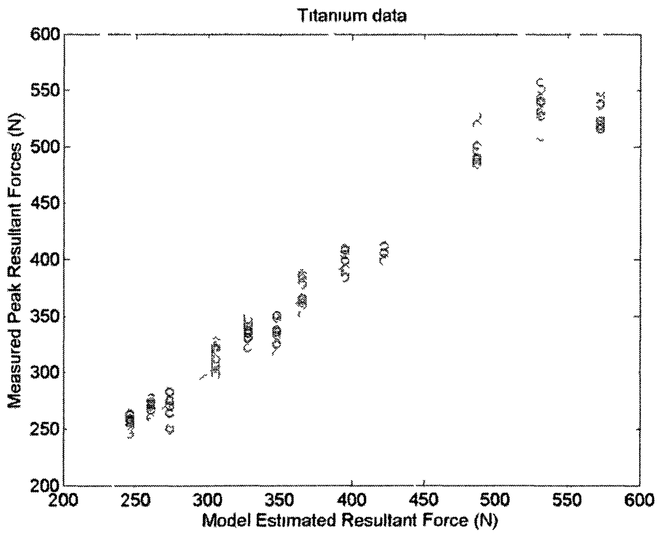

Figure 6.4 – Ratio Model Estimated vs. Measured Forces for Titanium 2

It can be seen from Figures 6.1-6.4 that the variation in the experimental peak resultant forces is less in Aluminum and Titanium. The variation increases in Steel1018 and SS304. This observation verifies the standard error values shown in Table 6.3. The experimental and simulated forces can be seen in Appendix C.

6.3 Summary

In this chapter the effect of estimating the radial coefficients on the force probability density functions is investigated. The radial coefficients are estimated by first getting the ratio statistics of K_{RC}/K_{TC} and K_{RE}/K_{TE}, i.e. the mean and the variance, of the calibrated tangential and radial coefficients. The mean and the variance of the coefficient ratios for each material are utilized in a multivariate normal random distribution and then multiplied with the tangential coefficients. Monte Carlo simulation is run with the calibrated tangential coefficients and the estimated radial coefficients to obtain a FS. For Aluminum the increase in FS is the minimal, from 1.17 to 1.19. For Steel 1018, the increase is the most significant, going from 1.17 to 1.26. For Stainless Steel 304, the FS increases from 1.16 to 1.21 and finally for Titanium Grade 2, FS increases from 1.16 to 1.19. These results show that estimating the radial coefficients increases FS slightly, meaning that cutting conditions become slightly more conservative than the case where a force dynamometer is used to determine FS. This is an important observation in process planning as a power sensor may be sufficient to estimate the resultant forces to set reasonable but more conservative cutting conditions.

In addition, it has been observed that there is no significant difference between the two methods, the ratio method and the calibrated coefficients method, in terms of the model accuracy. When the estimated forces are compared to the experimental forces, it was found that the standard error values associated with two methods are close to each other.

CHAPTER 7

CONCLUSIONS AND FUTURE WORK

7.1 Introduction

This chapter summarizes the thesis work and outlines the conclusions. Suggestions for future studies are also included.

7.2 Conclusions

The milling force model used in this study is calibrated by using the average cutting forces in the x and y direction. Constraints for the process planning are introduced to select the best possible cutting conditions using a properly calibrated force model. Quantifying the uncertainty of the force model resulted in a Factor of Safety that can be used to set safe cutting conditions.

The experiments for this research are performed on blocks of Aluminum 6061, Steel 1018, Stainless Steel 304 and Titanium Grade 2 with three different cutting geometries (¾, ½ and ¼ immersions), four different spindle speeds, and four different feedrates. At one of the spindle speeds the tests are repeated 14 times for each radial immersion. Force model coefficients calibrated from the regression matrices are sub-grouped into four categories to look at the variations with respect to changing cutting conditions: 1)Identical conditions 2) Spindle speed changes 3) Radial immersion changes 4) Spindle speed and radial immersion change

The calibrated model coefficients, K_{TC}, K_{TE}, K_{RC} and K_{RE} correlation matrices are obtained. The cutting force coefficients, C terms, and edge constants, E terms, are negatively correlated, exhibiting see-saw effect. Since there is correlation between the coefficients, it is not possible to add the effect of variation in the coefficients to the force estimation. Thus, Monte Carlo simulation is used to observe the variations in the force estimations. The results from the simulations indicate that for Aluminum 6061, Steel 1018 and Stainless Steel 304 spindle speed is a more significant source of variation in the peak resultant forces than the radial depth. However, in Titanium Grade 2, radial depth causes more variation than spindle speed. When cutting conditions are identical, the variation in the resultant forces is the smallest. On the contrary, when the sample includes the coefficients from all types of test conditions, the variation becomes larger.

The Monte Carlo results for Steel 1018 indicate that for safe and efficient cutting, process conditions (feedrate, spindle speed) should be set using the peak force estimates 18% less than the critical peak resultant forces. To ensure 99.86% confidence that the actual forces during machining will be less than the maximum allowable force based on tool failure or part deflection, a factor of safety value is needed. Results from the tests conducted with different types of inserts and conventional tools of different geometries at different tool radii, and axial depth show that when different types of inserts are used, the FS increases from 1.17 to 1.36. In addition, when the tests with conventional coated and uncoated solid carbide tools are combined with the inserts, FS increases from 1.36 to 1.5. Feedrates during the process planning should use the particular FS that is based on the difference between the planned cutting conditions and the cutting conditions used for calibration.

Experimental validation for the Monte Carlo simulations shows that a single FS should work over a full range of chip thicknesses. In addition, the actual resultant peak forces stay within the confidence intervals generated by the Monte Carlo simulations. Two types of case studies performed also show that the FS generated by the Monte Carlo simulations is valid and the measured peak forces for both down and upmilling fall below the critical threshold. This verifies that the FS obtained from Monte Carlo simulations can be used to enable safe and efficient cutting with 99.86% confidence, which is vital in process planning.

The Monte Carlo simulation results show that assigning a ratio between the tangential and the radial coefficients increases the peak resultant force variation to a small extent, leading to a small increase in FS for each material. Thus, in process planning the cutting conditions (feedrate, spindle speed) will be set slightly more conservative than the case when full coefficient calibration is utilized to obtain a FS. Since use of the coefficient ratio has little effect on the FS, the non-invasive power sensor can be used directly in process planning by calibrating only the tangential coefficients and assigning a ratio to estimate the radial coefficients.

7.3 Future Work

A reliable library of cutting coefficients is essential for process planning using cutting force models. There are many more combinations of materials, tools and cutting conditions that need to be tested before such a library could be completed. This study may be expanded to consider the effects of coolant, tool diameter and different tool shapes like helix angle, rake angle, relief angle and most importantly – tool wear. Cutting forces can increase by more than 100% due to tool wear [7]. As additional factors are introduced, the certainty is decreased and a greater factor of safety must be introduced. It might be preferable to use a system which continuously monitors coefficients [6, 7] as the part is being cut rather than relying on generic values for cutting coefficients.

In addition, it may be of interest to do the same analysis using the instantaneous tangential and radial forces in place of the average x and y forces. This requires a coordinate transformation of the dynamometer's instantaneous x and y forces. The reasons why the model coefficient calibrations from the Kistler dynamometer and LCI power sensor vary need further investigation.

This research demonstrates the need for "smart machining" sensors and systems. Sensors and models can only be combined effectively if models are calibrated continuously to ensure accurate model coefficients. A wireless "smart tool", such as [15] is currently being developed in the UNH research lab, would be of great value in the realization of such a system.

The underlying assumption in this study is that, the cutting coefficients are normally distributed. Observation of 36 sets of coefficients, from tests of 3 repetitions, shows that the coefficients are not normally distributed. However, 36 samples are not enough to draw a conclusion about the distribution of the coefficients. Thus, a larger sample, i.e. n>100, is needed to come to a conclusion about the distribution of the coefficients. The histogram plots showing the normality of the cutting coefficients can be seen in Appendix E. Also, the regression process creates a "see-saw" effect between the cutting coefficients. The data should be centered to eliminate this effect.

The radial immersion and the spindle speed create a systematic shift in the peak experimental forces which will not be observed in a normal distribution. The reasons for this should be investigated further. In addition, better models should be made and an outlier elimination procedure should be developed to extract the outliers from the data.

REFERENCES

[1] Jerard RB, Fussell BK, Xu M, Yalcin, C, (2006) "Process Simulation and Feedrate Selection for Three-axis Sculptured Surface Machining", *International Journal of Manufacturing Research*, 1(2), 136-156.

[2] Altintas, Y, 2000, *Manufacturing Automation: metal cutting mechanics, machine tool vibrations, and CNC design*, Cambridge University Press, ISBN 0-521-65973-6.

[3] Xu, M, Robert B Jerard, Barry K Fussell, (2007), "Energy Based Cutting Force Model Calibration for Milling", *Computer-Aided Design*, Vol. 4, Nos. 1-4, p 341-351.

[4] Yalcin, C, BK Fussell and RB Jerard (2007), "Comparison of Tangential Force Models for Feedrate Selection in Milling", Proceedings of the 2007 International Manufacturing Science And Engineering Conference, MSEC2007, October 15-17, Atlanta, Georgia, USA

[5] Budak E, Y Altintas and EJA Armarego (1996), "Prediction of Milling Force Coefficients from Orthogonal Cutting Data", *Journal of Manufacturing Science and Engineering*, May 1996, Volume 118, Issue 2, 216.

[6] Schuyler CK, M Xu, RB Jerard and BK Fussell, (2006) "Cutting power model-sensor integration for a smart machining system," *Transactions of the North American Manufacturing Research Conference,* Volume 34, NAMRC 34, Marquette University, May 23- 26.

[7] Yanjun Cui, BK Fussell, RB Jerard and DM Esterling (2009), "Tool Wear Monitoring For Milling By Tracking Cutting Force Model Coefficients", *Proceedings of the North American Manufacturing Research Conference*, May 19-22, 2009.

[8] Kurdi, M.H, Schmitz T. L, Haftka, R.T (2008), "Milling optimisation of removal rate and accuracy with uncertainty: part 2: parameter variation", *International Journal of Materials and Product Technology* 2009_Vol35, No:1/2 pp 26-46

[9] Zapata R, Traverso M, Abbas A, and Schmitz T, (2008), "Bayesian Updating of Stability Beliefs", Proceedings of American Society for Precision Engineering Annual Meeting, October 19-24, Portland, OR

[10] Ivester RW, L Deshayes and M McGlauflin, (2006) ,"Determination of Parametric Uncertainties for Regression- Based Modeling of Turning Operations", *Transactions of the North American Manufacturing Research Conference*, Volume 34, NAMRC 34, pp. 1-8, Marquette University, May23-26.

[11] *Machining Data Handbook 3rd Edition Vol. 1,* Machinability Data Center, Institute of Advanced Manufacturing Sciences, Inc.

[12] The MathWorks, Inc , R2007b, Natick, MA. www.mathworks.com, April 12, 2011

[13] Johnson, R. A. (2005) *Miller and Freund's Probability and Statistics for Engineers* Upper Saddle River, NJ: Pearson Prentice Hall

[14] Load Controls Incorporated, Universal Power Cell, Sturbridge, MA, www.loadcontrols.com, April 12, 2011

[15] Suprock, C. A., Nichols, J. S. (2009), "A Low Cost Wireless High Bandwidth Transmitter for Sensor-Integrated Metal Cutting Tools and Process Monitoring", *International Journal of Mechatronics and Manufacturing Systems 2009* - Vol. 2, No.4 pp. 441 - 454

APPENDIX A

EXPERIMENTS AND DATA ACQUISITION USER GUIDE

Introduction

This appendix includes the user guide to perform the experiments and data acquisition in order to replicate the results obtained from the tests performed for this research.

Experiments and Data Acquisition

To calibrate the cutting coefficients of a force model, a series of experiments must be performed. The experiments in this study utilized four different types of materials: aluminum 6061, steel 1018, stainless steel 304 and titanium grade 2. Cutting geometries of quarter immersion, half immersion and three quarters immersion with four different chip thicknesses and an axial depth of 0.125" were used in all of the four materials. Cutting blocks of these four different materials were mounted on the Kistler load cell. The surface of the cutting blocks must be flat. So, a clean cut with a small axial depth, about 0.01", must be done first. Then, a slot cut in y-offset direction must be created with an axial depth greater than the axial depth in the g-code. After that, tool and fixture offsets (x and y) must be set. To set the tool offset, the tool must be brought down to the top of the workpiece carefully with hand wheel knob. X fixture offset is set by bringing the tool to the left part of the workpiece and Y fixture offset is set by bringing the tool to the part where the slot cut was done. See **Figure A.1**.

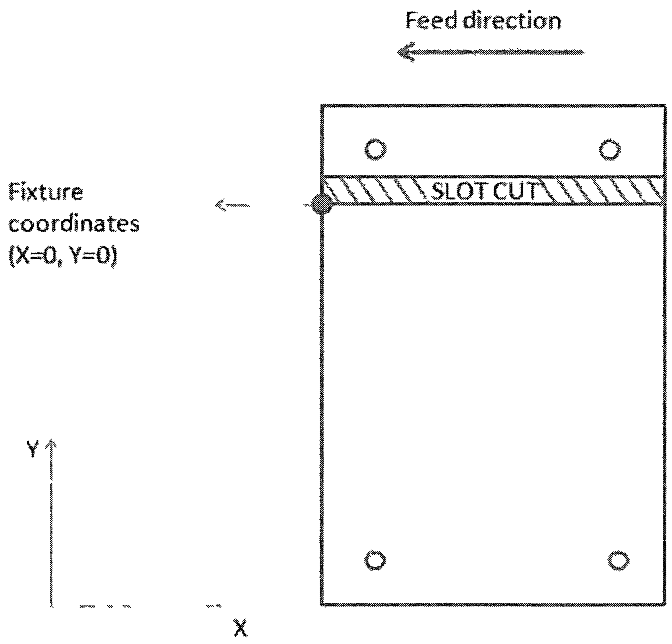

Figure A.1- Overhead view of block setup as used for test cuts

After setting the workpiece properly, the G-code written for the test must be loaded to the OpenCNC program part. In this research, G-codes were written so that cutting specifics are; down milling, ¼, ½ and ¾ immersions, a constant axial depth of 0.125" and with four different feedrates, depending on the material ,in order to apply a least squares fit to calibrate the force model. A typical cutting pass includes a single immersion at an axial depth of 0.125" and four different feedrates.

Predator (Vulcan Craft Performance) software is used for data acquisition. The experimenter can specify the sampling rate and number of sampling revolutions in the setup dialog box in the software, which can be seen in **Figure A.2**.

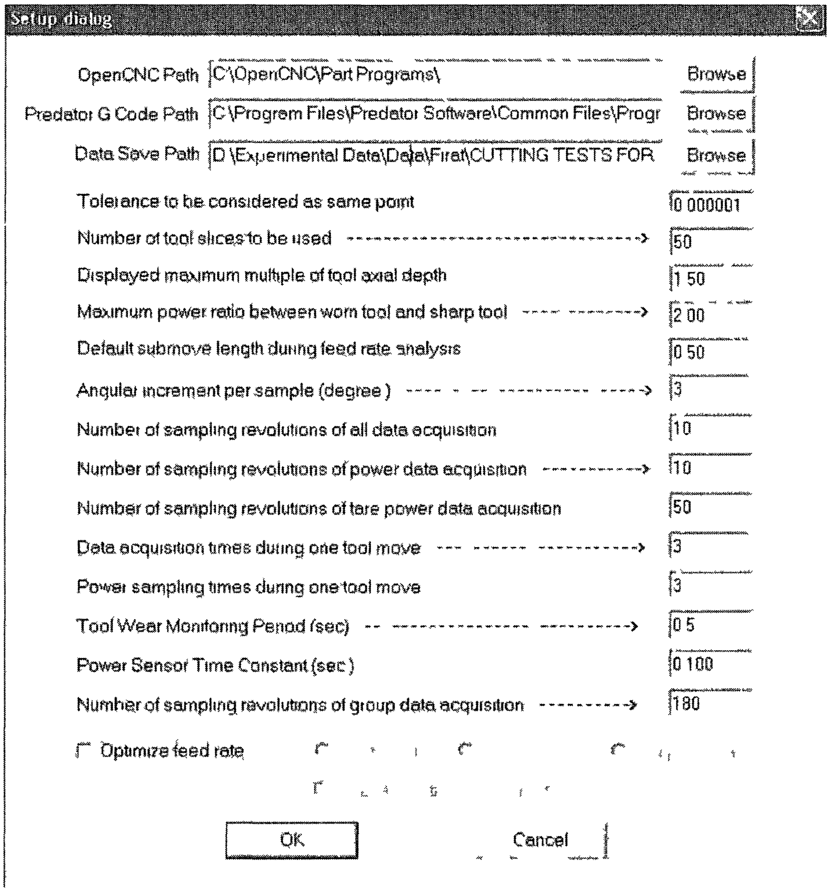

Figure A.2 – Data acquisition Setup Dialog

After setting the sampling parameters in the software, the user should switch to the MDSI window to set EOBBlock (End of Block) on so that the g-codes line will be executed line by line. That is necessary as the Predator software requires sampling of tare power of the spindle motor before starting to collect data. So, the spindle should be allowed to rotate and the tare power should be sampled until a somewhat constant value is reached. After observing that the tare power has a constant reading, EOBBlock should be switched to off and then the program is ready to run. All of the cutting data, force and power data, obtained from the cutting test will be stored into the folder specified in the dialog box. A sample G code for the experiments performed can be seen below.

A Sample G Code for the cutting tests

```
N1 (CALIBRATIONG-CODESETFOR10REVOLUTIONS)
N2 (SAN_0.500)
N3 (FLUTE=1HELIX=0.0)
N4 (TOOLMATERIAL=CARBIDE)
N5 (WORKPIECEMATERIAL=ALUMINUM)
N6 G17G20G40G90
N7 T1M6
N8 H1M42E1
N9 M3S4990M8
N10 (1/4IMMERSIONDOWNMILLSIDECUT)
N20 G0X-1Y0.125Z2.0
N30 G1Z-0.125F50
N40 G1X0.5F5
N50 G1X1.5F10.472
N60 G1X2.5F20.944
N70 G1X4.0F31.416
N80 G1X5.0F41.888
N90 G1X7.0F12
N100 G1Z2.0F50
N110 (1/2IMMERSIONDOWNMILLSIDECUT)
N120 G0X-1.0Y-0.125Z2.0
N130 G1Z-0.125F50
N140 G1X0.5F5
N150 G1X1.5F7.854
N160 G1X2.5F15.708
N170 G1X4.0F23.562
N180 G1X5.0F31.416
N190 G1X7.0F12
N200 G1Z2.0F50
N210 (3/4IMMERSIONDOWNMILLSIDECUT)
N220 G0X-1.0Y-0.5Z2.0
N230 G1Z-0.125F50
N240 G1X0.5F5
N250 G1X1.5F6.981
N260 G1X2.5F13.963
N270 G1X4.0F20.944
N280 G1X5.0F27.925
N290 G1X7.0F12
N300 G1Z2.0F50
N317 M5M9H0E0
N322 M41
N327 G0Z0
N332 G0X0Y0
N337 M30
```

APPENDIX B

USER GUIDE FOR DATA PROCESSING AND PROGRAMS

Introduction

This appendix introduces the methods for data processing and lists the MATLAB programs written for the automation of the force model coefficient calibration process and Monte Carlo simulations

Data Processing and Matlab Programs

The force model introduced by Altintas in [1] suggests the use of average x and y forces in order to calibrate the four cutting coefficients, K_{TC}, K_{TE}, K_{RC} and K_{RE}. In order to do that, average x and y forces should be processed and then calibrated by a least squares fit.

Several MATLAB m-files were written for data acquisition purposes. First program is *main_Altintas_KrKt_feed.m*. In this program the user has to enter the name of the .lst extension file, which is stored in the folder created after the cutting test is completed. This file contains the geometric information of the cut like axial, radial depths, contact area rate for each G- code line as well as the feedrates, RPM information. The file's format is like the following: "G-Code name-NewMoveInfo". That file must be added to the working directory in MATLAB. *main_Altintas_KrKt_feed.m* program runs the *automate2.m* program which gets the average x and y forces. The user should enter the name of the file in which the cutting data is stored in ".xlsx" format in *automate2.m*. Also, that file should be in the working directory.

Depending on the sampling rate and sampling revolutions, necessary changes should be made in the program (lines 12, 16, 20, 21), i.e. if the user sets the angular increment per sample to 2 and the number of sampling revolutions of all data acquisition to 10, then 360/2 * 10 = 1800 lines of data will be in the excel spreadsheet for each g-code line, if the user sets the angular increment per sample to 3 and number of sampling revolutions of all data acquisition to 10, then 360/3 * 10 = 1200 lines of data will be in the excel spreadsheet for each g-code line.

After the average x and y forces are calculated, *main_Altintas_KrKt_feed.m* program applies least squares on the data to obtain the four cutting coefficients. These cutting coefficients are written in a different excel spreadsheet specified in the program in order to use them for the Monte Carlo simulation analysis.

Monte Carlo simulation is used to get a force probability distribution which will help to find the factor of safety. To get the force distribution, *montecarlo.m* file should be run. This program runs *peaks_monte.m* program, which uses the coefficients to determine the angle at which the maximum force occurs. The user should specify the RPM used in the cut and the average chip thickness. The maximum chip thickness giving the maximum force can be calculated and used in *montecarlo.m* program to find the distribution of the maximum forces utilizing a normal distribution. Thus; it is possible to determine a factor of safety for force by looking at the mean and standard deviation of the distribution.

List of programs

MATLAB m-file to calculate the average x and y forces

```
% Program to automate the procedure to find average x and y forces
  collected out of Kistler dynamometer to an excel spreadsheet.
  It processes 4 lines, starting from the input line and next three
lines
  Important: excel work book must be converted from xls--> xlsx
% Save 1st file in the matlab workspace directory to get the feedrate
info      from that file
% by Firat Eren on August 1, 2009
% Design and Manufacturing Lab. University of New Hampshire

function [F] = automate2()
clc
clear
global x
[a b c]=xlsread('Al 3819-1.xlsx');
x=[50;150;250];

for r=1:3
    j=1;
    for y=x(r):10:x(r)+30
        k=int2str(y);
        for i=1:18
        t=b(2+1201*(i-1),2); % 1200 will change according to the
sampling                                  % rate
        f=cell2mat(t);          Program is set to get 10 rotations and
sample                                  % at every degrees so there will be
360/3 * 10
        z=findstr(f,k);         lines for each g-code line

          if(size(z)>0)
             row = 2+1201*(i-1);
            break
          end
        end
  Fx_cell=c(row+1:row+1200,2);     1200 will change according to the
        Fy_cell=c(row+1:row+1200,3);  % sampling rate
        Fxt=cell2mat(Fx_cell);
        Fyt=cell2mat(Fy_cell);
Fx_avg=mean(Fxt)*4.44822162;  % unit conversion from pounds to
Fy_avg=mean(Fyt)*4.44822162;  % newtons
        Fx(j,r)=Fx_avg;
        Fy(j,r)=Fy_avg;
        j=j+1;
    end
end
g=1;
for v=1:3

F(1:4,g:g+1)=[Fx(:,v) Fy(:,v)];
g=g+2;
end
```

MATLAB m-file to calibrate the cutting coefficients K_{TC}, K_{TE}, K_{RC} and K_{RE}

```
  Program to estimate both cutting coefficient pairs Kts and Krs
- using the Altintas' equations on page 46
  Firat Eren on 12 Nov 2009
  updated on March 11 2010, gets 4 coefficient for all three radial
  immersions and writes them into an excel file
  [f]=fpt(spindle speed, no of teeth, feed1, feed2, feed3, feed4)
' important: save 1st file in the matlab workspace directory to get the
  feedrate info from that file

clear
N=1;   number of teeth
a=in_mm(0.125);  % axial depth for Yanjun's steel cut
F= automate2();   changed to automate_scan, was automate()

info = xlsread('c:\Users\firateren\Documents\MATLAB\confidence radial
coefs\First tests\Aluminum\aluminum 3819-1-NewMoveInfo.xlsx','a1:n19');
feedinfo=[info(2:5,14) info(8:11,14) info(14:17,14)];
rpm=3819;
exit=180*pi/180 ;
k=1;
for j=1:3
   Calculation of feed per tooth and entry angles
    if j==1
        enter=120*pi/180 ;

      f=fpt(rpm,1,feedinfo(1,1),feedinfo(2,1),feedinfo(3,1),feedinfo(4,
      1));

          elseif j==2
              enter=90*pi/180;

      f=fpt(rpm,1,feedinfo(1,2),feedinfo(2,2),feedinfo(3,2),feedinfo(4,
      2));

          elseif j==3
              enter=60*pi/180;

      f=fpt(rpm,1,feedinfo(1,3),feedinfo(2,3),feedinfo(3,3),feedinfo(4,
      3));
          end

    Fx=F(:,k);
    Fy=F(:,k+1);
    k=k+2;
    A1x=zeros(4,1);
    A2x=zeros(4,1);
    A3x=zeros(4,1);
    A4x=zeros(4,1);
    A1y=zeros(4,1);
    A2y=zeros(4,1);
    A3y=zeros(4,1);
    A4y=zeros(4,1);
    Bx=zeros(4,1);
    By=zeros(4,1);
```

```
     for i=1:4
        A1x(i)= N*a*f(i)/(8*pi)*(cos(2*exit) - cos(2*enter));
        A2x(i)= (-(N*a)/(2*pi))*(sin(exit) - sin(enter));
              A3x(i)=-N*a*f(i)/(8*pi)*(2*exit-2*enter-
      sin(2*exit)+sin(2*enter));
        A4x(i)=N*a/(2*pi)*(cos(exit)-cos(enter));
        Bx(i)= Fx(i);

              A1y(i)=N*a*f(i)/(8*pi)*(2*exit-2*enter-
      sin(2*exit)+sin(2*enter));
        A2y(i)=-N*a/(2*pi)*(cos(exit)-cos(enter));
        A3y(i)=N*a*f(i)/(8*pi)*(cos(2*exit)-cos(2*enter));
        A4y(i)=-N*a/(2*pi)*(sin(exit)-sin(enter));
        By(i)=Fy(i);
    end

    M=[A1x(1) A2x(1) A3x(1) A4x(1);A1y(1) A2y(1) A3y(1) A4y(1);
    A1x(2) A2x(2) A3x(2) A4x(2);A1y(2) A2y(2) A3y(2) A4y(2);
    A1x(3) A2x(3) A3x(3) A4x(3);A1y(3) A2y(3) A3y(3) A4y(3);
    A1x(4) A2x(4) A3x(4) A4x(4);A1y(4) A2y(4) A3y(4) A4y(4)];
    Bg=[Bx(1);By(1);Bx(2);By(2);Bx(3);By(3);Bx(4);By(4)];
    K(1:4,1)=inv(M'*M)*M'*Bg ;
end

% REST OF THE CODE IS FOR WRITING COEFFICIENTS INTO AN EXCEL
SPREADSHEET
col={'quarter 1mm','half 1mm','three quarters'};
sp={'';'';'';''};
Ks={'Ktc'; 'Kte'; 'Krc'; 'Kre'};
xlswrite('coefficients of Aluminum.xlsx',col,'d2:f2');
data=xlsread('coefficients of Aluminum.xlsx');

if size(data)==0
   data=zeros(3);
end

if max(size(data))==3
    for i=max(size(data))-2:max(size(data))+1
    a1{i,1}=sprintf('%c', 'D' + i-1 );
    b1{i,1}=num2str(i+2);
    c1{i,1}=sprintf('%c', 'B' + i-1 );
    d1{i,1}=sprintf('%c', 'A' + i-1 );
    w1{i,1}=int2str(max(size(data))-2);
    end

else
    for i=1:4
    a1{i,1}=sprintf('%c', 'D' + i-1 );
    b1{i,1}=num2str(max(size(data))+i+3);
    c1{i,1}=sprintf('%c', 'B' + i-1 );
    d1{i,1}=sprintf('%c', 'A' + i-1 );
    w1{i,1}=int2str((max(size(data))+1)/5 +1);

    end
```

```
end
    t=sprintf('%c','A' -7);
    h(1)=strcat(a1(1),b1(1)) ;
    h(2)=strcat(a1(3),b1(4));
    g(1)=strcat(c1(1),b1(1));
    g(2)=strcat(c1(1),b1(4));

    r=int2str(rpm);
    p=char(strcat(d1(1),b1(1)));
    p1=char(strcat(p,t,p));

    k=char(strcat(h(1),t,h(2)));
    l=char(strcat(g(1),t,g(2)));

    e=sprintf('%c','A' -20);
    m=char(strcat(r,e));
    y{1}=char(strcat(m,w1(1)));

xlswrite('coefficients of Aluminum.xlsx',Ks,l);
xlswrite('coefficients of Aluminum.xlsx',y,p1);
xlswrite('coefficients of Aluminum.xlsz',K,k);
```

MATLAB m-file to find the chip thickness at which the maximum force occurs

```
% program to get the angle and chip thickness at which the force is
maximum
% written by Jeff Nichols
% modified by Firat Eren

clear;clc
close all
run outlier_tang % get the tangential coefficients and extract outliers
run outlier_rad  the radial coefficients and extract outliers

exy=Mt; % Mt is from outlier_tang (tangential coefficients)
RPM=1800; %spindle speed -------------------- may be changed 2313
originally
N = 1; % number of teeth
Fs=RPM*3;

feed1=2.827;
RPS=RPM/60;
SPR=round(Fs/RPS); %samples per revolution    .
alpha_helix =12 * pi / 180; % helix angle in radians 12
R = 6.35; % radius of cutter in mm ------R and a may be changed 9.525
originally
a = in_mm(0.125); % axial depth in mm---2.54 originally
radial=R/2; %radial immersion ---------------for  slot cutting it was
2*R
fpt=fpt1(RPM,N,feed1);
phi = linspace(0, 2*pi, SPR);
%
NXY=length(exy);  % comment out unless you find nominal (find min max)
Ktc1=exy(:,1);Kte1=exy(:,2);% comment out unless you find nominal (find
% min max)
%% add radial components into play
Krc1=Mr(:,1);Kre1=Mr(:,2);
rho = 0.00; beta = 0;runout = rho * exp(i*beta);
phi_st = pi-acos((R-radial)/R);
phi_ex = pi;F_xn1=[];F_xx1=[];F_xen1=[];F_yn1=[];F_yx1=[];F_yen1=[];
F_hypotmn=[];F_hypotmx1=[];F_hypoten1=[]; %last three added by firat

for ij=1:NXY;  %% comment out unless you find nominal (find min max)
    K1=[Ktc1(ij),Kte1(ij);Krc1(ij),Kre1(ij)];% comment out unless you
find nominal (find min max)
%      K1=[Ktc1, Kte1 ; Krc1, Kre1] % comment in when you find nominal
    [F1,T1,X1] = getcoefficients(phi, N, 100, a, K1, alpha_helix, R,
runout, phi_st, phi_ex);
    [F_x,F_y,F_hypot] = getforces2(F1,phi,fpt);
    F_xx1=[F_xx1;max(F_x)];
    F_yx1=[F_yx1;max(F_y)];
    F_hypotmx1=[F_hypotmx1;max(F_hypot)];

      end
      F_xmin=min(F_xx1);
      Ktc_xmin=Ktc1(find(F_xx1==F_xmin));
Kte_xmin=Kte1(find(F_xx1==F_xmin));
F_xmax=max(F_xx1);
```

```
Ktc_xmax=Ktc1(find(F_xx1==F_xmax));
Kte_xmax=Kte1(find(F_xx1==F_xmax));
F_ymin=min(F_yx1);
Ktc_ymin=Ktc1(find(F_yx1==F_ymin));
Kte_ymin=Kte1(find(F_yx1==F_ymin));
F_ymax=max(F_yx1);
Ktc_ymax=Ktc1(find(F_yx1==F_ymax));
Kte_ymax=Kte1(find(F_yx1==F_ymax));
F_rmin=min(F_hypotmx1);
Ktc_hmin=Ktc1(find(F_hypotmx1==F_rmin)) ;
Kte_hmin=Kte1(find(F_hypotmx1==F_rmin));
F_rmax=max(F_hypotmx1);
Ktc_hmax=Ktc1(find(F_hypotmx1==F_rmax));
Kte_hmax=Kte1(find(F_hypotmx1==F_rmax));

F_xmin=min(F_xx1);
Krc_xmin=Krc1(find(F_xx1==F_xmin));
Kre_xmin=Kre1(find(F_xx1==F_xmin));
F_xmax=max(F_xx1);
Krc_xmax=Krc1(find(F_xx1==F_xmax));
Kre_xmax=Kre1(find(F_xx1==F_xmax));
F_ymin=min(F_yx1);
Krc_ymin=Krc1(find(F_yx1==F_ymin));
Kre_ymin=Kre1(find(F_yx1==F_ymin));
F_ymax=max(F_yx1);
Krc_ymax=Krc1(find(F_yx1==F_ymax));
Kre_ymax=Kre1(find(F_yx1==F_ymax));
F_rmin=min(F_hypotmx1);
Krc_hmin=Krc1(find(F_hypotmx1==F_rmin));
Kre_hmin=Kre1(find(F_hypotmx1==F_rmin)) ;
F_rmax=max(F_hypotmx1);
Krc_hmax=Krc1(find(F_hypotmx1==F_rmax));
Kre_hmax=Kre1(find(F_hypotmx1==F_rmax));

Ktc=[Ktc_xmin;Ktc_xmax;Ktc_ymin;Ktc_ymax;Ktc_hmin;Ktc_hmax];
Kte=[Kte_xmin;Kte_xmax;Kte_ymin;Kte_ymax;Kte_hmin;Kte_hmax];
Krc=[Krc_xmin;Krc_xmax;Krc_ymin;Krc_ymax;Krc_hmin;Krc_hmax];
Kre=[Kre_xmin;Kre_xmax;Kre_ymin;Kre_ymax;Kre_hmin;Kre_hmax];

figure(1);
hold on

color=['r','b','g','k','c'];
for j=1:1    for plotting purposes
K = [Ktc_hmax,Kte_hmax;Krc_hmax,Kre_hmax];
rho = 0.00;  runout magnitude in mm
beta = 0;    locating angle of runout in radians
runout = rho * exp(i*beta);    runout
phi_st = pi-acos((R-radial)/R);    entry angle in radians
phi_ex = pi;    exit angle in radians
a = 3.175; -----changed it was 2.54
[F,T,X] = getcoefficients(phi, N, 100, a, K, alpha_helix, R, runout,
phi_st, phi_ex);
[F_x2,F_y2,F_hypot2] = getforces2(F,phi,fpt);
T_x = gettorques2(T,phi,fpt);
[X_haR, X_aR] = getX(X,fpt);
```

```
plotforces2(F_x2,F_y2,F_hypot2,phi,'N',1,color(j));
T_x=repmat(T_x./1000,20,1);
haR=repmat(X_haR,20,1);
aR=repmat(X_aR,20,1);

Wn=[10]/(Fs/2); %corner frequency of 10 Hz
[b,a] = butter(2,Wn,'high'); %2nd order butterworth
T_x = filter(b,a,T_x-mean(T_x));

end
minu=F_rmin;
maxi=F_rmax;
avgc=(minu+maxi)/2;
in=find(F_hypot==max(F_hypot));
   an=phi(in)*180/pi;
   h=fpt*sind(an) ;
```

MATLAB m-file for Monte Carlo simulation

```
%Monte Carlo Simulation program. User has to define the number of
%experiments to run, in n variable.
% by Firat Eren, 2010, Design and Manufacturing Lab. UNH
close all
clear;clc
run peaks_monte  % run this file to get the simulation info (angle)

% Evaluates the dependent multivariate random variables for Monte Carlo
in=find(F_hypot==max(F_hypot));
an=phi(in)*180/pi;
h=fpt*sind(an);

M=[Mt Mr];
Ktc1=M(:,1);
Kte1=M(:,2);
Krc1=M(:,3);
Kre1=M(:,4);

C=corr(M);
df=length(Ktc1)-1; % degree of freedom how many points does the sample
have ?
n=100000;  % number of points to be generated
mu = mean(M);
sigma = std(M);
t = bsxfun(@plus,mu,bsxfun(@times,sigma,mvtrnd(C,df,n)));

Ktc=t(:,1);
Kte=t(:,2);
Krc=t(:,3);
Kre=t(:,4);
Ft=zeros(length(Kte),1);Fr=zeros(length(Kte),1);Fres=zeros(length(Kte),
1);

a=inch_mm(0.125); % axial depth in mm

% Basic force estimation
for i=1:length(Kte)
    Ft(i)=Ktc(i)*a*h+Kte(i)*a;
    Fr(i)=Krc(i)*a*h+Kre(i)*a;
    Fres(i)=sqrt(Ft(i)^2+ Fr(i)^2);
end
figure
histfit(Fres,100);title('Peak force distribution for steel 1018
identical havg=0.001"','FontSize',17);xlabel('Force
(N)','FontSize',14);ylabel('Number of times','FontSize',14);
max(F_hypot)
deviation=std(Ft);
avg=mean(Ft);
upperlimit=avg+3*deviation;
kov=cov(M);
A=(Fres-avg)/deviation;
figure
```

```
histfit(A,100);title('Norm. peak force distribution for steel 1018
identical havg=0.001"','FontSize',17);xlabel('Force
(N)','FontSize',14);ylabel('Number of times','FontSize',14);
```

Force Simulation Program including runout

```
clear all;  % Matlab command to clear out all variables from workspace
close all;  % Matlab command to close all open plots

%   Author:  D M Esterling          Date;   10/06/2006
%   Revised 06/30/2008 to clean up the input & output sections
%   Comments from original 10/06/2006 program removed for clarity
%   Modified by Firat Eren
%   Sign error for Fx fixed on 07/08/2008
%
%  Input lengths are in inches
%
%
%  ****************************************
%
%  Start of input
%
%  ****************************************
%
%  All angles will be in radians !!
%  Important: ALL angles start at zero along the +Y axis
%  All input lengths are in inches. Time is in seconds.

n_cycles = 3;  % number of spindle periods for the data
% Note that the simulation runs for one spindle period before any
% data is taken (this is time_skip defined below)
% Simulation assumes up milling (see phi_enter & phi_exit below)

Cutting_energy_tang = 1883.22 ;  % tangential cutting energy N/mm^2
(aluminum)
Cutting_energy_edge_tang =  57.64;  % tangential edge cutting energy
N/mm (aluminum)

Cutting_energy_rad=1105.78; % radial cutting energy
Cutting_energy_edge_rad=87.43; % radial edge cutting energy
Kn  = 1/3;  % Kn is the ratio of the normal to the tangential force
constant

Run_Out = 0.0004; % runout in inches
Run_Out_Angle = 145;  %locator angle in degrees

% Run_Out = 0.0; % runout in inches
% Run_Out_Angle = 0;  %locator angle in degrees

num_teeth = 3;  %number of teeth on tool (assumed FEM shape)
tool_diam = 1; % tool diameter in inches
tool_length = 1.5;  % tool (gauge) length in inches
      % only used for stress and displacement calculations
helix_angle = 12;  % helix angle in degrees

Radial_Depth = 0.75*tool_diam; % radial depth in inches
```

```
adoc = 0.1; % axial depth of cut in inches
num_adoc = 40;  % number of slices in the axial direction

omega = 3500; % spindle speed in RPM
% feed_per_tooth = 0.002;  % feed per tooth in inches;

feed=29.8;
feed_per_tooth=fpt1(omega,num_teeth,feed);
%  ****************************
%
%   end of input
%
% ****************************

% Convert to mm & radian & rev per second units
tool_diam = tool_diam*25.4; % tool diameter in mm
tool_radius = 0.5*tool_diam;
tool_length = tool_length*25.4;
Run_Out = Run_Out*25.4;
Run_Out_Angle = Run_Out_Angle*pi/180.0;
Radial_Depth = Radial_Depth*25.4;
adoc = adoc*25.4;
helix_angle = helix_angle*(pi/180.0);
% feed_per_tooth = feed_per_tooth*25.4;
omega = omega/60.0;  % spindle rev per second

period = 1/omega;

feed = feed_per_tooth * num_teeth * omega;
feed_ipm = feed*60/25.4;    % feed rate in inches per minute
% feed is in mm

% The following come into play if we want to do dynamics
Stiffness = 4.e06; % cutter stiffness in N/M. Not used
Mass = 0.88;  % mass in Kg. Not used.

delta_theta = 2.0*(pi/180.0);
% 2 degree change in angle between each data segment in surface arc

time_cycle = 1./omega;  % time for one spindle rotation (seconds)

time_start = 0;
time_skip = time_cycle; % time to start storing data
time_skip = time_skip - (12/360)*period;
% This funky shift by -12 degrees in rotation angle is to get
% my plot in phase with the Altintas p.44 m file result.
%  Not sure where the phase lag is coming from.

time_end = time_skip + n_cycles*time_cycle; % time to end simulation

theta_step = 0.75*delta_theta;  % change in angle in each time step
time_step = (theta_step/(2.0*pi))/omega;
% time step in simulation.
```

```
% theta_step < delta_step guarantees at least one cut per
%   delta_theta rotation by the spindle
%
num_time_steps = floor( time_end/time_step) + 1;

RDOC_Phi = acos((tool_radius - Radial_Depth)/tool_radius);  % acos( (R
- radial depth of cut) / R);
RDOC = (RDOC_Phi/pi)*100;  % rdoc immersion in percent (!)

% Number of linear segments in surface segment that maintains
%  where the cut surface is located.
Num_seg = floor( 0.01*RDOC*pi/delta_theta )+ 1;

% upmill

phi_enter = 0.0; % entrance and exit angle for RDOC
phi_exit = phi_enter + Num_seg*delta_theta;

% downmill

% phi_exit=pi;
% phi_enter=phi_exit-Num_seg*delta_theta;

tooth_angle_step = (2.0*pi)/num_teeth;  % angular spacing between teeth

helix_tan = tan(helix_angle);
helix_angle_step = helix_tan*2/tool_diam; % Altintas eqn 2.87
%  The tooth angle has changed by Z*helix_angle_step
%    as you go up a distance Z along the tool axis,

helix_step = helix_angle_step*adoc*180/pi;

pitch_angle = tooth_angle_step;

%  adoc_1 is the AD where the total force on the tool should be zero
%   (see Tlusty, p. 555) for rigid tool, no runout and
%   circular approximation

           adoc_1 = tool_diam*pitch_angle/(2.0*helix_tan);
%  adoc = adoc_1
adoc_step = adoc/(num_adoc - 1); % Thickness of an axial slice

%C_Tlusty = Cutting_energy*adoc_step;  % eqn 9.59 Tlusty, needs h

x_step = feed*time_step;
% distance the tool center moves in one time step (no dynamics)
x_end = x_step*num_time_steps;

% initialize Lin_Seg array, which describes the cut surface.

% Initial location of tool center is X_init, Y_init

X_init = 0.0;
```

```
Y_init = 0.0;
Seg_length = (pi*tool_radius)*(delta_theta/pi);

for i_adoc = 1: (num_adoc-1)
   for i_seg = 1:Num_seg
      phi = phi_enter + (i_seg - 1)*delta_theta;
      if (phi <= phi_exit)
         Last_seg(i_adoc) = i_seg;  % Last_seg will be last segment
         %  number that is above the RDOC line, for this ADOC slice

         % Set initial z, y, angle and time for starting cut surface
         X_seg(i_adoc, i_seg) = X_init + tool_radius*sin(phi);
         Y_seg(i_adoc, i_seg) = Y_init + tool_radius*cos(phi);
         Phi_seg(i_adoc, i_seg) = phi;
         Time_seg(i_adoc, i_seg) = time_start;
                Tooth_seg(i_adoc, i_seg) = -1;  % -1 means no tooth has
actually cut this segment
      end;  % end of case where tooth angle is less than or equal to
phi_exit
   end; % end of loop over i_seg

   % Put the lowest adoc data points into an array for plotting
   %  Later we will follow how these points are moved as the surface is
cut
   %
   if (i_adoc == 1)
        for i = 1:Last_seg(1)
                xx(i) = X_seg(1,i);
                yy(i) = Y_seg(1,i);
                end;

                %plot(xx, yy, 'bo');
      %hold on;
   end;

end; % end of loop over i_adoc

% End of initializing the linear segment (data point) array

% Now initialize the y buffer data
%
% Note that we could extend the Y buffer x range to before the start
and after the
%  end of the tool center positions. What you would see is a profile of
the tool
%  outline (with some spiral effect due to the non-zero feed as the
tooth rotates)
%  but these Y values would not contribute to the surface roughness
measure.

x_buffer_start = 0.0;
x_buffer_end = x_end;
x_buffer_number = 100;
x_buffer_step = (x_buffer_end - x_buffer_start)/x_buffer_number;
```

```
for i_adoc = 1:(num_adoc-1)
    for ix = 1:(x_buffer_number +1)
        x_buffer(i_adoc, ix) = x_buffer_start + (ix-1)*x_buffer_step;
        y_buffer(i_adoc, ix) = tool_radius - Radial_Depth;  %
initialize end of y buffer stalk to Y = 0
    end;
end;

% Set the min and max angles to search for Y buffer intersections,
%  for the tooth angle relative to the current tool center.

tooth_angle_min = -0.25*pi;  % In fact, most cutting for  upmilling
will start at
   % zero angle, but due to cycloidal motion and tool dynamics, some
cutting
   % can happen before the "noon" position. -pi/4 is a safe angle to
start
   % the intersection test
tooth_angle_max = RDOC_Phi + 0.1*pi;  % Again a safe distance past the
RDOC line
if (tooth_angle_max > pi )
    tooth_angle_max = pi;  % For slot cutting or near slot cutting,
truncate
     %  intersection test to Y buffer lines in front of the tool.
end;

pi2 = 2.0*pi;
Toolsq = tool_radius^2;

time = time_start;
angle = 0.0; % angle will be the spindle rotation angle. It is also
%  the angle the first tooth makes with the positive Y axis.

i_time_end = num_time_steps;

for i_time = 1: num_time_steps

    % Find the i_time value for the starting time
   force_time(i_time) = 0.0;
   time_time(i_time) = time;

   if (time <= time_skip)
       i_time_skip = i_time;      % update i_time_skip unitl time >
time_skip
   end;

   for i_adoc = 1: (num_adoc - 1)
    Fx(i_adoc, i_time) = 0.0;   % Total x component of the force at time
t
    Fy(i_adoc, i_time) = 0.0;   % Total y component of the force at
time t
   end;

   % MyChip is debug stuff to follow the chip thickness as
   %    a function of time.  MyChip_h is circular approx to
```

```
%    chip thickness
   MyChip(i_time) = 0.0;
   MyChip_h(i_time) = 0.0;

      % (Xold, Yold) is the current center of the tool at this time,
      %  where there is NO dynamic deflection of the tool.
      Xold = Run_Out*sin(angle + Run_Out_Angle) + (time -
time_start)*feed;
      Yold = Run_Out*cos(angle + Run_Out_Angle);


     for i_adoc = 1: (num_adoc -1)

       for i_tooth = 1: num_teeth

         tooth_angle_base = (i_tooth -1)*tooth_angle_step + angle;
         % This is the angle of the i_th tooth at the base of the tool

         tooth_adoc = (i_adoc -1)*adoc_step;
         % tooth_adoc is distance from base of tool to this tooth
         tooth_angle = tooth_angle_base + tooth_adoc*helix_angle_step;
         % This is the angle of i_tooth at this z value
         tooth_angle = mod(tooth_angle, pi2);
         if( tooth_angle > pi)
            tooth_angle = tooth_angle - pi2;  % fold tooth_angle from -
pi to +pi
         end;

         %  Ok, now have the tooth angle for the current tooth and adoc
         % Next we do the y buffer calculation and, at the end of that,
         %  we will do the linked segment chip thickness and force
         %  calculation
         %
         %
            %  Test if tooth angle is at least at the first segment
angle or
         %    more than one time step beyond the last segment angle.
         %  The tooth angle is allowed to go just beyond the last
segment angle
         %    so the tests below can test the very last segment point.
         %
         angle_time(i_time) = tooth_angle;
         x_tooth = Xold + tool_radius*sin(tooth_angle);
         y_tooth = Yold + tool_radius*cos(tooth_angle);

         if(i_tooth == 1)
            x_t1(i_time) = x_tooth;
            y_t1(i_time) = y_tooth;
        end;

        if(i_tooth == 2)
            x_t2(i_time) = x_tooth;
            y_t2(i_time) = y_tooth;
              end;
```

```
         if ( (tooth_angle > tooth_angle_min) & (tooth_angle <
tooth_angle_max) )
             % Trim Y buffer lines for this tooth

             % Search Y buffer lines near the tip of the tool or buffer
line at ix_center.
             ix_center = round( (x_tooth -
x_buffer_start)/x_buffer_step + 1);
                 % xx_step is how far the tooth tip moves in the x
direction in one time step.
                 % ix step is the change in the y buffer index over
that x distance
                 % Add one more point in for safety... near Seg_angle =
0
             xx_step = abs( tool_radius* ( sin(tooth_angle +
theta_step) - sin(tooth_angle) ) );
             ix_step = round( ( xx_step/ x_buffer_step) + 1);
             ix_start = ix_center - ix_step;
             ix_end = ix_center + ix_step;
             do_loop = 1; % == 1 if the tool tip "ahadow" is over the y
buffer lines
             if (ix_end < 1)
                 do_loop = 0;
             end;
             if (ix_start > (x_buffer_number + 1))
                 do_loop = 0;
             end;
             if (do_loop == 1)
                if (ix_start < 1)
                    ix_start = 1;
                end;
                if ( ix_end > (x_buffer_number + 1) )
                 ix_end = x_buffer_number + 1;
                end;
            end;

             if (do_loop == 1 )

                 for ix = ix_start: ix_end
                     % Find the y coordinate the tooth was at when at
this x coordinate
                     x_test = x_buffer(i_adoc, ix);
                     if (abs( x_test - Xold) < tool_radius)
                        y_test = sqrt( tool_radius^2 - (x_test -
Xold)^2) + Yold;
                        if (y_buffer(i_adoc, ix) < y_test)
                            y_buffer(i_adoc, ix) = y_test;
                        end;
                    end;  %end of case that the intersection point
                    %  on the y buffer line is less than the tool
radius
                    %  in distance from the current tool center
                 end;  % end of trimming y buffer near the tip of the
tool
             end; % end of do_loop test if y buffer lines near the tool
tip
```

```
        end; % end of case where tooth tip angle is such that
intersection is possible

        %  End of Y buffer calculation
        %
        % Start of linked segment calculation
        %

        %  Test if tooth angle is at least at the first segment angle
or
        %    more than one time step beyond the last segment angle.
        %  The tooth angle is allowed to go just beyond the last
segment angle
        %    so the tests below can test the very last segment point.
        %
        if ( (tooth_angle < Phi_seg(i_adoc, 1) ) | (tooth_angle > ( P
      hi_seg(i_adoc, Last_seg(i_adoc) ) + delta_theta) ) )
           i_seg = -1; % indicate that this tooth is not cutting
        else

           % search phi_segs until tooth_angle is at or just past
phi_seg

           for j_seg = 1: Last_seg(i_adoc)
              if (Phi_seg(i_adoc, j_seg) <= tooth_angle )
                 i_seg = j_seg;
              end;
           end;
        end;


        if (i_seg >= 1)
           %  Test to see if the tooth is cutting this segment. Use
the
           %   coordinates of the first segment point on the surface
segment which includes
           %   the current tooth angle

              R1 =  sqrt( (X_seg(i_adoc, i_seg) - Xold)^2 + (
Y_seg(i_adoc, i_seg) - Yold)^2 );
              chip_thickness_1 = tool_radius - R1;

              if (chip_thickness_1 > 0)
                 % then tooth is cutting this segment. Re-set surface
position
                 %  of the FIRST point on the surface segment.
                 Seg_angle = Phi_seg(i_adoc, i_seg);  % Use most
recent
                 % value for the angle of the first segment point
                 X_seg(i_adoc, i_seg) = Xold +
tool_radius*sin(Seg_angle);
                 Y_seg(i_adoc, i_seg) = Yold +
tool_radius*cos(Seg_angle);
                 Phi_seg(i_adoc, i_seg) = atan2(X_seg(i_adoc, i_seg)-
Xold, Y_seg(i_adoc, i_seg) - Yold);
```

```
                  Tooth_seg(i_adoc, i_seg) = i_tooth;
                  Time_seg(i_adoc, i_seg) = time;
               end;
               if (i_seg < Last_seg(i_adoc) )
                   % then use the SECOND point on the segment to
determine
                   %  the chip thickness, forces and so on. But this
SECOND
                   %  point's surface coordinate is not changed, since
the
                   %  tooth has not reached it yet.
                    R2 =  sqrt( (X_seg(i_adoc, i_seg+1) - Xold)^2 + (
Y_seg(i_adoc, i_seg+1) - Yold)^2 );
                    chip_thickness_2 = tool_radius - R2;
                    if ((chip_thickness_2 > 0)& (time > time_skip) )
                               % record chip thickness for this tooth
and axial doc and at this time
                                chip(i_time, i_adoc, i_tooth) =
chip_thickness_2;
                                Ftang_step =
Cutting_energy_tang*adoc_step*chip_thickness_2;
                        Ftang_step = Ftang_step +
Cutting_energy_edge_tang*adoc_step;  % add in edge effect

Frad_step=Cutting_energy_rad*adoc_step*chip_thickness_2;
                       Frad_step = Frad_step +
Cutting_energy_edge_rad*adoc_step;  % add in edge effect
%
%  Fix on 07/08/2008
%
% changed Fx so sign agrees with Altintas p. 42 M code
%
%                         Fx(i_adoc, i_time) = Fx(i_adoc, i_time) +
Ftang_step*( -cos(tooth_angle) - Kn*sin(tooth_angle) );
%                         Fy(i_adoc, i_time) = Fy(i_adoc, i_time) +
Ftang_step*( sin(tooth_angle) - Kn*cos(tooth_angle) );

                        % 2 LINES BELOW TAKE RADIAL COEFFICIENTS INTO
ACCOUNT
                        Fx(i_adoc, i_time) = Fx(i_adoc, i_time) -
Ftang_step*cos(tooth_angle) - Frad_step*sin(tooth_angle) ;
                        Fy(i_adoc, i_time) = Fy(i_adoc, i_time) +
Ftang_step*sin(tooth_angle) - Frad_step*cos(tooth_angle) ;
                        if ( (i_adoc == 1) & (i_tooth == 1) )
                                MyChip(i_time) =  chip(i_time, i_adoc,
i_tooth);
                                MyChip_h(i_time) =
feed_per_tooth*sin(tooth_angle);
                        end; % end of debug test of iadoc = 1, itooth =
1
                     end; % end of chip_thickness_2 > 0
                  else % i_seg = Last_seg
                     % If here, then at the last surface segment.  This
segment
                     %   goes from the last point to the RDOC surface
(phi_exit)
```

```
                        % So the "second" point on this surface may be
considered to
                        % have zero chip thickness (just past the RDOC
surface).
                        % But, we need to consider if this last point is
cut and, if so,
                        % then add the chip thickness and resulting
force to
                        % the total force. We only do this ONCE, at the
first
                        % time the last segment is cut by this
particular tooth
                        % for this particular rotation of the spindle.
If the tooth
                        % continues to cut this segment (i.e. a short
time later
                        % it is cutting), for simplicity of logic, I
ignore this
                        % and treat this tooth as not cutting (as past
the
                        % RDOC surface line, even it it is not quite
there yet.
                        % For sure, the tooth angle is within
delta_theta of
                        % the RDOC surface, so this is a small error.
                        % Ok, now to test if this is the first time that
the
                        %  current tooth is cutting this last point over
the
                        %  current spindle rotation.

                        if ( (Tooth_seg(i_adoc, i_seg) ~= i_tooth) | (
(time - Time_seg(i_adoc, i_seg) ) > 0.75*time_cycle )  )
                           Seg_angle = Phi_seg(i_adoc, i_seg);  % Use most
recent
                                          % value for the angle of the last
segment point
                           X_seg(i_adoc, i_seg) = Xold +
tool_radius*sin(Seg_angle);
                           Y_seg(i_adoc, i_seg) = Yold +
tool_radius*cos(Seg_angle);
                           Phi_seg(i_adoc, i_seg) = atan2(X_seg(i_adoc,
i_seg)- Xold, Y_seg(i_adoc, i_seg) - Yold);
                           Tooth_seg(i_adoc, i_seg) = i_tooth;
                           Time_seg(i_adoc, i_seg) = time;

                           R1 =  sqrt( (X_seg(i_adoc, i_seg) - Xold)^2 + (
Y_seg(i_adoc, i_seg) - Yold)^2 );
                           chip_thickness_1 = tool_radius - R1;
                           if ( (chip_thickness_1 > 0) & (time >
time_skip) )
                                        % record chip thickness for this tooth
and azial doc and at this time
                                          chip(i_time, i_adoc, i_tooth) =
chip_thickness_2;Ftang_step =
Cutting_energy*adoc_step*chip_thickness_2;
```

```
Ftang_step = Ftang_step + Cutting_energy_edge*adoc_step;  % add in edge
effect

Frad_step=Cutting_energy_rad*adoc_step*chip_thickness_2;
                                        Frad_step = Frad_step +
Cutting_energy_edge_rad*adoc_step;
%                                        Fx(i_adoc, i_time) = Fx(i_adoc, i_time) -
Ftang_step*( cos(tooth_angle) + Kn*sin(tooth_angle) );
%            Fy(i_adoc, i_time) = Fy(i_adoc, i_time) + Ftang_step*(
sin(tooth_angle) - Kn*cos(tooth_angle) );

% 2 LINES BELOW TAKE RADIAL COEFFICIENTS

                                Fx(i_adoc, i_time) = Fx(i_adoc, i_time) -
Ftang_step*cos(tooth_angle) - Frad_step*sin(tooth_angle) ;
                                Fy(i_adoc, i_time) = Fy(i_adoc, i_time) +
Ftang_step*sin(tooth_angle) - Frad_step*cos(tooth_angle) ;
                                        if ( (i_adoc == 1) & (i_tooth == 1) )
                                                MyChip(i_time) =  chip(i_time,
i_adoc, i_tooth);
                                                MyChip_h(i_time) =
feed_per_tooth*sin(tooth_angle);
                                        end;  % end of debug, iadoc = itooth = 1
case
                                end; % end of chip_thickness > 0 for last
segment point
                            end;  % end of first time this last segment point
has been cut for this tooth, spindle rotation

                        end; % end of if .. else... for i_seg < Last_seg or
is == Last_seg
                  end; % end of test on i_seg >= 1
                  %
                  %  End of linked segment calculation for a particular
tooth
                  %    axial segment and time step
                  %

      end; % end of loop over number of teeth

   end;  % end of loop over adoc slices

        Fx_tot(i_time) = 0.0;
        Fy_tot(i_time) = 0.0;

        for i_adoc = 1: (num_adoc -1)
             Fx_tot(i_time) = Fx_tot(i_time) + Fx(i_adoc, i_time);
             Fy_tot(i_time) = Fy_tot(i_time) + Fy(i_adoc, i_time);
        end;

                      Ftot(i_time) = sqrt( Fx_tot(i_time)^2
      +Fy_tot(i_time)^2 );
             MyTime(i_time) = time;

            % Change spindle angle and time for next time step
```

```
                angle = angle + theta_step;
        time = time + time_step;

end;    end of loop over time steps

  All of the data analysis and plotting at the end of the 10/06/2006
  version has been removed.

  Now let's find the peak bending stress and the peak displacement.
  Only the displacement perpendicular to the face is considered or in
    the y direction.

  Using beam theory, BUT the total force is assumed concentrated
  at the tip, as used in cncx.  A better solution would calculate
  bending stress and displacement using a distributed force model.


  Find peak Ftot and peak Fy.

Ftot_peak = 0.0;
Fy_peak = 0.0;

for i_time = i_time_skip:i_time_end
    if (Ftot(i_time) > Ftot_peak )
        Ftot_peak = Ftot(i_time);    max total force
    end;

    if (abs(Fy_tot(i_time)) > Fy_peak)
        Fy_peak = abs(Fy_tot(i_time));    peak Y force
        if(Fy_tot(i_time) > 0 )
            y_direction = +1;    is Y force towards or away from
surface?
        else
            y_direction = -1;
        end;
    end;

end;

  Ko approx for effective radius of fluted tool
R_eff_meters = 0.8*tool_radius/1000;
Inertia = pi*R_eff_meters^4/4;    Eqn 13.20 in C&J
  Peak bending momment with forces taken at tip of tool
Mxy = Ftot_peak*(tool_length/1000);     lengths all in meters

E_modulus = 200*10^9;    this is E for STEEL (the tool) in Pascals
L = tool_length/1000;    length in meters

   ****************************

             Output  SI UNITS !!!!!!!!!!!

        ****************************

      Ftot_peak     Newtons
```

```
Fy_peak     % Newtons
y_direction;  % +1 => force towards the cutting surface
%displacement in microns
displacement = y_direction*(10^6)*(Fy_peak*L^3)/(3*E_modulus*Inertia)

% Peak bending stress in MPa
Max_stress = (10^(-6))* Mxy*(tool_radius/1000)/Inertia

% This is easy enough to convert to a more accurate bending stress
% since we have Fx and Fy at each axial depth of cut and time:
%  Fx(i_adoc, i_time), Fy(i_adoc, i_time)
%  for i_time = i_time_skip: i_time_end
%
% Where is the center of the i adoc slice?
  Answer: A distance of adoc_step from the tool tip
%
figure(1);
% Convert from time to rotation angle with zero angle at time_skip
%
angle_time = ((time_time - time_skip)/period)*360;
plot(angle_time, Fy_tot);     y force is in blue
hold on;
plot(angle_time, Fx_tot, 'r');  % x force is in red
% axis([0 180 -300 300]);


figure;
Fres=hypot(Fx_tot,Fy_tot);
plot(angle_time,Ftot)
% figure(2);
%plot(x_buffer(1,:), y_buffer(1,:));
phi_exit*180/pi
phi_enter*180/pi
```

APPENDIX C

THE FORCE MODEL COEFICIENTS AND THE EXPERIMENTAL FORCES

Introduction

This section includes the calibration results for the cutting force model coefficients, K_{TC}, K_{TE}, K_{RC} and K_{RE} as well as the average forces for all of the tests performed for this study. Experimental forces for two types of case study are also included.

Aluminum Results

RPM - TEST NO	IMMERSION	K_{TC} (N/mm^2)	K_{TE} (N/mm)	K_{RC} (N/mm^2)	K_{RE} (N/mm)
2600-1	¼	850.96	23.62	353.80	26.26
	½	750.63	22.10	273.07	25.61
	¾	798.92	20.97	330.70	25.18
2600-2	¼	870.28	21.50	406.49	22.58
	½	727.84	22.67	288.85	24.38
	¾	830.37	19.62	339.96	23.14
2600-3	¼	797.90	21.75	375.17	21.82
	½	750.91	15.55	306.88	28.12
	¾	830.74	20.16	350.12	22.87
3819-1	¼	777.04	20.18	353.63	24.62
	½	702.83	18.35	262.71	23.37
	¾	782.51	16.21	313.25	21.88
3819-2	¼	744.79	18.77	301.98	24.42
	½	709.61	20.71	268.10	20.95
	¾	758.29	18.43	306.96	20.47
3819 -3	¼	698.58	18.72	275.31	22.40
	½	735.20	17.77	317.95	20.80
	¾	768.78	17.30	316.74	22.02
3819-4	¼	723.52	22.26	300.45	22.68
	½	708.90	18.63	282.76	21.35

	¾	764.91	18.34	298.29	24.55
3819-5	¼	756.10	21.68	352.17	20.62
	½	685.62	22.83	292.75	21.48
	¾	768.27	17.31	311.09	22.61
3819-6	¼	698.80	24.11	297.89	20.67
	½	775.49	17.04	325.75	21.85
	¾	806.60	16.81	341.33	20.41
3819-7	¼	762.76	20.78	345.67	17.79
	½	737.92	18.59	288.91	22.23
	¾	785.97	17.92	278.94	23.68
3819-8	¼	722.93	23.15	329.28	19.68
	½	729.50	19.20	279.29	20.18
	¾	800.05	17.26	294.31	23.82
3819-9	¼	794.69	20.07	320.94	18.40
	½	751.97	16.63	287.30	19.12
	¾	764.10	18.79	312.40	20.40
3819-10	¼	719.46	22.34	283.45	21.16
	½	731.95	20.39	277.56	20.51
	¾	786.30	18.51	303.37	22.46
3819-11	¼	730.23	19.89	311.40	22.89
	½	735.50	18.63	275.45	24.44
	¾	818.24	16.24	320.28	19.19
3819-12	¼	763.48	19.41	302.10	23.71
	½	711.62	19.43	277.77	23.09
	¾	758.53	20.34	299.33	24.90
3819-13	¼	751.56	18.74	317.22	23.94
	½	751.46	16.69	293.04	24.15
	¾	820.31	17.45	353.63	20.93
3819-14	¼	737.80	21.69	325.68	19.85
	½	745.96	18.86	270.00	23.24
	¾	799.59	18.27	311.86	20.58
5000 -1	¼	731.23	20.57	300.44	22.72
	½	703.37	16.56	268.03	19.23
	¾	747.58	15.22	283.00	19.49
5000 – 2	¼	640.08	21.10	172.13	21.82
	½	660.72	20.65	254.53	21.91
	¾	750.20	16.48	280.08	21.10

5000 -3	¼	718.49	14.71	277.92	24.87
	½	728.95	15.92	283.12	19.45
	¾	747.58	15.82	288.61	21.00
6200 -1	¼	720.80	16.87	265.78	18.57
	½	732.16	12.02	241.56	22.41
	¾	713.27	14.47	275.13	21.09
6200 -2	¼	682.69	17.27	301.39	20.08
	½	660.06	16.49	235.89	23.08
	¾	687.11	16.10	266.35	20.61
6200 – 3	¼	650.07	20.16	239.13	18.14
	½	802.37	16.29	289.50	14.50
	¾	734.74	13.69	271.65	21.95

Table C.1: Coefficients from Aluminum tests

Aluminum Average Forces and the Geometry Matrices

1/4

mm2	mm	mm2	mm
0 010	0 438	-0 008	-0 253
0 008	0 253	0 010	0 438
0 020	0 438	-0 016	-0 253
0 016	0 253	0 020	0 438
0 031	0 438	0 025	-0 253
0 025	0 253	0 031	0 438
0 040	0 438	-0 033	0 253
0 033	0 253	0 040	0 438

1/2

mm2	mm	mm2	mm
0 010	0 505	-0 016	-0 505
0 016	0 505	0 010	0 505
0 020	0 505	0 031	-0 505
0 031	0 505	0 020	0 505
0 030	0 505	-0 047	-0 505
0 047	0 505	0 030	0 505
0 040	0 505	-0 063	-0 505
0 063	0 505	0 040	0 505

3/4

mm2	mm	mm2	mm
0 007	0 438	0 023	-0 758
0 023	0 758	0 007	0 438
0 013	0 438	0 045	-0 758
0 045	0 758	0 013	0 438
0 020	0 438	0 068	0 758
0 068	0 758	0 020	0 438
0 027	0 438	0 090	0 758
0 090	0 758	0 027	0 438

		1/4	1/2	3/4
2600-1	Fx1 (N)	8 99	1 08	-11 52
	Fy1	27 36	38 40	46 39
	Fx2	15 25	5 21	-14 70
	Fy2	39 11	53 53	67 99
	Fx3	21 35	7 92	-16 58
	Fy3	50 42	67 92	88 33
	Fx4	25 79	10 93	-17 92
	Fy4	58 84	82 14	106 93

		1/4	1/2	3/4
2600 2	Fx1 (N)	8 74	2 06	-10 58
	Fy1	25 40	37 82	45 72
	Fx2	14 76	4 35	-13 42
	Fy2	39 30	52 64	66 77
	Fx3	20 68	7 41	-16 19
	Fy3	49 95	67 39	88 97
	Fx4	24 80	10 20	-16 68
	Fy4	59 42	80 78	108 21

2600 3	Fx1 (N)	8 74	-3 91	-10 82
	Fy1	24 72	36 19	45 98
	Fx2	13 93	-0 65	-12 83
	Fy2	35 72	52 89	67 43
	Fx3	19 45	1 86	-16 30
	Fy3	48 46	67 01	89 38
	Fx4	23 36	4 24	-17 43
	Fy4	54 95	81 16	108 81

3819 1	Fx1 (N)	7 30	-0 03	-11 45
	Fy1	25 62	34 39	41 87
	Fx2	12 67	3 79	-13 31
	Fy2	35 70	49 73	61 66
	Fx3	17 61	6 60	-14 34
	Fy3	46 91	61 80	80 68
	Fx4	22 05	8 79	-17 24
	Fy4	55 18	76 35	101 71

3819 -2	Fx1 (N)	6 61	2 43	-9 27
	Fy1	24 17	34 01	42 07
	Fx2	12 51	5 97	-11 15
	Fy2	34 68	50 15	61 75
	Fx3	17 62	9 16	-13 17
	Fy3	42 74	63 56	80 36
	Fx4	21 64	11 07	-14 79
	Fy4	52 15	76 06	100 07

3819 -3	Fx1 (N)	7 31	0 50	-10 95
	Fy1	22 75	34 10	41 73
	Fx2	11 74	3 64	13 61
	Fy2	31 94	49 63	62 41
	Fx3	17 51	5 80	-14 75
	Fy3	40 57	64 05	82 04
	Fx4	21 31	7 72	-17 27
	Fy4	48 37	78 84	100 40

3819 -4	Fx1 (N)	8 88	1 20	-12 56
	Fy1	23 71	34 20	43 88
	Fx2	13 33	3 97	-13 54
	Fy2	34 85	48 29	62 97
	Fx3	18 96	6 96	14 90

3819-5	Fx1 (N)	8 74	2 73	11 87
	Fy1	23 29	34 88	41 89
	Fx2	13 52	5 57	-12 25
	Fy2	35 00	51 36	63 01
	Fx3	19 59	7 53	-16 13

	Fy3	42 61	62 97	83 74
	Fx4	23 05	9 11	-17 49
	Fy4	51 15	76 28	101 47

	Fy3	45 18	65 24	81 44
	Fx4	22 45	9 67	16 86
	Fy4	52 57	76 33	100 80

3819 6	Fx1 (N)	9 67	0 01	10 68
	Fy1	23 44	34 72	42 51
	Fx2	14 80	3 25	-12 60
	Fy2	32 72	51 62	62 45
	Fx3	19 26	5 51	14 54
	Fy3	42 87	66 33	83 37
	Fx4	23 48	8 13	-17 74
	Fy4	49 32	81 76	104 17

3819 7	Fx1 (N)	9 13	1 06	10 69
	Fy1	22 84	35 00	43 04
	Fx2	14 80	3 84	12 95
	Fy2	32 88	50 22	64 61
	Fx3	19 03	6 77	13 02
	Fy3	41 89	64 48	82 24
	Fx4	23 85	9 64	-14 13
	Fy4	52 46	78 97	102 84

3819 8	Fx1 (N)	9 37	2 56	11 76
	Fy1	22 90	33 96	44 44
	Fx2	14 70	5 18	-13 01
	Fy2	34 21	48 80	63 16
	Fx3	19 22	8 35	14 61
	Fy3	42 64	63 76	82 52
	Fx4	23 10	11 29	-15 52
	Fy4	51 07	76 92	105 07

3819-9	Fx1 (N)	9 54	1 87	-9 41
	Fy1	22 57	32 43	42 00
	Fx2	14 92	4 64	10 74
	Fy2	33 20	48 33	62 68
	Fx3	20 03	7 92	13 16
	Fy3	42 69	62 66	81 84
	Fx4	25 72	10 90	-15 08
	Fy4	52 09	77 06	100 38

3819 10	Fx1 (N)	9 17	3 00	9 61
	Fy1	22 99	34 10	42 34
	Fx2	14 24	5 59	13 82
	Fy2	33 59	49 91	64 22
	Fx3	19 79	9 33	-12 93
	Fy3	41 35	65 96	86 30
	Fx4	23 71	11 71	15 21
	Fy4	49 75	76 77	101 22

3819 11	Fx1 (N)	7 66	0 43	-8 99
	Fy1	24 11	34 96	42 20
	Fx2	12 61	2 84	11 66
	Fy2	32 91	52 48	61 19
	Fx3	17 28	5 98	11 88
	Fy3	43 88	65 17	82 26
	Fx4	22 08	9 57	14 78
	Fy4	51 04	78 87	104 22

3819 12	Fx1 (N)	7 61	0 63	11 29
	Fy1	24 27	34 54	44 28
	Fx2	12 89	4 20	13 84
	Fy2	34 28	51 31	66 84
	Fx3	18 52	6 40	-15 09
	Fy3	43 92	63 54	83 42
	Fx4	23 09	9 16	-16 49
	Fy4	52 24	77 41	102 81

3819 13	Fx1 (N)	7 15	1 02	-11 42
	Fy1	24 05	35 62	43 20
	Fx2	12 04	2 26	-13 13
	Fy2	34 92	49 98	64 39
	Fx3	17 02	5 31	-13 79
	Fy3	43 42	65 69	85 65
	Fx4	22 03	7 76	-19 53
	Fy4	52 58	79 96	106 06

3819-14	Fx1 (N)	8 98	1 01	9 03
	Fy1	23 18	34 86	42 19
	Fx2	14 32	4 41	-11 14
	Fy2	33 35	51 95	63 63
	Fx3	18 84	7 37	13 19
	Fy3	42 60	64 70	85 49
	Fx4	23 31	10 85	-13 98
	Fy4	51 37	79 11	102 34

5000-1	Fx1 (N)	8 21	1 15	-9 11
	Fy1	24 15	31 06	39 02
	Fx2	12 93	4 79	-11 28
	Fy2	33 26	46 83	57 39
	Fx3	18 06	7 38	-12 68
	Fy3	42 69	60 33	77 20
	Fx4	22 84	9 79	-13 26
	Fy4	51 29	72 79	95 30

5000-2	Fx1 (N)	8 80	1 35	-9 72
	Fy1	21 80	33 46	40 22
	Fx2	13 49	5 61	-11 60
	Fy2	29 37	49 18	59 67
	Fx3	19 34	7 26	-13 36
	Fy3	35 47	60 85	79 43
	Fx4	23 66	9 59	-13 48
	Fy4	43 21	73 09	96 66

5000-3	Fx1 (N)	5 04	1 42	-10 70
	Fy1	23 04	31 45	39 24
	Fx2	9 84	3 46	-11 27
	Fy2	31 72	47 67	59 97
	Fx3	15 71	6 80	14 47
	Fy3	42 54	61 81	78 45
	Fx4	19 61	9 88	-14 69
	Fy4	48 61	74 83	96 10

6200-1	Fx1 (N)	7 20	-1 51	-10 85
	Fy1	20 34	31 86	37 60
	Fx2	13 36	1 97	-12 90
	Fy2	30 51	45 96	55 40
	Fx3	18 70	4 76	-13 99
	Fy3	38 84	57 64	78 16
	Fx4	22 38	9 45	-15 29
	Fy4	46 43	74 89	90 22

6200-2	Fx1 (N)	6 80	-0 14	-9 38
	Fy1	21 41	32 55	37 54
	Fx2	11 55	2 24	-12 50
	Fy2	31 01	47 07	58 28
	Fx3	15 47	5 23	-12 53
	Fy3	39 66	56 92	72 25
	Fx4	20 20	8 63	-14 10
	Fy4	47 54	72 18	90 91

6200 3	Fx1 (N)	8 87	5 11	11 22
	Fy1	20 16	30 60	38 14
	Fx2	13 18	7 56	13 28
	Fy2	29 21	47 61	56 39
	Fx3	18 39	10 12	15 85
	Fy3	37 31	63 09	77 98
	Fx4	22 45	15 98	14 42
	Fy4	43 47	77 70	92 69

Table C2: Aluminum Average Forces and the Geometry Matrices

Steel 1018 Results

RPM – TEST NO	IMMERSION	K_{TC} (N/mm^{2})	K_{TE} (N/mm)	K_{RC} (N/mm^{2})	K_{RE} (N/mm)
2400-1	¼	1517.50	82.07	774.23	95.20
	½	1745.86	73.05	968.91	100.42
	¾	1678.06	74.24	1050.44	103.23
2400-2	¼	1824.42	73.86	960.10	96.22
	½	1925.05	74.42	1329.98	93.59
	¾	2025.50	67.61	1283.35	100.34
2400-3	¼	2368.95	58.83	1157.37	90.66
	½	1748.56	75.94	888.02	103.48
	¾	1650.22	79.23	1016.99	105.15
4000-1	¼	1935.23	61.06	1253.65	93.03
	½	1861.64	59.25	1130.58	93.88
	¾	1906.12	73.37	1061.20	89.85
4000-2	¼	1814.15	48.28	851.96	77.40
	½	1864.06	42.75	1032.44	82.90
	¾	1932.10	43.83	992.01	80.23
4000 -3	¼	1837.79	52.97	929.16	77.22
	½	1875.05	50.74	923.33	87.12
	¾	1904.16	50.14	1176.02	78.67
4000-4	¼	2023.71	51.84	1081.58	76.45
	½	1910.69	52.29	863.85	87.81
	¾	1828.29	52.14	1012.38	82.65
4000-5	¼	1891.97	57.42	969.61	77.85
	½	1830.27	52.02	873.05	88.28
	¾	1809.12	53.62	1055.02	82.65
4000-6	¼	1994.57	56.23	1002.54	88.03
	½	1806.18	59.31	949.04	89.08
	¾	1859.03	51.17	991.94	85.55
4000-7	¼	1955.81	55.62	1027.17	84.10
	½	1956.10	46.53	1117.40	83.97

	¾	1919.67	51.71	1114.39	82.65
4000-8	¼	1829.47	58.87	799.31	83.47
	½	1855.99	51.85	933.81	86.02
	¾	2057.34	47.08	1228.50	76.01
4000-9	¼	2007.13	53.76	940.74	87.99
	½	1809.49	55.11	901.17	87.85
	¾	1940.26	49.18	1070.91	81.33
4000-10	¼	2051.77	58.26	1346.78	86.90
	½	2000.16	49.66	963.81	82.26
	¾	1884.35	50.69	1041.97	82.09
4000-11	¼	1932.20	57.11	949.05	84.85
	½	1745.25	59.82	789.94	93.94
	¾	1894.17	51.45	1060.35	81.63
4000-12	¼	1949.44	55.55	906.84	82.04
	½	1889.11	52.22	946.46	80.98
	¾	1914.32	50.40	1050.92	80.90
4000-13	¼	1841.10	52.32	883.45	79.00
	½	1755.82	52.54	912.75	91.23
	¾	1776.77	54.69	1069.49	81.85
4000-14	¼	1961.61	53.34	982.76	84.05
	½	2062.61	45.10	996.18	82.78
	¾	1817.07	54.87	1032.56	83.77
5600 -1	¼	2462.86	39.68	1515.22	72.74
	½	1910.55	48.74	1128.74	83.10
	¾	1821.11	55.91	1265.03	81.20
5600 - 2	¼	1961.57	56.06	1287.27	86.81
	½	1850.71	52.32	1000.92	91.36
	¾	1708.34	57.52	1098.52	91.68
5600 -3	¼	1950.16	59.28	1188.43	100.00
	½	1755.85	57.25	911.71	97.91
	¾	1904.65	50.49	1228.42	82.44
6400 -1	¼	1713.45	61.69	938.88	82.40
	½	1855.62	50.25	1030.71	85.54
	¾	1912.36	41.84	1156.13	76.57
6400 -2	¼	1815.80	53.74	859.50	82.04
	½	1952.94	48.35	1172.57	82.79
	¾	2099.89	44.01	1584.66	60.25
6400 - 3	¼	1849.30	54.90	1093.15	82.88
	½	1617.74	59.29	1086.62	90.80
	¾	2238.61	42.23	1482.12	68.49

Table C.3: Coefficients from Steel1018 tests

Steel1018 Average Forces and the Geometry Matrices

1/4

mm2	mm	mm2	mm
0 010	0 438	-0 008	-0 253
0 008	0 253	0 010	0 438
0 013	0 438	-0 010	-0 253
0 010	0 253	0 013	0 438
0 015	0 438	-0 012	-0 253
0 012	0 253	0 015	0 438
0 020	0 438	-0 017	-0 253
0 017	0 253	0 020	0 438

1/2

mm2	mm	mm2	mm
0 010	0 505	-0 016	-0 505
0 016	0 505	0 010	0 505
0 013	0 505	-0 020	-0 505
0 020	0 505	0 013	0 505
0 015	0 505	-0 024	-0 505
0 024	0 505	0 015	0 505
0 020	0 505	0 032	-0 505
0 032	0 505	0 020	0 505

3/4

mm2	mm	mm2	mm
0 007	0 438	-0 023	-0 758
0 023	0 758	0 007	0 438
0 008	0 438	-0 028	-0 758
0 028	0 758	0 008	0 438
0 010	0 438	-0 034	-0 758
0 034	0 758	0 010	0 438
0 013	0 438	-0 045	-0 758
0 045	0 758	0 013	0 438

		1/4	1/2	3/4
2400 1	Fx1 (N)	21 05	11 60	-57 63
	Fy1	84 46	123 57	145 60
	Fx2	22 49	11 20	62 29
	Fy2	86 11	135 64	158 45
	Fx3	25 62	-10 25	-64 56
	Fy3	92 16	145 10	169 92
	Fx4	29 65	-9 40	64 56
	Fy4	103 88	161 60	169 92

		1/4	1/2	3/4
2400 2	Fx1 (N)	17 72	11 56	62 27
	Fy1	84 59	132 72	144 79
	Fx2	22 04	-12 20	67 72
	Fy2	92 53	136 74	167 76
	Fx3	23 94	-11 09	-66 05
	Fy3	98 70	147 42	179 96
	Fx4	28 64	-13 44	-78 69
	Fy4	109 68	175 12	201 48

2400-3	Fx1 (N)	17 02	-11 04	56 80
	Fy1	86 40	122 92	150 25
	Fx2	20 96	8 54	60 84
	Fy2	93 61	141 86	157 23
	Fx3	24 32	8 57	-61 96
	Fy3	100 03	146 33	178 61
	Fx4	31 44	-7 01	-69 18
	Fy4	117 62	162 27	192 38

4000 -1	Fx1 (N)	11 99	16 89	-48 01
	Fy1	84 93	117 49	145 51
	Fx2	14 57	-16 72	-49 55
	Fy2	91 55	129 08	157 54
	Fx3	17 87	15 24	51 98
	Fy3	99 27	139 28	170 34
	Fx4	21 09	-16 18	58 98
	Fy4	113 34	158 73	195 63

4000 -2	Fx1 (N)	12 57	-17 84	-49 59
	Fy1	69 09	102 15	117 36
	Fx2	15 80	-17 04	-55 67
	Fy2	75 95	114 35	132 95
	Fx3	18 74	-16 95	-55 61
	Fy3	81 89	124 44	144 47
	Fx4	23 89	-15 29	-60 17
	Fy4	92 85	142 60	168 54

4000-3	Fx1 (N)	14 48	-14 08	-52 25
	Fy1	71 80	107 25	121 89
	Fx2	17 30	-13 40	-54 41
	Fy2	77 99	119 61	138 44
	Fx3	19 96	-11 46	-57 88
	Fy3	83 62	129 15	148 85
	Fx4	25 36	9 98	-65 79
	Fy4	96 39	146 90	173 99

4000 -4	Fx1 (N)	14 70	-11 99	-50 62
	Fy1	74 13	108 97	123 47
	Fx2	17 90	-11 52	-53 40
	Fy2	81 29	121 61	135 40
	Fx3	20 58	-9 51	55 11
	Fy3	87 69	127 61	149 80
	Fx4	26 26	-6 68	-61 38
	Fy4	101 84	149 05	171 36

4000 5	Fx1 (N)	16 49	-12 80	-49 86
	Fy1	73 50	106 05	122 76
	Fx2	19 35	-13 97	-54 91
	Fy2	80 64	121 95	139 52
	Fx3	22 06	-11 04	-57 32
	Fy3	87 14	127 03	149 29
	Fx4	27 58	8 88	-62 11
	Fy4	99 03	145 80	172 10

4000-6	Fx1 (N)	14 00	-11 95	-52 40
	Fy1	78 91	110 69	124 60
	Fx2	17 26	-10 68	-53 95
	Fy2	85 74	124 81	137 63
	Fx3	20 35	-10 70	-58 94
	Fy3	93 70	133 93	149 55
	Fx4	25 87	-8 57	-61 88
	Fy4	105 36	149 97	173 56

4000 7	Fx1 (N)	13 94	-17 43	-53 51
	Fy1	76 79	106 69	127 07
	Fx2	17 38	-16 16	-54 62
	Fy2	84 51	119 79	138 66
	Fx3	20 36	-15 16	57 46
	Fy3	90 96	130 66	151 03
	Fx4	25 29	15 29	-65 42
	Fy4	103 53	149 51	177 79

4000-8	Fx1 (N)	16 48	-13 29	-51 19
	Fy1	74 23	107 73	123 19
	Fx2	19 63	-12 61	-54 57
	Fy2	80 53	119 35	137 85
	Fx3	22 29	-11 14	57 58
	Fy3	86 57	127 55	152 03
	Fx4	28 39	9 48	-65 20
	Fy4	97 46	147 18	178 17

4000-9	Fx1 (N)	13 48	-12 62	-50 90
	Fy1	77 99	110 03	123 29
	Fx2	16 96	-11 78	-54 73
	Fy2	85 39	119 83	137 88
	Fx3	20 46	-10 20	56 94
	Fy3	90 38	128 06	149 46
	Fx4	25 97	-8 74	-62 40
	Fy4	104 39	148 03	174 93

4000 10	Fx1 (N)	13 11	-11 26	-50 16
	Fy1	83 27	107 64	122 06
	Fx2	15 49	-10 74	-55 55
	Fy2	90 88	119 58	138 38
	Fx3	17 89	-9 17	-55 34
	Fy3	98 53	127 74	149 96

4000-11	Fx1 (N)	14 96	-11 48	-50 47
	Fy1	76 46	112 21	124 15
	Fx2	18 33	-12 53	-53 68
	Fy2	84 35	124 22	138 44
	Fx3	21 16	-8 51	-56 32
	Fy3	89 76	130 16	149 22

	Fx4	22 66	-6 55	-62 00
	Fy4	113 76	149 68	172 67

	Fx4	26 71	7 21	-61 86
	Fy4	102 40	148 88	174 74

4000-12	Fx1 (N)	15 49	-10 66	-49 84
	Fy1	74 57	106 21	123 00
	Fx2	19 08	9 30	53 61
	Fy2	81 90	117 51	138 01
	Fx3	21 92	-8 34	-55 39
	Fy3	88 37	126 21	149 28
	Fx4	27 79	-6 51	-61 10
	Fy4	99 99	146 17	174 07

4000-13	Fx1 (N)	13 97	15 70	-50 44
	Fy1	71 22	109 84	124 71
	Fx2	17 17	-16 35	-53 50
	Fy2	79 04	119 14	137 49
	Fx3	20 08	-14 59	56 39
	Fy3	83 63	127 38	147 04
	Fx4	25 30	12 88	-62 73
	Fy4	95 87	147 02	172 57

4000-14	Fx1 (N)	13 58	-14 10	-51 15
	Fy1	75 76	106 58	126 05
	Fx2	16 69	12 85	-53 04
	Fy2	83 32	118 91	139 74
	Fx3	19 98	11 22	-55 90
	Fy3	89 98	128 76	148 99
	Fx4	25 23	9 12	-62 11
	Fy4	102 05	149 79	174 79

5600-1	Fx1 (N)	11 20	-16 48	52 88
	Fy1	78 01	107 53	124 85
	Fx2	14 63	-15 39	55 58
	Fy2	86 39	119 43	142 35
	Fx3	17 31	-14 64	-65 92
	Fy3	94 13	129 41	154 74
	Fx4	23 64	-14 97	-68 29
	Fy4	113 63	149 50	175 75

5600 2	Fx1 (N)	11 35	17 59	-58 20
	Fy1	80 46	111 73	128 78
	Fx2	14 46	-15 66	-58 05
	Fy2	89 27	121 55	141 97
	Fx3	16 47	15 02	67 99
	Fy3	96 65	132 74	153 86
	Fx4	20 71	14 50	-70 09
	Fy4	109 96	150 94	175 19

5600 3	Fx1 (N)	10 25	-18 76	-54 88
	Fy1	89 89	116 32	123 48
	Fx2	13 01	-15 85	-59 08
	Fy2	91 12	121 45	137 52
	Fx3	15 96	-13 63	-64 13
	Fy3	98 80	136 89	157 52
	Fx4	20 11	-15 19	-69 86
	Fy4	116 61	151 68	174 36

6400-1	Fx1 (N)	15 18	-13 99	-52 69
	Fy1	73 56	106 77	113 86
	Fx2	18 94	-16 25	-58 49
	Fy2	83 97	122 02	129 70
	Fx3	20 20	-15 06	-57 31
	Fy3	86 21	125 98	145 80
	Fx4	25 14	12 31	-67 06
	Fy4	98 59	148 40	165 22

6400 2	Fx1 (N)	13 34	16 17	-49 13
	Fy1	70 94	106 31	118 17
	Fx2	17 23	-15 88	53 85
	Fy2	83 70	118 60	132 39
	Fx3	20 27	-16 12	56 86
	Fy3	82 33	137 42	146 70
	Fx4	24 77	-14 99	71 00
	Fy4	96 94	148 53	176 30

6400 3	Fx1 (N)	11 47	17 21	-52 13
	Fy1	74 76	111 32	123 35
	Fx2	16 61	-16 62	-57 05
	Fy2	85 55	123 95	138 23
	Fx3	17 73	-17 13	-60 18
	Fy3	89 04	129 31	150 95
	Fx4	21 84	17 89	-70 87
	Fy4	102 34	149 10	184 18

Table C4: Steel 1018 Average Forces and the Geometry Matrices

Stainless Steel 304 Results

RPM - TEST NO	IMMERSION	K_{TC} (N/mm^2)	K_{TE} (N/mm)	K_{RC} (N/mm^2)	K_{RE} (N/mm)
1600-1	¼	2790.46	43.14	1979.97	77.94
	½	2957.31	36.26	1894.67	76.92
	¾	2438.85	47.25	1644.86	91.07
1600-2	¼	2465.09	39.72	1453.78	72.87
	½	2464.72	38.51	1442.60	72.64
	¾	2603.80	34.94	1679.29	69.54
1600-3	¼	2899.11	32.21	1958.41	61.36
	½	2516.74	37.59	1629.01	68.62

	¾	2535.69	36.63	1661.83	69.51
2400-1	¼	2251.54	42.84	1335.00	64.38
	½	2537.14	35.42	1524.81	66.39
	¾	2999.35	23.05	1688.73	62.22
2400-2	¼	2898.54	29.54	1926.95	50.22
	½	2186.93	45.73	1302.62	73.70
	¾	2031.84	46.18	1429.54	75.03
2400 -3	¼	2442.88	35.84	1492.65	67.55
	½	2859.34	27.57	1890.98	50.25
	¾	2001.51	47.86	1166.47	80.57
2400-4	¼	2174.94	47.90	1397.82	72.80
	½	2221.13	40.88	1339.77	69.28
	¾	2116.83	42.25	1260.94	77.69
2400-5	¼	1942.99	51.80	1021.52	81.35
	½	2089.27	42.52	1172.78	74.73
	¾	2335.12	37.87	1270.89	78.31
2400-6	¼	2168.16	45.44	1153.37	77.14
	½	2455.02	36.25	1568.79	68.22
	¾	1745.99	52.95	964.95	93.95
2400-7	¼	2610.58	38.97	1413.97	70.41
	½	2346.71	42.22	1346.69	75.46
	¾	2531.08	36.52	1439.45	78.65
2400-8	¼	2714.19	35.03	1836.98	63.96
	½	2008.34	48.52	1165.97	83.48
	¾	2131.03	47.02	1430.18	82.85
2400-9	¼	2476.94	38.55	1596.72	63.61
	½	2347.33	39.06	1252.81	78.14
	¾	2263.18	38.49	1252.58	86.23
2400-10	¼	1997.08	53.73	1078.67	93.66
	½	2109.59	48.38	1068.12	90.87
	¾	2167.43	41.90	1318.77	84.87
2400-11	¼	2109.62	47.96	1260.97	77.53
	½	2529.39	35.50	1232.71	84.91
	¾	2453.37	40.45	1268.33	90.15
2400-12	¼	2289.47	43.12	1309.22	80.05
	½	2002.70	54.69	1162.80	88.79
	¾	2231.29	41.51	1152.39	93.66
2400-13	¼	2096.49	52.17	1250.14	86.33
	½	2220.27	45.81	1170.86	91.82
	¾	2080.57	45.64	915.98	107.37
2400-14	¼	2622.33	40.11	1466.38	82.36

	½	2330.23	41.02	1339.14	77.92
	¾	2313.96	44.34	910.00	98.13
3200 -1	¼	2653.40	25.42	1495.62	55.20
	½	2351.09	29.78	1423.61	55.36
	¾	2378.24	29.99	1323.91	62.79
3200 - 2	¼	2448.00	38.35	1359.81	72.18
	½	2469.11	35.37	1515.75	73.07
	¾	2377.86	37.99	1253.22	87.77
3200 -3	¼	2525.29	38.64	1524.07	79.70
	½	2424.26	36.66	1411.54	78.62
	¾	2513.86	34.48	1240.27	90.73
4400 -1	¼	2371.03	28.56	1270.52	58.41
	½	2255.61	33.00	1170.54	65.67
	¾	2279.72	30.72	1185.91	70.19
4400 -2	¼	2424.17	32.97	1479.74	62.07
	½	2351.46	33.56	1367.92	65.97
	¾	2646.61	27.58	1599.96	73.71
4400 - 3	¼	2476.53	29.22	1830.55	54.04
	½	2583.85	25.08	1539.42	52.95
	¾	2582.54	24.84	1324.54	68.40

Table C5: Coefficients from StSt304 tests

Stainless Steel 304 Average Forces and the Geometry Matrices

1/4				1/2				3/4			
mm2	mm	mm2	mm	mm2	mm	mm2	mm	mm2	mm	mm2	mm
0 008	0 438	-0 006	0 253	0 008	0 505	-0 012	-0 505	0 005	0 438	-0 017	-0 758
0 006	0 253	0 008	0 438	0 012	0 505	0 008	0 505	0 017	0 758	0 005	0 438
0 010	0 438	-0 008	-0 253	0 010	0 505	-0 016	-0 505	0 007	0 438	-0 023	-0 758
0 008	0 253	0 010	0 438	0 016	0 505	0 010	0 505	0 023	0 758	0 007	0 438
0 013	0 438	-0 010	-0 253	0 013	0 505	-0 020	-0 505	0 008	0 438	-0 028	-0 758
0 010	0 253	0 013	0 438	0 020	0 505	0 013	0 505	0 028	0 758	0 008	0 438
0 015	0 438	-0 012	-0 253	0 015	0 505	-0 024	-0 505	0 010	0 438	-0 034	-0 758
0 012	0 253	0 015	0 438	0 024	0 505	0 015	0 505	0 034	0 758	0 010	0 438

		1/4	**1/2**	**3/4**
1600-1	Fx1 (N)	8 28	-20 27	-62 79
	Fy1	77 14	107 40	124 42
	Fx2	10 66	-21 17	-70 34
	Fy2	88 30	122 88	142 68
	Fx3	13 74	-21 19	-75 79
	Fy3	98 35	137 21	160 01
	Fx4	17 10	-20 42	-78 33
	Fy4	109 72	157 70	173 75

		1/4	**1/2**	**3/4**
1600-2	Fx1 (N)	8 89	-15 30	-50 34
	Fy1	67 60	96 31	109 02
	Fx2	11 48	15 62	-61 03
	Fy2	77 28	109 16	128 00
	Fx3	14 80	-15 35	-64 32
	Fy3	86 58	123 91	144 92
	Fx4	18 52	-13 72	-66 34
	Fy4	93 75	136 16	161 77

1600-3	Fx1 (N)	8 67	-15 46	-50 75
	Fy1	67 69	93 19	107 75
	Fx2	11 42	-16 11	-58 71
	Fy2	78 53	112 44	128 50
	Fx3	14 49	-17 82	-63 54
	Fy3	89 90	126 56	146 19
	Fx4	18 56	15 24	-66 27
	Fy4	100 39	135 51	158 88

2400 -1	Fx1 (N)	11 72	-14 15	-52 95
	Fy1	63 31	89 38	106 66
	Fx2	12 90	13 85	-51 34
	Fy2	68 86	111 67	118 53
	Fx3	18 15	-15 87	-60 34
	Fy3	82 60	122 75	146 89
	Fx4	19 70	12 29	-65 06
	Fy4	85 43	132 02	163 45

2400 -2	Fx1 (N)	10 60	12 88	-49 53
	Fy1	60 70	96 29	109 93

2400 3	Fx1 (N)	7 85	-12 91	-51 39
	Fy1	64 60	89 60	113 51

	Fx2	13 39	-12 68	54 81
	Fy2	75 84	104 93	121 15
	Fx3	16 08	-12 98	-64 68
	Fy3	81 37	126 09	140 67
	Fx4	20 79	-11 60	-61 88
	Fy4	94 96	129 09	149 90

	Fx2	10 88	-11 83	-50 45
	Fy2	73 98	102 77	122 65
	Fx3	14 05	12 56	56 97
	Fy3	83 66	115 56	135 65
	Fx4	17 04	-13 59	60 05
	Fy4	90 70	138 97	153 60

2400 -4	Fx1 (N)	10 75	-13 37	-51 50
	Fy1	70 34	91 65	106 37
	Fx2	12 65	-13 33	54 42
	Fy2	73 55	105 01	125 68
	Fx3	15 01	12 86	57 82
	Fy3	81 94	116 81	135 77
	Fx4	18 61	-12 54	62 34
	Fy4	94 23	128 31	150 15

2400-5	Fx1 (N)	10 74	-14 35	-52 89
	Fy1	69 08	92 78	107 95
	Fx2	13 03	-13 82	54 60
	Fy2	76 13	104 07	122 71
	Fx3	15 74	13 26	-60 77
	Fy3	77 54	116 05	146 22
	Fx4	19 13	-12 46	-61 77
	Fy4	90 53	126 24	151 44

2400-6	Fx1 (N)	9 14	-16 94	-56 43
	Fy1	63 87	94 01	117 58
	Fx2	13 03	-16 27	56 93
	Fy2	77 66	107 11	124 63
	Fx3	16 75	14 10	-60 70
	Fy3	86 93	121 35	138 51
	Fx4	18 18	-17 73	-63 63
	Fy4	85 38	134 86	151 42

2400-7	Fx1 (N)	10 05	-15 02	-54 79
	Fy1	65 20	97 08	112 14
	Fx2	14 71	-14 55	-58 27
	Fy2	81 65	110 97	129 10
	Fx3	16 57	13 81	-66 59
	Fy3	82 00	122 74	146 24
	Fx4	21 62	-13 32	65 04
	Fy4	94 89	135 46	162 40

2400-8	Fx1 (N)	8 54	-16 22	57 10
	Fy1	68 41	98 87	115 64
	Fx2	11 34	-15 79	-59 43
	Fy2	78 20	110 91	130 11
	Fx3	13 83	15 94	-62 49
	Fy3	84 54	121 39	142 36
	Fx4	17 86	-14 69	-71 18
	Fy4	100 38	131 70	159 91

2400 9	Fx1 (N)	9 31	-16 68	57 30
	Fy1	64 21	95 61	110 22
	Fx2	12 71	-16 52	63 54
	Fy2	73 63	108 92	128 56
	Fx3	16 30	-14 37	64 45
	Fy3	86 60	124 61	141 69
	Fx4	17 93	-14 21	-67 98
	Fy4	90 33	131 92	155 70

2400 10	Fx1 (N)	8 44	-18 04	-58 34
	Fy1	76 68	102 56	111 89
	Fx2	11 00	-18 49	-60 16
	Fy2	79 48	115 79	127 59
	Fx3	13 55	-13 81	-64 73
	Fy3	88 88	125 94	141 10
	Fx4	16 93	-15 96	-69 59
	Fy4	96 34	136 01	155 80

2400-11	Fx1 (N)	9 82	-20 94	-57 90
	Fy1	69 01	100 75	116 75
	Fx2	12 09	-17 78	-66 35
	Fy2	75 86	109 91	136 20
	Fx3	14 48	18 56	-64 65
	Fy3	83 25	131 67	150 32
	Fx4	18 07	15 69	68 69
	Fy4	91 64	137 27	165 59

2400-12	Fx1 (N)	7 69	-15 74	-61 42
	Fy1	69 71	101 72	115 22
	Fx2	11 09	-15 82	-63 56
	Fy2	78 36	121 22	131 88
	Fx3	14 11	-14 76	-66 62
	Fy3	86 26	126 33	145 61
	Fx4	16 90	-14 62	-69 67
	Fy4	93 81	136 25	159 34

2400 13	Fx1 (N)	9 36	-19 90	68 54
	Fy1	73 38	101 97	121 65
	Fx2	11 45	20 38	-65 15
	Fy2	79 76	121 54	134 41
	Fx3	14 62	-17 92	69 73
	Fy3	90 61	126 65	148 56
	Fx4	17 31	-17 51	-72 66
	Fy4	94 69	139 42	161 44

2400 14	Fx1 (N)	7 58	-16 84	60 03
	Fy1	77 06	97 10	123 69
	Fx2	11 23	-15 67	-57 98
	Fy2	79 42	110 38	131 55
	Fx3	14 12	-17 45	-61 64
	Fy3	87 43	125 80	146 80
	Fx4	18 55	-14 34	-63 04
	Fy4	104 73	133 99	167 51

3200-1	Fx1 (N)	8 32	-12 05	-44 30
	Fy1	57 79	81 47	96 03
	Fx2	11 27	-11 46	-48 89
	Fy2	68 27	94 16	114 06
	Fx3	14 81	-12 10	53 17
	Fy3	77 01	109 11	130 32
	Fx4	19 13	-10 88	-54 53
	Fy4	85 66	119 45	142 90

3200-2	Fx1 (N)	8 70	-18 17	-58 46
	Fy1	66 29	95 23	113 24
	Fx2	11 70	-18 21	-62 62
	Fy2	75 53	109 47	129 63
	Fx3	15 76	-18 47	-67 01
	Fy3	84 32	123 26	146 82
	Fx4	18 55	-17 34	67 33
	Fy4	91 60	135 93	159 40

3200-3	Fx1 (N)	6 60	-19 64	-61 28
	Fy1	70 98	97 06	114 36
	Fx2	9 21	-19 11	-65 84
	Fy2	81 75	111 18	131 50
	Fx3	13 27	-18 58	68 13
	Fy3	90 61	125 39	147 99
	Fx4	15 97	-18 08	-69 85
	Fy4	98 17	136 16	163 25

4400-1	Fx1 (N)	8 13	-12 91	-46 46
	Fy1	56 59	85 18	96 86
	Fx2	10 73	-12 68	54 24
	Fy2	65 86	97 79	116 52

4400-2	Fx1 (N)	7 79	13 88	57 57
	Fy1	60 67	86 05	107 92
	Fx2	11 19	15 84	-62 82
	Fy2	71 68	105 27	122 25

	Fx3	14 36	-11 83	-54 14
	Fy3	73 29	109 26	128 16
	Fx4	18 10	-9 69	-56 12
	Fy4	81 08	121 00	142 69

	Fx3	13 93	13 72	-65 90
	Fy3	79 72	113 61	139 51
	Fx4	17 06	12 88	71 92
	Fy4	87 08	125 84	161 12

4400 3	Fx1 (N)	6 36	-12 53	-49 69
	Fy1	59 59	80 75	96 48
	Fx2	9 12	-12 55	-54 73
	Fy2	70 55	96 29	118 81
	Fx3	11 69	-12 62	-56 83
	Fy3	80 28	112 01	136 15
	Fx4	13 71	-11 11	59 54
	Fy4	88 74	122 59	146 91

Table C6: Stainless Steel 304 Average Forces and the Geometry Matrices

Titanium Grade 2 Results

RPM - TEST NO	IMMERSION	K_{TC} (N/mm²)	K_{TE} (N/mm)	K_{RC} (N/mm²)	K_{RE} (N/mm)
1200-1	¼	1649.97	21.59	964.95	35.07
	½	1913.29	23.93	1255.78	37.98
	¾	1994.47	22.34	1349.27	37.48
1200-2	¼	1958.42	22.81	1300.46	35.11
	½	1952.62	23.05	1286.28	37.69
	¾	2008.08	22.30	1332.02	38.48
1200-3	¼	1602.49	25.27	876.49	38.48
	½	1848.21	25.40	1204.52	39.41
	¾	1993.88	22.74	1324.33	38.97
1800-1	¼	2048.70	14.21	1476.19	21.96
	½	1958.18	21.34	1104.09	37.48
	¾	2020.64	11.48	1337.41	17.77
1800-2	¼	1913.57	19.42	1120.00	34.34
	½	2088.46	12.54	1569.63	18.47
	¾	1671.57	19.08	879.54	30.44
1800 -3	¼	1582.11	18.51	867.21	34.49
	½	1976.31	20.59	1153.43	39.74
	¾	2217.54	15.13	1326.11	29.87
1800-4	¼	1855.79	19.99	1064.51	33.48
	½	2069.61	15.82	1346.71	29.33
	¾	1801.57	20.01	1002.16	32.15
1800-5	¼	1149.64	26.07	443.38	47.10
	½	1827.75	18.56	1232.80	32.84
	¾	1819.46	21.71	1038.00	37.47
1800-6	¼	1888.45	22.19	1094.47	39.19
	½	1934.04	19.62	1098.15	34.48
	¾	1859.52	20.21	1097.06	34.60

1800-7	¼	1725.02	24.22	994.97	39.56
	½	1848.56	19.90	1088.03	34.12
	¾	1662.33	24.05	921.95	40.02
1800-8	¼	1930.66	21.12	1113.16	37.64
	½	1880.31	21.13	1124.60	35.83
	¾	2001.84	18.70	1164.69	35.23
1800-9	¼	1906.57	19.22	1108.87	36.26
	½	1862.40	19.34	1026.78	36.48
	¾	1653.06	23.72	1011.60	37.60
1800-10	¼	2005.11	17.74	1361.53	29.63
	½	1745.72	24.69	978.71	41.50
	¾	1806.45	23.98	1098.87	39.66
1800-11	¼	1781.99	20.70	1074.67	35.93
	½	1965.10	18.11	1075.88	35.52
	¾	1765.88	20.86	1031.91	37.56
1800-12	¼	1701.18	21.77	950.98	38.78
	½	1714.69	23.11	883.37	43.33
	¾	1893.96	19.71	1228.80	36.40
1800-13	¼	1804.84	20.41	1016.89	40.13
	½	1989.42	19.03	933.97	41.09
	¾	1812.80	20.62	988.53	39.56
1800-14	¼	1788.69	20.58	1021.31	39.08
	½	1815.23	20.25	1161.50	35.75
	¾	1889.04	17.87	1120.82	36.30
2400 -1	¼	1692.51	20.86	1161.73	35.17
	½	1759.96	22.05	1064.45	37.68
	¾	1972.09	18.76	1211.01	37.82
2400 - 2	¼	2179.84	15.18	1500.01	28.14
	½	1788.54	20.82	1149.90	37.37
	¾	1814.96	19.90	1180.75	37.56
2400 -3	¼	1884.94	16.72	1440.23	26.21
	½	1915.46	20.41	1352.29	33.05
	¾	1914.23	17.83	1190.46	36.32
2700 -1	¼	1883.46	19.36	1163.81	37.95
	½	1858.25	18.66	1169.61	35.94
	¾	1849.00	20.10	1237.11	36.08
2700 -2	¼	1951.09	15.97	1491.38	29.06
	½	1863.01	20.91	1155.63	39.35
	¾	1865.96	20.89	1211.69	39.83
2700 - 3	¼	1850.32	24.31	1162.49	43.58
	½	1859.48	20.09	1173.41	39.32

¾	1853.08	23.09	1232.01	36.24

Table C.7: Coefficients from Titanium 2 tests

Titanium 2 Average Forces and the Geometry Matrices

1/4

mm2	mm	mm2	mm
0 005	0 438	-0 004	-0 253
0 004	0 253	0 005	0 438
0 008	0 438	-0 006	-0 253
0 006	0 253	0 008	0 438
0 010	0 438	-0 008	-0 253
0 008	0 253	0 010	0 438
0 015	0 438	-0 012	-0 253
0 012	0 253	0 015	0 438

1/2

mm2	mm	mm2	mm
0 005	0 505	-0 008	0 505
0 008	0 505	0 005	0 505
0 008	0 505	-0 012	0 505
0 012	0 505	0 008	0 505
0 010	0 505	-0 016	0 505
0 016	0 505	0 010	0 505
0 015	0 505	-0 024	0 505
0 024	0 505	0 015	0 505

3/4

mm2	mm	mm2	mm
0 003	0 438	-0 011	-0 758
0 011	0 758	0 003	0 438
0 005	0 438	-0 017	-0 758
0 017	0 758	0 005	0 438
0 007	0 438	-0 023	-0 758
0 023	0 758	0 007	0 438
0 010	0 438	-0 034	-0 758
0 034	0 758	0 010	0 438

		1/4	1/2	3/4
1200 1	Fx1 (N)	5 30	7 35	27 01
	Fy1	30 50	52 10	59 78
	Fx2	6 85	7 39	-31 58
	Fy2	40 60	63 75	74 91
	Fx3	8 83	-8 03	36 19
	Fy3	44 62	74 83	88 03
	Fx4	13 85	-7 87	-44 13
	Fy4	55 00	95 34	114 23

		1/4	1/2	3/4
1200 2	Fx1 (N)	5 64	7 82	27 72
	Fy1	35 41	52 40	60 61
	Fx2	7 69	7 95	32 23
	Fy2	43 34	64 07	75 40
	Fx3	10 30	7 85	-35 78
	Fy3	50 69	74 01	88 05
	Fx4	14 56	-8 53	-44 48
	Fy4	64 81	96 67	115 22

1200-3	Fx1 (N)	5 84	7 16	-27 72
	Fy1	33 11	52 04	60 82
	Fx2	8 04	-7 43	-32 42
	Fy2	40 67	64 48	75 38
	Fx3	10 13	7 78	-36 03
	Fy3	46 19	75 63	88 98
	Fx4	14 76	-7 62	-44 44
	Fy4	55 63	93 94	114 91

1800 1	Fx1 (N)	5 30	-7 62	-24 34
	Fy1	29 66	49 02	57 76
	Fx2	6 62	6 56	30 99
	Fy2	36 78	59 64	74 12
	Fx3	8 93	-4 80	30 33
	Fy3	44 21	69 73	83 25
	Fx4	13 59	-5 73	-36 04
	Fy4	61 39	88 47	105 21

1800 -2	Fx1 (N)	5 31	-7 90	-24 98
	Fy1	35 14	50 74	59 53
	Fx2	7 76	7 03	-31 15
	Fy2	42 28	63 17	72 27
	Fx3	10 33	6 96	-31 18
	Fy3	49 63	71 18	83 27
	Fx4	15 92	-6 06	-38 74
	Fy4	62 50	92 45	108 07

1800-3	Fx1 (N)	5 26	6 36	-24 75
	Fy1	25 94	47 39	55 00
	Fx2	7 15	-6 12	-27 25
	Fy2	32 87	58 08	66 95
	Fx3	10 29	5 32	-30 03
	Fy3	41 06	71 32	79 52
	Fx4	14 43	-4 34	-37 01
	Fy4	55 96	88 86	102 50

1800 -4	Fx1 (N)	4 57	-6 52	-24 12
	Fy1	32 53	47 31	54 59
	Fx2	7 96	-6 48	-27 82
	Fy2	41 91	58 79	69 80
	Fx3	9 49	5 67	-30 37
	Fy3	46 40	68 33	79 41
	Fx4	14 94	-5 27	-35 51
	Fy4	60 50	88 21	107 18

1800-5	Fx1 (N)	4 55	7 40	-25 95
	Fy1	28 63	51 77	54 67
	Fx2	7 26	-6 16	-27 29
	Fy2	35 26	57 07	67 51
	Fx3	8 98	-5 73	-30 13
	Fy3	43 75	72 51	81 04
	Fx4	12 85	5 58	-37 10
	Fy4	61 38	87 57	101 63

1800-6	Fx1 (N)	5 22	-7 09	26 28
	Fy1	29 78	47 71	56 56
	Fx2	7 91	-5 91	-26 45
	Fy2	34 72	56 24	66 93
	Fx3	10 62	-4 90	-28 74
	Fy3	40 80	68 71	77 41
	Fx4	14 86	5 57	-35 87
	Fy4	52 28	87 37	101 34

1800 7	Fx1 (N)	3 41	7 38	-28 27
	Fy1	30 30	49 81	59 89
	Fx2	6 63	6 01	-28 03
	Fy2	36 38	59 56	69 13
	Fx3	7 95	-5 78	-30 20
	Fy3	41 89	67 98	80 52
	Fx4	12 54	5 01	36 21
	Fy4	52 28	85 69	104 18

1800-8	Fx1 (N)	4 16	-8 02	-27 72
	Fy1	35 37	50 10	57 48
	Fx2	6 83	6 64	-29 72
	Fy2	45 46	61 69	68 65
	Fx3	9 28	-5 83	-32 49
	Fy3	50 02	71 40	80 72

1800-9	Fx1 (N)	4 62	-6 66	-26 82
	Fy1	32 59	49 69	55 84
	Fx2	8 17	-6 59	30 78
	Fy2	42 23	59 24	71 05
	Fx3	9 96	6 63	-30 90
	Fy3	46 42	69 67	79 40

	Fx4	14 62	-6 02	-42 52
	Fy4	64 33	92 26	108 32

	Fx4	16 33	5 53	38 28
	Fy4	65 13	90 66	104 66

1800 10	Fx1 (N)	4 97	-7 61	-27 65
	Fy1	32 44	50 23	58 11
	Fx2	7 50	-7 18	27 41
	Fy2	39 23	59 46	70 07
	Fx3	11 10	6 16	-30 59
	Fy3	46 31	68 65	84 82
	Fx4	14 80	-5 94	34 79
	Fy4	58 55	93 53	109 01

1800-11	Fx1 (N)	4 05	-8 01	26 20
	Fy1	32 18	48 48	56 71
	Fx2	6 95	-7 13	28 82
	Fy2	40 33	59 16	68 87
	Fx3	9 72	6 83	30 57
	Fy3	46 68	69 66	80 50
	Fx4	13 88	-6 24	36 50
	Fy4	63 16	89 93	104 47

1800-12	Fx1 (N)	5 61	7 76	26 62
	Fy1	31 47	47 27	55 64
	Fx2	7 92	-7 29	29 28
	Fy2	38 14	58 58	69 07
	Fx3	10 63	-4 66	30 30
	Fy3	43 90	68 96	80 22
	Fx4	15 46	-5 51	-37 89
	Fy4	56 65	87 39	103 42

1800 13	Fx1 (N)	3 61	-6 06	24 65
	Fy1	32 10	48 66	55 54
	Fx2	5 48	-6 91	-28 90
	Fy2	40 34	58 53	67 30
	Fx3	7 12	-7 06	-33 45
	Fy3	41 30	67 92	80 24
	Fx4	11 57	5 60	-38 80
	Fy4	47 42	85 20	104 25

1800 14	Fx1 (N)	3 88	-6 74	25 26
	Fy1	32 15	46 71	54 05
	Fx2	5 76	7 34	29 42
	Fy2	39 36	57 32	67 71
	Fx3	8 57	-6 76	-33 57
	Fy3	48 39	70 33	79 90
	Fx4	12 02	-8 25	-38 06
	Fy4	59 56	91 87	104 63

2400-1	Fx1 (N)	3 93	-7 66	26 75
	Fy1	33 01	48 18	55 91
	Fx2	6 34	7 22	30 22
	Fy2	40 69	59 51	72 03
	Fx3	7 06	-6 62	-37 51
	Fy3	46 16	70 75	83 61
	Fx4	11 65	-6 77	-40 50
	Fy4	59 09	87 06	109 57

2400 2	Fx1 (N)	4 50	-8 22	-26 96
	Fy1	32 97	47 27	55 79
	Fx2	6 63	-7 80	-30 51
	Fy2	40 06	60 38	68 55
	Fx3	8 92	-10 06	-34 70
	Fy3	50 12	71 89	80 71
	Fx4	14 05	-8 05	-41 42
	Fy4	65 65	87 79	104 97

2400-3	Fx1 (N)	3 94	-7 84	-26 74
	Fy1	30 28	49 34	55 50
	Fx2	5 90	7 89	30 33
	Fy2	37 21	58 20	67 79
	Fx3	8 61	-7 79	-33 85
	Fy3	48 22	72 87	80 19
	Fx4	10 99	-9 92	-40 85
	Fy4	59 86	92 52	106 79

2700-1	Fx1 (N)	3 54	-8 70	27 17
	Fy1	35 03	48 28	56 17
	Fx2	5 84	-8 31	29 42
	Fy2	42 24	58 63	68 42
	Fx3	8 47	-8 75	-33 69
	Fy3	48 61	68 41	81 42
	Fx4	12 87	-8 36	-42 39
	Fy4	62 43	89 56	106 35

2700-2	Fx1 (N)	3 34	-9 27	-28 84
	Fy1	32 50	51 24	58 12
	Fx2	5 00	-8 60	-32 73
	Fy2	39 55	60 80	71 89
	Fx3	7 22	-8 97	-34 50
	Fy3	48 42	71 90	83 05
	Fx4	10 61	-8 61	-44 03
	Fy4	63 34	92 12	109 05

2700 3	Fx1 (N)	4 04	-10 02	-25 55
	Fy1	38 59	50 83	58 09
	Fx2	6 41	-8 98	-28 75
	Fy2	45 66	60 39	71 58
	Fx3	8 94	-9 71	-32 19
	Fy3	52 18	71 81	83 53
	Fx4	13 09	-9 55	-40 93
	Fy4	65 66	91 80	108 72

Table C8: Titanium Average Forces and the Geometry Matrices

Cutting coefficients from the tests performed on Steel 1018 with Sandvik 08M-PM insert

	K_{TC} (N/mm^2)	K_{TE} (N/mm)	K_{RC} (N/mm^2)	K_{RE} (N/mm)
Sandvik -1 1/4	1800.61	47.29	761.80	52.87
Sandvik -1 3/4	1682.07	62.75	1100.82	69.06
Sandvik -2 1/4	1528.60	45.89	566.68	56.56
Sandvik -2 3/4	1404.31	49.32	424.11	77.84
Sandvik -3 1/4	2100.64	49.91	1274.56	59.97
Sandvik -3 3/4	2068.93	51.30	1318.73	63.08
Sandvik -4 1/4	1571.09	42.92	672.27	52.48
Sandvik -4 3/4	1537.02	51.97	892.32	54.79
Sandvik -5 1/4	1942.27	46.02	1050.19	77.41
Sandvik -5 3/4	1820.53	52.69	1213.04	62.45
Sandvik -6 1/4	1415.63	45.27	1092.78	80.03
Sandvik -6 3/4	1692.02	47.73	693.66	58.43
Sandvik -7 1/4	1536.32	46.79	732.24	62.32
Sandvik -7 3/4	1722.82	46.91	976.92	59.87
Sandvik -8 1/4	1431.52	38.91	447.55	57.18
Sandvik -8 3/4	1495.37	36.78	589.00	52.84

Table C.9: Coefficients from Sandvik 08M-PM tests on Steel 1018

Cutting coefficients from the tests performed on Steel 1018 with Kennametal KC725M insert

	K_{TC} (N/mm^2)	K_{TE} (N/mm)	K_{RC} (N/mm^2)	K_{RE} (N/mm)
KC725M -1 1/4	1377.54	85.78	509.25	115.25
KC725M -1 3/4	1453.81	84.28	806.04	122.10
KC725M -2 1/4	1820.60	40.51	702.81	59.18
KC725M -2 3/4	1387.59	69.27	829.64	66.26
KC725M -3 1/4	1370.96	92.86	460.66	115.52
KC725M -3 3/4	1954.53	71.99	1231.82	110.33
KC725M -4 1/4	1456.17	67.30	586.59	66.54
KC725M -4 3/4	1768.28	53.27	873.91	68.96
KC725M -5 1/4	1987.10	54.91	1129.44	91.02
KC725M -5 3/4	2038.93	54.13	1390.31	84.02
KC725M -6 1/4	1766.88	48.10	765.99	60.13
KC725M -6 3/4	1968.25	53.81	1081.89	60.64
KC725M -7 1/4	2032.95	44.63	879.39	84.97
KC725M -7 3/4	1725.45	56.96	940.83	98.94
KC725M -8 1/4	1773.08	45.20	957.52	74.46
KC725M -8 3/4	1752.48	48.91	769.27	61.70

Table C.10: Coefficients from Kennametal KC725M insert tests on Steel 1018

Cutting coefficients from the tests performed on Steel 1018 with Kennametal KC935M insert

	K_{TC} (N/mm^2)	K_{TE} (N/mm)	K_{RC} (N/mm^2)	K_{RE} (N/mm)
KC935M -1 1/4	1400.13	94.88	318.35	120.10
KC935M -1 3/4	1798.20	85.32	1060.00	119.34
KC935M -2 1/4	2037.46	76.76	851.29	71.79
KC935M -2 3/4	2318.77	61.63	1180.01	74.57
KC935M -3 1/4	2234.25	80.15	1094.25	93.85
KC935M -3 3/4	2700.18	72.83	1797.88	108.46
KC935M -4 1/4	1637.53	91.46	952.56	122.68
KC935M -4 3/4	2617.12	64.92	1558.57	59.78
KC935M -5 1/4	2033.13	64.31	1370.57	98.33
KC935M -5 3/4	2206.65	65.04	1421.66	103.98
KC935M -6 1/4	1482.13	105.78	837.22	69.67
KC935M -6 3/4	2088.70	80.95	1078.30	73.97
KC935M -7 1/4	1945.88	66.95	998.17	83.44
KC935M -7 3/4	1978.22	55.31	1162.43	93.05
KC935M -8 1/4	1717.45	58.45	690.17	93.68
KC935M -8 3/4	2060.72	63.81	1115.03	68.32

Table C.11: Coefficients from Kennametal KC935M insert tests on Steel 1018

Cutting coefficients from the tests performed on Steel 1018 with Uncoated Solid Carbide Cutter of 30^o helix angle

	K_{TC} (N/mm^2)	K_{TE} (N/mm)	K_{RC} (N/mm^2)	K_{RE} (N/mm)
Uncoated -1 1/4	1974.20	36.26	931.25	43.41
Uncoated -1 3/4	2396.83	25.46	1281.99	27.40
Uncoated -2 1/4	1980.41	38.53	1062.16	62.70
Uncoated -2 3/4	2002.59	41.54	1111.34	56.34
Uncoated -3 1/4	2114.98	28.77	1070.32	35.63
Uncoated -3 3/4	2704.64	13.95	1523.72	11.97
Uncoated -4 1/4	2090.03	71.68	1018.01	103.76
Uncoated -4 3/4	1806.14	85.77	841.27	114.68
Uncoated -5 1/4	1798.63	42.07	762.44	43.03
Uncoated -5 3/4	1853.32	42.56	932.05	50.76
Uncoated -6 1/4	1820.72	96.84	874.37	101.32
Uncoated -6 3/4	1438.79	100.37	992.55	107.01
Uncoated -7 1/4	1885.29	38.57	855.17	45.01
Uncoated -7 3/4	2168.63	26.71	1062.95	37.74
Uncoated -8 1/4	2316.23	33.05	1434.48	43.35
Uncoated -8 3/4	2377.84	27.84	1121.14	48.30

Table C.12: Coefficients from Uncoated Solid Carbide Cutter of 30^o helix angle tests on Steel 1018

Cutting coefficients from the tests performed on Steel 1018 with Coated Solid Carbide Cutter of 30° helix angle

	K_{TC} (N/mm²)	K_{TE} (N/mm)	K_{RC} (N/mm²)	K_{RE} (N/mm)
Coated -1 1/4	1892.87	27.40	818.19	27.71
Coated -1 3/4	1844.33	28.51	853.58	31.86
Coated -2 1/4	1670.17	31.25	712.18	43.85
Coated -2 3/4	1731.59	32.37	593.51	56.36
Coated -3 1/4	921.30	53.41	366.26	59.82
Coated -3 3/4	490.76	68.41	79.17	79.44
Coated -4 1/4	711.44	50.68	468.67	60.55
Coated -4 3/4	477.15	61.20	76.68	65.85
Coated -5 1/4	523.63	67.88	134.93	73.26
Coated -5 3/4	553.90	67.30	126.00	81.71
Coated -6 1/4	579.12	49.93	36.03	60.63
Coated -6 3/4	559.83	53.85	56.43	65.37
Coated -7 1/4	1732.65	33.74	724.96	39.03
Coated -7 3/4	1808.60	32.39	812.18	45.95
Coated -8 1/4	1586.71	29.39	697.68	59.04
Coated -8 3/4	1625.78	39.28	640.48	62.38

Table C.13: Coefficients from Coated Solid Carbide Cutter of 30° helix angle tests on Steel 1018

Steel 1018 with Sandvik 08M-PM, KC725M, KC935M, uncoated solid carbide and coated solid carbide cutters Average Forces and the Geometry Matrices

G matrix for tests 1 2-7-8

	1/4					3/4		
mm2	mm	mm2	mm		mm2	mm	mm2	mm
0 010	0 438	-0 008	-0 253		0 007	0 438	-0 023	0 758
0 008	0 253	0 010	0 438		0 023	0 758	0 007	0 438
0 013	0 438	-0 010	-0 253		0 008	0 438	-0 028	-0 758
0 010	0 253	0 013	0 438		0 028	0 758	0 008	0 438
0 015	0 438	-0 012	-0 253		0 010	0 438	-0 034	-0 758
0 012	0 253	0 015	0 438		0 034	0 758	0 010	0 438
0 020	0 438	-0 017	-0 253		0 013	0 438	-0 045	-0 758
0 017	0 253	0 020	0 438		0 045	0 758	0 013	0 438

G matrix for tests 3-4-5 6

	1/4					3/4		
mm2	mm	mm2	mm		mm2	mm	mm2	mm
0 006	0 263	0 005	-0 152		0 004	0 263	-0 014	-0 455
0 005	0 152	0 006	0 263		0 014	0 455	0 004	0 263
0 008	0 263	-0 006	-0 152		0 005	0 263	-0 017	0 455
0 006	0 152	0 008	0 263		0 017	0 455	0 005	0 263
0 009	0 263	-0 007	-0 152		0 006	0 263	-0 020	-0 455
0 007	0 152	0 009	0 263		0 020	0 455	0 006	0 263
0 012	0 263	-0 010	-0 152		0 008	0 263	-0 027	-0 455
0 010	0 152	0 012	0 263		0 027	0 455	0 008	0 263

		1/4	3/4
Sandvik-1	Fx1 (N)	19 38	-36 92
	Fy1	57 95	121 70
	Fx2	21 99	-40 32
	Fy2	63 08	133 11
	Fx3	25 04	-50 92
	Fy3	68 56	151 52
	Fx4	31 14	-49 73

		1/4	3/4
Sandvik 2	Fx1 (N)	16 53	38 02
	Fy1	54 19	105 61
	Fx2	19 24	36 50
	Fy2	59 01	114 01
	Fx3	21 83	-38 48
	Fy3	65 18	125 60
	Fx4	27 27	37 62

		1/4	3/4
Sandvik-3	Fx1 (N)	9 86	24 85
	Fy1	41 50	72 53
	Fx2	11 97	27 43
	Fy2	44 71	81 01
	Fx3	14 74	-29 13
	Fy3	52 22	92 67
	Fx4	16 23	34 54

	Fy4	80 37	166 39

	Fy4	72 38	139 86

	Fy4	58 97	105 60

Sandvik-4	Fx1 (N)	8 83	-18 28
	Fy1	30 81	62 72
	Fx2	11 54	-18 26
	Fy2	35 22	70 43
	Fx3	13 12	-18 65
	Fy3	40 50	71 65
	Fx4	15 26	-23 99
	Fy4	42 72	88 10

Sandvik-5	Fx1 (N)	6 79	23 55
	Fy1	43 49	69 52
	Fx2	8 47	-26 07
	Fy2	46 94	77 82
	Fx3	10 48	-28 49
	Fy3	51 34	85 16
	Fx4	13 30	32 73
	Fy4	59 28	99 34

Sandvik-6	Fx1 (N)	2 53	-16 74
	Fy1	40 35	62 94
	Fx2	4 11	-17 17
	Fy2	46 74	69 59
	Fx3	4 60	-17 96
	Fy3	47 85	75 11
	Fx4	5 89	19 27
	Fy4	54 88	88 86

Sandvik 7	Fx1 (N)	13 65	-35 64
	Fy1	59 88	106 42
	Fx2	17 01	-37 98
	Fy2	63 68	119 50
	Fx3	19 23	-40 30
	Fy3	68 50	130 89
	Fx4	23 32	-46 15
	Fy4	79 68	152 35

Sandvik-8	Fx1 (N)	12 89	-27 99
	Fy1	50 43	88 44
	Fx2	15 85	-27 46
	Fy2	55 19	98 77
	Fx3	19 77	-28 34
	Fy3	60 99	107 86
	Fx4	23 54	-30 97
	Fy4	66 70	126 47

KC725M 1	Fx1 (N)	18 36	66 23
	Fy1	91 22	153 52
	Fx2	20 04	-64 81
	Fy2	89 98	170 46
	Fx3	23 15	-66 43
	Fy3	95 79	171 31
	Fx4	27 79	-73 98
	Fy4	106 33	194 45

KC725M 2	Fx1 (N)	15 06	-27 90
	Fy1	56 86	114 45
	Fx2	18 47	-33 57
	Fy2	65 08	134 27
	Fx3	22 12	-34 33
	Fy3	70 12	135 37
	Fx4	27 60	-38 27
	Fy4	79 61	154 68

KC725M 3	Fx1 (N)	13 21	-38 57
	Fy1	56 15	91 92
	Fx2	14 01	-41 97
	Fy2	53 63	100 27
	Fx3	15 78	-48 25
	Fy3	58 57	112 92
	Fx4	19 03	-47 23
	Fy4	64 34	123 00

KC725M-4	Fx1 (N)	13 96	-21 51
	Fy1	39 09	69 25
	Fx2	14 49	-22 85
	Fy2	40 45	76 34
	Fx3	16 20	-26 39
	Fy3	43 53	85 59
	Fx4	19 62	-26 02
	Fy4	49 50	96 57

KC725M-5	Fx1 (N)	6 94	34 06
	Fy1	48 34	78 52
	Fx2	8 67	-37 72
	Fy2	53 96	89 13
	Fx3	10 44	-40 66
	Fy3	57 03	98 44
	Fx4	13 37	-44 91
	Fy4	65 44	112 21

KC725M-6	Fx1 (N)	10 16	-20 04
	Fy1	36 72	70 90
	Fx2	12 50	-22 59
	Fy2	39 63	80 41
	Fx3	13 79	-22 90
	Fy3	42 92	86 61
	Fx4	17 23	27 15
	Fy4	50 01	102 56

KC725M-7	Fx1 (N)	11 32	-60 61
	Fy1	75 82	128 11
	Fx2	14 86	-61 47
	Fy2	79 41	148 59
	Fx3	17 49	-64 08
	Fy3	85 19	154 12
	Fx4	24 67	-69 95
	Fy4	100 89	176 17

KC725M-8	Fx1 (N)	10 63	-30 33
	Fy1	67 47	106 30
	Fx2	13 51	-33 64
	Fy2	75 10	122 94
	Fx3	16 43	-33 36
	Fy3	80 99	132 50
	Fx4	20 63	-36 58
	Fy4	92 11	152 53

KC935M 1	Fx1 (N)	22 93	-67 52
	Fy1	91 35	168 82
	Fx2	24 94	-66 00
	Fy2	93 44	172 57
	Fx3	28 78	-69 07
	Fy3	100 92	186 77
	Fx4	34 10	-78 44
	Fy4	105 32	214 59

KC935M 2	Fx1 (N)	28 16	-45 02
	Fy1	74 37	139 27
	Fx2	31 51	-38 79
	Fy2	81 72	151 68
	Fx3	38 59	-44 65
	Fy3	93 89	175 97
	Fx4	41 24	-53 82
	Fy4	99 32	198 06

KC935M-3	Fx1 (N)	15 73	-44 93
	Fy1	57 30	105 50
	Fx2	16 39	-47 79
	Fy2	56 67	119 27
	Fx3	18 14	-47 17
	Fy3	61 02	123 51
	Fx4	23 54	-58 80
	Fy4	73 85	150 80

KC935M-4	Fx1 (N)	10 44	-20 48
	Fy1	59 11	87 14
	Fx2	10 08	-23 57
	Fy2	62 01	99 08
	Fx3	16 27	-26 43
	Fy3	70 70	105 56
	Fx4	14 70	-31 18
	Fy4	72 26	129 75

KC935M-5	Fx1 (N)	6 86	-39 99
	Fy1	54 15	91 22
	Fx2	9 53	-43 98
	Fy2	60 23	103 72
	Fx3	10 50	-46 03
	Fy3	60 10	109 97
	Fx4	12 70	-50 78
	Fy4	73 36	128 01

KC935M 6	Fx1 (N)	22 47	-17 24
	Fy1	46 63	87 65
	Fx2	22 72	-21 52
	Fy2	49 00	98 01
	Fx3	24 34	-22 49
	Fy3	54 41	106 72
	Fx4	27 02	-24 14
	Fy4	58 61	120 79

KC935M 7	Fx1 (N)	19 14	58 23
	Fy1	78 04	132 45
	Fx2	22 57	-61 99
	Fy2	86 94	149 20
	Fx3	26 00	69 11
	Fy3	94 39	166 11
	Fx4	30 57	-70 93
	Fy4	104 57	185 41

KC935M-8	Fx1 (N)	13 68	35 07
	Fy1	76 49	132 35
	Fx2	16 24	-38 16
	Fy2	82 24	146 28
	Fx3	19 32	-41 30
	Fy3	88 21	159 29
	Fx4	25 19	-46 49
	Fy4	97 64	186 63

Uncoated 1	Fx1 (N)	17 26	-22 38
	Fy1	54 04	92 89
	Fx2	20 08	-26 37
	Fy2	60 30	108 78
	Fx3	23 05	-28 49
	Fy3	66 26	130 01
	Fx4	29 42	-35 59
	Fy4	79 72	155 18

Uncoated-2	Fx1 (N)	11 66	-37 27
	Fy1	62 64	107 07
	Fx2	14 65	-37 96
	Fy2	70 44	121 33
	Fx3	19 49	-41 84
	Fy3	81 78	140 47
	Fx4	22 66	-48 37
	Fy4	89 39	159 44

Uncoated-3	Fx1 (N)	9 14	-10 90
	Fy1	29 82	51 63
	Fx2	12 10	-13 72
	Fy2	36 20	62 55
	Fx3	13 52	-18 30
	Fy3	38 88	76 21
	Fx4	16 92	-20 54
	Fy4	47 41	94 22

Uncoated 4	Fx1 (N)	10 88	35 29
	Fy1	55 23	97 23
	Fx2	12 77	34 49
	Fy2	59 85	105 44
	Fx3	13 84	33 33
	Fy3	60 01	108 58
	Fx4	18 56	39 28
	Fy4	72 27	125 86

Uncoated 5	Fx1 (N)	12 02	17 44
	Fy1	31 95	61 11
	Fx2	12 86	18 66
	Fy2	34 04	69 67
	Fx3	15 20	18 64
	Fy3	37 27	75 96
	Fx4	18 85	22 76
	Fy4	45 19	90 44

Uncoated 6	Fx1 (N)	16 85	29 67
	Fy1	55 42	99 48
	Fx2	18 20	31 70
	Fy2	59 55	101 28
	Fx3	20 22	34 83
	Fy3	62 51	107 61
	Fx4	23 42	37 24
	Fy4	69 91	122 06

Uncoated 7	Fx1 (N)	17 20	25 42
	Fy1	53 71	92 19
	Fx2	20 53	29 78
	Fy2	59 60	108 80
	Fx3	23 79	31 68
	Fy3	65 68	120 30
	Fx4	29 18	35 41
	Fy4	77 84	149 27

Uncoated 8	Fx1 (N)	14 53	32 52
	Fy1	61 75	103 22
	Fx2	18 34	36 44
	Fy2	68 74	119 35
	Fx3	21 09	-40 81
	Fy3	76 84	134 64
	Fx4	26 25	-42 05
	Fy4	95 03	164 75

Coated 1	Fx1 (N)	17 25	19 29
	Fy1	42 81	81 88
	Fx2	21 01	19 20
	Fy2	50 71	96 44
	Fx3	22 70	22 43
	Fy3	52 37	106 94
	Fx4	29 87	25 65
	Fy4	67 57	130 11

Coated 2	Fx1 (N)	13 48	30 82
	Fy1	47 94	90 88
	Fx2	16 26	30 32
	Fy2	53 24	106 84
	Fx3	19 24	31 06
	Fy3	58 86	111 65
	Fx4	24 41	32 38
	Fy4	68 86	135 88

Coated 3	Fx1 (N)	8 60	17 53
	Fy1	31 22	57 88
	Fx2	10 00	15 46
	Fy2	32 50	60 88
	Fx3	10 30	18 62
	Fy3	32 36	64 36
	Fx4	12 53	15 84
	Fy4	38 10	64 95

Coated-4	Fx1 (N)	5 93	12 31
	Fy1	29 93	51 05
	Fx2	7 04	12 94
	Fy2	31 66	53 92
	Fx3	6 81	13 69
	Fy3	32 95	56 61
	Fx4	8 13	11 51
	Fy4	36 35	57 98

Coated 5	Fx1 (N)	8 60	18 88
	Fy1	32 68	59 19
	Fx2	10 63	18 47
	Fy2	34 06	62 55
	Fx3	10 52	19 44
	Fy3	34 75	65 26
	Fx4	11 49	18 17
	Fy4	36 22	67 45

Coated 6	Fx1 (N)	7 41	13 85
	Fy1	27 04	48 45
	Fx2	8 02	13 77
	Fy2	27 67	52 90
	Fx3	8 67	13 79
	Fy3	26 71	53 32
	Fx4	10 70	12 38
	Fy4	30 28	57 01

Coated 7	Fx1 (N)	16 36	25 92
	Fy1	46 88	90 38
	Fx2	19 40	29 64
	Fy2	52 87	103 71
	Fx3	21 97	30 18
	Fy3	58 33	114 23
	Fx4	27 90	32 75
	Fy4	68 60	137 27

Coated 8	Fx1 (N)	7 99	33 10
	Fy1	53 42	97 70
	Fx2	10 64	35 60
	Fy2	58 35	108 90
	Fx3	13 81	35 07
	Fy3	63 55	119 21
	Fx4	18 17	37 19
	Fy4	73 50	139 00

Table C14: Steel 1018 with Sandvik 08M-PM, KC725M, KC935M, uncoated solid carbide and coated solid carbide cutters Average Forces and the Geometry Matrices

Experimental Forces (Peak Resultant) for Case Study 1

Milling Type	
Down Mill (N)	**Up Mill (N)**
560.2	604.9
568	601.1
628.4	598.3
586.6	587.1
538.7	556.5
603.9	554
630.9	577.7
624.5	574.5

561.4	545.3
597.1	548.4
632.9	580
621.8	593
533.7	567.2
547.3	531.3
588.4	571.5
600.1	561.3

Table C.15: Experimental Forces for Case Study 1

Experimental Forces (Peak Resultant) for Case Study 2

Milling Type	
Down Mill (N)	**Up Mill (N)**
312.3	339.8
381.4	371.9
359.7	348
325.9	351.5
327.2	345.9
387.8	374.5
374.8	371.8
329.7	366.2
341.5	360.4
406	394.4
407.6	410.7
365.4	411.1
348.3	411.3
416.5	412.9
421.4	410.8
396.2	420.1

Table C.16: Experimental Forces for Case Study 2

Experimental Peak Resultant Forces for the Cone Plots (Figures 5.1-5.4)

Aluminum (N)	Steel1018 (N)	StSt304 (N)	Titanium 2 (N)
192.5	607.8	565.4	262.4
187.6	620.1	498.4	263.1
195.8	608.5	500.1	263.9
171.6	553.6	495.1	257.2
173	519.8	479.6	258.5
193.1	541.4	482.9	255.7
180.4	529.1	443.1	259.6
178.9	532.2	473.8	258.2
177.1	534.1	504.5	252.2

Aluminum (N)	Steel1018 (N)	StSt304 (N)	Titanium 2 (N)
174.7	530	449.5	245.5
178.6	544.2	495.3	259.8
174.7	539.7	456.3	254.6
274.5	669.3	646.5	328.1
285.9	696.5	580.6	327.9
290.5	681.4	586.1	323.5
265	644.6	550.4	322
261.7	571	545.2	311.9
276.2	592	531.7	300.4
270.2	585.1	516.4	320.5
270.1	588.7	542.2	317.3
274.4	592.8	584.4	317
271.3	582.1	520.3	297.4
269.9	603.1	568.6	307.9
267	616.7	537.2	305.5
355.5	722.6	715.7	386.5
358.3	729.8	659.1	383.8
388	728.8	652.3	391.2
360	677.7	634.8	365.7
370.1	611.4	610.6	377.4
367.6	654.7	611.1	351.2
348.9	639.5	576.4	387.8
360	649.5	620.2	379.3
354.4	639.9	656.9	362
366.2	643.3	585.6	358.9
354.7	655.5	630.2	363.8
356.9	657.8	587.9	366.4
431.9	811.9	768.7	527.4
428.2	827.7	703	519.5
462.7	817.2	688.7	529.4
452.1	776.4	689.3	487.2
430.1	721.5	683.6	500.2
450.7	735.4	678	484.5
428.4	740.4	630.3	501.6
424.7	731.6	682.2	495.8
424.8	724.1	681.9	489.1
431.4	766.1	632.5	490
432.7	749.8	682.2	491.3
448.4	765.1	658.5	486.4
196.6	643.3	600.9	277.7

Aluminum (N)	Steel1018 (N)	StSt304 (N)	Titanium 2 (N)
200	676.8	560.9	277.4
213.4	682.4	548.2	287.9
202.6	650	554.1	271.1
204.1	580.7	560.1	267.1
202.5	611.5	563	260.2
191.7	627.8	512.7	267.4
198.2	643.4	598.4	269.5
204.7	650.8	592.3	272.2
181.8	622.1	515.2	274.7
188.9	634	537.7	273
185.8	635.2	511.2	277.2
312.2	728.8	710.8	346.3
316	751.3	669.6	350.3
304.3	736.3	634.1	334.5
298	700.2	650.3	337
288.1	646.7	660.9	336.4
311.4	672.8	653.1	330.9
283.9	696.7	604.1	343.3
301.8	742.6	659.9	341.3
300.2	743.8	685.8	338
281.7	683.7	611.9	322.1
294.2	693.9	631.9	335
292.2	699.4	628.1	330
401.5	782.4	786.6	425
395.7	798.1	758.5	422.4
368.5	806.2	744.3	410.4
377	769.5	727.7	385.5
387.2	705.8	715.8	398.2
410.8	731.8	731.6	391.6
375	765.3	690.3	388
384	773.1	745.9	408.6
394.5	808.8	756.4	399.7
374.1	759.4	686.2	384.2
379.5	795.5	713.3	404.6
381.4	778.8	716.4	408
504.8	863.3	883.9	551
502.5	883.9	825.7	556.9
518.4	879.6	833.3	543.5
493.2	863.3	802.1	509.3
479.9	853.1	777	538.9

Aluminum (N)	Steel1018 (N)	StSt304 (N)	Titanium 2 (N)
515.3	832.4	792.8	540.2
466.1	862	741.8	527.1
477.4	901.3	818.2	530.6
479.3	895.8	853.8	531.9
463.3	861.2	756	527.6
469.9	899	776.3	540
462.6	892.8	779.1	541
221.4	607.3	558	295.9
226	648.3	598.8	282.8
222.5	661	560.7	270.1
212.9	638.5	571.1	251.1
212	556	573.4	283.2
207.6	598.8	563.4	249.5
209.1	596.6	508.2	274.8
204.5	656.7	574.9	270.4
197.4	657.3	581.8	264.5
200	629.4	501.9	264.1
202.9	628	539.3	275.5
198.5	629.2	513.6	273.4
329.6	694.8	675.4	350.7
349.2	714.3	702.7	348.1
324.6	721	693.7	337.8
337.4	674.3	681.1	313.3
331.7	634.5	659.5	350.51
318.4	642.1	629.4	316.3
317.7	695.5	612.5	338.6
270.8	715.7	671.1	335.5
309	716.6	635.7	333.6
310.8	681.7	605.9	324.8
293.8	675.8	633.8	336.8
290.7	706.7	605	326
436.2	743.1	801	433.7
443.9	776.6	798.5	411.3
451.6	779.3	743	405.8
426.7	755.4	751.3	366.8
419.6	690.2	765.3	406.7
409	720.4	779.2	372.4
406.1	774.9	702.2	385
357.7	798.6	778.7	393.9
390.4	788.5	732.9	399.1

Aluminum (N)	Steel1018 (N)	StSt304 (N)	Titanium 2 (N)
393.7	772	676	406.4
379.4	774.4	722.9	401.6
371	780.4	690.2	412.4
525.2	850	894.1	544.4
529.2	866.3	871	516.4
537.7	862.2	830.8	525.9
519.2	857.7	829.4	498.2
516.4	767.2	834.1	548.6
493.5	829.2	840.8	523.3
485.2	872.3	778.2	519
444.2	930	861.6	538.7
477.8	915	839	537.1
475.7	889.9	769.5	518.6
462.6	888.5	790	515.6
449.2	903.9	763.4	522

Table C.17: Experimental Peak Resultant Forces for the Cone Plots (144 samples)

Model Estimated Forces with Two Methods (The Calibrated Coefficients and the Ratio Method)

Aluminum		Steel1018		StSt304		Titanium	
Ratio (N)	Calibrated Coefs (N)	Ratio (N)	Calibrated Coefs (N)	Ratio (N)	Calibrated Coefs (N)	Ratio (N)	Calibrated Coefs (N)
177.34	174.75	553.79	563.61	484.36	472.5	245.6	249.97
266.08	262.58	612.39	623.25	558.58	552.12	305.25	311.26
355.72	351.22	671.19	683.33	633.84	632.06	365.47	372.97
446.2	440.39	790.07	803.58	709.51	712.69	486.51	497.46
188.1	185.17	582.63	582.73	511.35	500.66	260.28	259.61
288.15	283.56	648.34	647.03	595.2	647.03	327.33	325.97
388.9	383.96	714.8	711.92	680.04	711.92	394.94	392.81
489.94	482.79	848.75	841.92	765.12	770.45	531.07	527.08
198.14	195.1	608.5	619.52	536.5	528.37	273.43	278.69
308.1	304.16	681.54	693.42	629.27	627.48	347.57	354.72
419.2	413.84	754.31	767.73	722.44	726.43	422.21	431.44
530.23	524.45	902.13	917.27	816.4	826.87	572.27	585.38

Table C.18: Model Estimated Peak Resultant Forces (Calibrated Coefficients and the Ratio Method)

Covariance Table for the Sandvik 08M-PM tests on Steel 1018 coefficients

$Cov(x_1,x_2)$	K_{TC}	K_{TE}	K_{RC}	K_{RE}
K_{TC}	49986.52	482.62	48937.6	-60.27
K_{TE}	482.62	34.857	971.16	15.74
K_{RC}	48937.6	971.16	85222.59	702.86
K_{RE}	-60.27	15.74	702.8653	83.13

Table C.19: Covariance Table for the Sandvik 08M-PM tests on Steel 1018 coefficients

Covariance Table for the Kennametal KC725M tests on Steel 1018 coefficients

$Cov(x_1,x_2)$	K_{TC}	K_{TE}	K_{RC}	K_{RE}
K_{TC}	59695.12	-2841.74	48503.70	-1616.25
K_{TE}	-2841.74	257.40	-1610.64	273.28
K_{RC}	48503.70	-1610.64	63951.96	-365.91
K_{RE}	-1616.25	273.28	-365.91	503.53

Table C.20: Covariance Table for the Kennametal KC725M tests on Steel 1018 coefficients

Covariance Table for the Kennametal KC935M tests on Steel 1018 coefficients

$Cov(x_1,x_2)$	K_{TC}	K_{TE}	K_{RC}	K_{RE}
K_{TC}	130906.83	-2898.91	109943.75	-2418.82
K_{TE}	-2898.91	208.47	-2282.84	75.57
K_{RC}	109943.75	-2282.84	121851.65	-1043.38
K_{RE}	-2418.82	75.57	-1043.38	408.69

Table C.21: Covariance Table for the Kennametal KC935M tests on Steel 1018 coefficients

Covariance Table for the Uncoated Solid Carbide Cutter of 30° helix angle on Steel 1018 coefficients

$Cov(x_1,x_2)$	K_{TC}	K_{TE}	K_{RC}	K_{RE}
K_{TC}	91615.82	-6003.54	51818.10	-6357.19
K_{TE}	-6003.54	709.22	-2952.26	788.87
K_{RC}	51818.10	-2952.26	44176.97	-3353.71
K_{RE}	-6357.19	788.87	-3353.71	969.45

Table C.22: Covariance Table for the Uncoated Solid Carbide Cutter of 30° helix angle on Steel 1018 coefficients

Covariance Table for the Coated Solid Carbide Cutter of 30° helix angle on Steel 1018 coefficients

$Cov(x_1,x_2)$	K_{TC}	K_{TE}	K_{RC}	K_{RE}
K_{TC}	358728.90	-8664.70	182457.98	-7707.72
K_{TE}	-8664.70	235.08	-4430.36	208.35
K_{RC}	182457.98	-4430.36	100462.41	-4106.92
K_{RE}	-7707.72	208.35	-4106.92	246.80

Table C.23: Covariance Table for the Coated Solid Carbide Cutter of 30° helix angle on Steel 1018 coefficients

APPENDIX D

G CODES FOR CASE STUDY

Introduction

This chapter includes the g-codes used for the case study performed on Steel 1018 to verify the Monte Carlo simulation results. Method 1 is the case where cutting conditions, spindle speed, feedrate and average chip thickness h_{avg} is known and force is calculated in the simulation program. Method 2 is the case where allowable force is found by either using deflection or tool bending stress as a constraint. Feedrates are found by iteration to match the target force which is constrained by one of the formulas.

G-Code for Method 1

Tool rotation speed is 3000 rpm, h_{avg} is 0.03175 mm. 3 teeth insert tool in upmilling configuration.

```
N1 (CALIBRATIONG-CODESETFOR10REVOLUTIONS,2DEGREESPERSAMPLE)
N2 (SAN_0.500)
N3 (FLUTE=1HELIX=0.0)
N4 (TOOLMATERIAL=CARBIDE)
N5 (WORKPIECEMATERIAL=STEEL1018)
N6 G17G20G40G90
N7 T1M6
N8 H1M42E1
N9 M3S3000M8
```

```
N10 (SLOTCUT)
N20 G0X1.0Y-0.5Z2.0
N30 G1Z-0.1F50
N40 G1X-0.5F17.671
N50 G1X-3F17.671
N60 G1X-5F17.671
N70 G1X-7F17.671
N100 G1Z2.0F50
N110 (3/4IMMERSIONDOWNMILLSIDECUT)
N120 G0X1.0Y-1.25Z2.0
N130 G1Z-0.1F50
N140 G1X-0.5F15.708
N150 G1X-3F15.708
N160 G1X-5F15.708
N170 G1X-7F15.708
N200 G1Z2.0F50
N210 (1/2IMMERSIONDOWNMILLSIDECUT)
N220 G0X1.0Y-1.75Z2.0
N230 G1Z-0.1F50
N240 G1X-0.5F17.671
N250 G1X-3F17.671
N260 G1X-5F17.671
N270 G1X-7F17.671
N300 G1Z2.0F50
N310 (1/4IMMERSIONDOWNMILLSIDECUT)
N320 G0X1.0Y-2.0Z2.0
N330 G1Z-0.1F50
N340 G1X-0.5F23.562
N350 G1X-3F23.562
N360 G1X-5F23.562
```

```
N370 G1X-7F23.562
N400 G1Z2.0F50
N410 M5M9H0E0
N420 M41
N430 G0Z0
N440 G0X0Y0
N450 M30
```

G-Code for Method2

Feedrates are optimized for a target force of 400 N in the simulation program for each radial depth including runout. Tool rotation speed is 4000 rpm, with downmill configuration.

```
N1 (CALIBRATIONG-CODESETFOR10REVOLUTIONS,2DEGREESPERSAMPLE)
N2 (SAN_0.500)
N3 (FLUTE=1HELIX=0.0)
N4 (TOOLMATERIAL=CARBIDE)
N5 (WORKPIECEMATERIAL=STEEL1018)
N6 G17G20G40G90
N7 T1M6
N8 H1M42E1
N9 M3S4000M8
N10 (SLOTCUT)
N20 G0X-1.0Y-0.5Z2.0
N30 G1Z-0.1F50
N40 G1X0.5F7.7
N50 G1X3F7.7
N60 G1X5F7.7
N70 G1X7F7.7
```

```
N100 G1Z2.0F50
N110 (3/4IMMERSIONDOWNMILLSIDECUT)
N120 G0X-1.0Y-1.25Z2.0
N130 G1Z-0.1F50
N140 G1X0.5F7.7
N150 G1X3F7.7
N160 G1X5F7.7
N170 G1X7F7.7
N200 G1Z2.0F50
N210 (1/2IMMERSIONDOWNMILLSIDECUT)
N220 G0X-1.0Y-1.75Z2.0
N230 G1Z-0.1F50
N240 G1X0.5F7.7
N250 G1X3F7.7
N260 G1X5F7.7
N270 G1X7F7.7
N300 G1Z2.0F50
N310 (1/4IMMERSIONDOWNMILLSIDECUT)
N320 G0X-1.0Y-2.0Z2.0
N330 G1Z-0.1F50
N340 G1X0.5F8.8
N350 G1X3F8.8
N360 G1X5F8.8
N370 G1X7F8.8
N400 G1Z2.0F50
N410 M5M9H0E0
N420 M41
N430 G0Z0
N440 G0X0Y0
N450 M30
```

APPENDIX E

NORMALITY OF THE CUTTING COEFFICIENTS

Introduction

This section includes the residual plots of the cutting coefficients for Aluminum, Steel 1018, Stainless Steel and Titanium Grade 2.

Aluminum

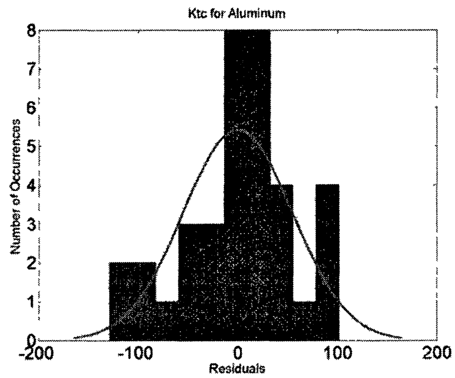

Figure E.1: K_{TC} Residual Histogram for Aluminum

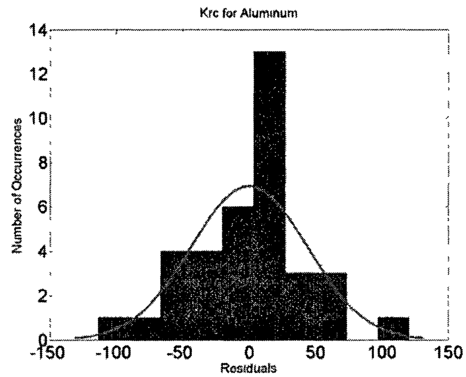

Figure E.3: K_{RC} Residual Histogram for Aluminum

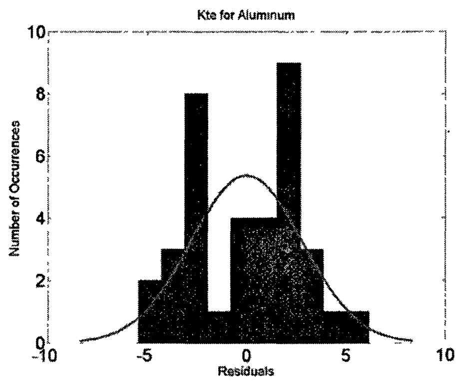

Figure E.2: K_{TE} Residual Histogram for Aluminum

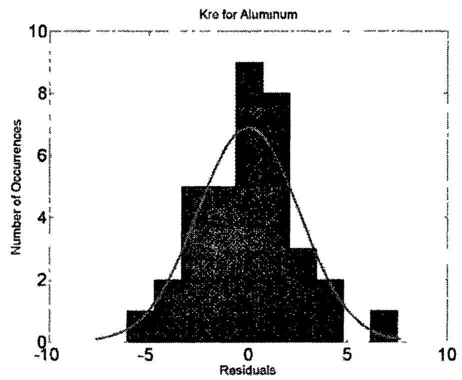

Figure E.4: K_{RE} Residual Histogram for Aluminum

Steel 1018

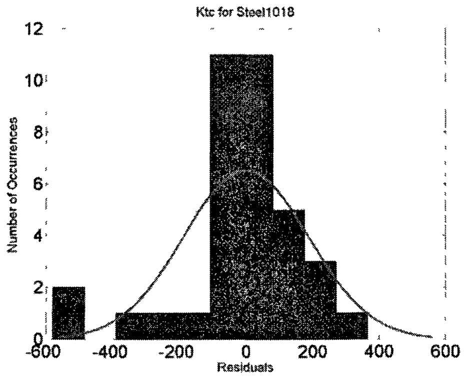

Figure E.5: K_{TC} Residual Histogram for Steel 1018

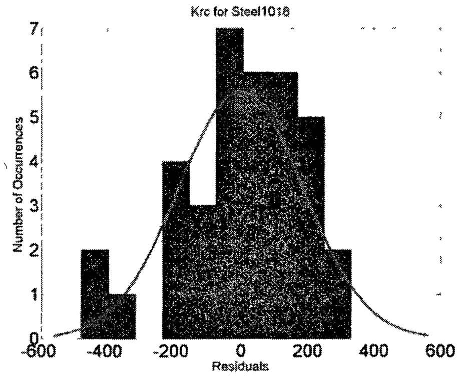

Figure E.7: K_{RC} Residual Histogram for Steel 1018

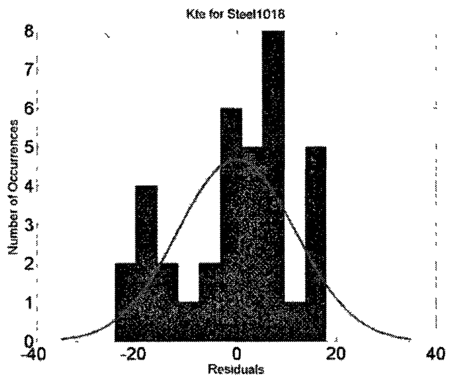

Figure E.6: K_{TE} Residual Histogram for Steel 1018

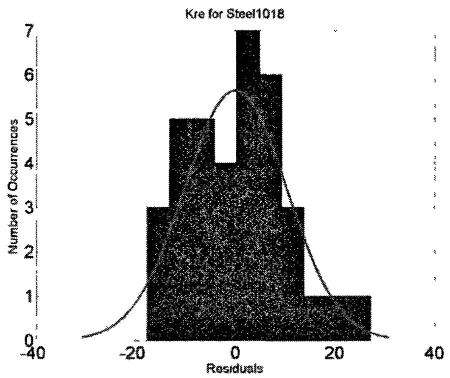

Figure E.8: K_{RE} Residual Histogram for Steel 1018

Stainless Steel 304

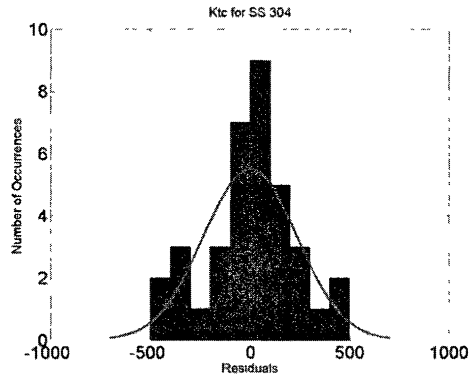

Figure E.9: K_{TC} Residual Histogram for Stainless Steel 304

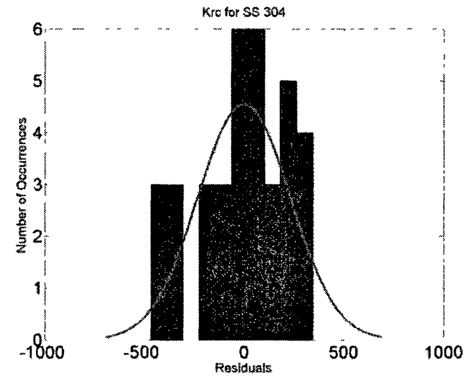

Figure E.11: K_{RC} Residual Histogram for Stainless Steel 304

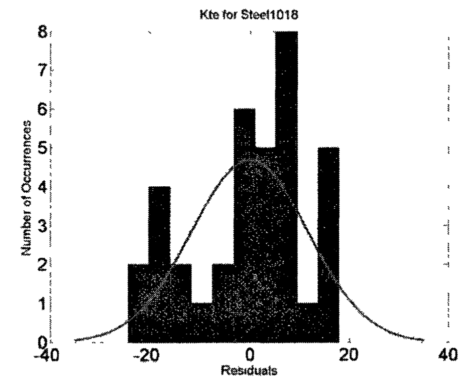

Figure E.10: K_{TE} Residual Histogram for Stainless Steel 304

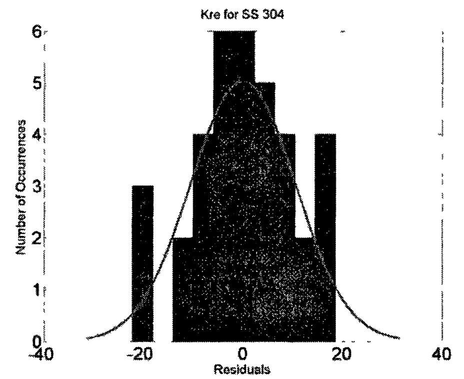

Figure E.12: K_{RE} Residual Histogram for Stainless Steel 304

Titanium Grade 2

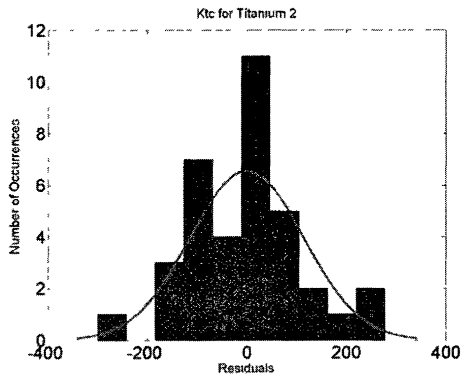

Figure E.13: K_{TC} Residual Histogram for Titanium Grade 2

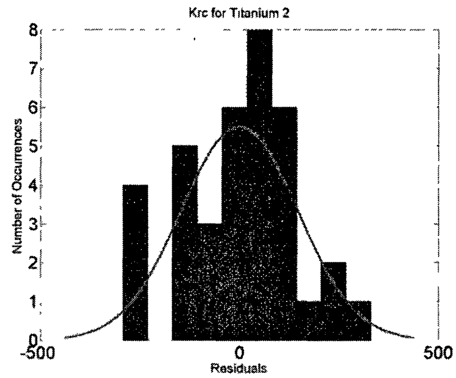

Figure E.15: K_{RC} Residual Histogram for Titanium Grade 2

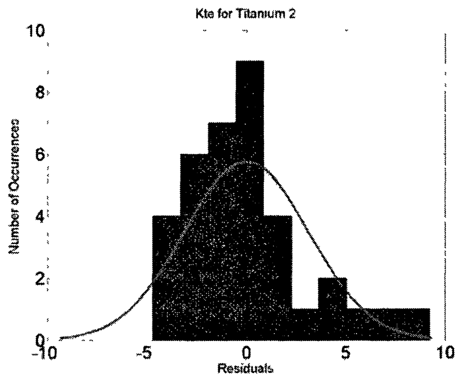

Figure E.14: K_{TE} Residual Histogram for Titanium Grade 2

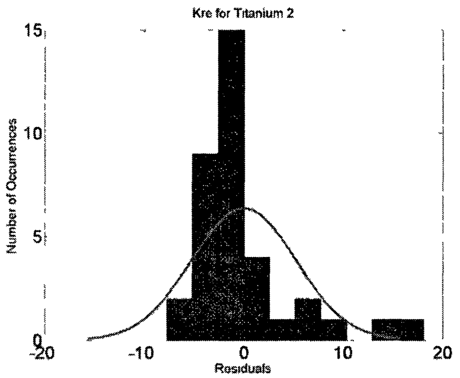

Figure E.16: K_{RE} Residual Histogram for Titanium Grade 2